ADAPTIVE CONTROL OF SYSTEMS IN CASCADE WITH SATURATION

A Thesis
Presented to
The Academic Faculty

by

Suresh K. Kannan

In Partial Fulfillment
of the Requirements for the Degree
Doctor of Philosophy

School of Aerospace Engineering
Georgia Institute of Technology
December 2005

ADAPTIVE CONTROL OF SYSTEMS IN CASCADE WITH SATURATION

Approved by:

Professor Eric N. Johnson
Committee Chair
School of Aerospace Engineering
Georgia Institute of Technology

Professor Daniel P. Schrage
School of Aerospace Engineering
Georgia Institute of Technology

Professor Eric Feron
School of Aerospace Engineering
Georgia Institute of Technology

Professor J.V.R. Prasad
School of Aerospace Engineering
Georgia Institute of Technology

Professor George J. Vachtsevanos
School of Electrical Engineering
Georgia Institute of Technology

Date Approved: 22 November 2005

அப்பா, அம்மா

for my father and mother

ACKNOWLEDGEMENTS

My deepest gratitude is to my advisors Dr. Eric N. Johnson and Dr. Daniel P. Schrage for their advice and guidance over the years. Eric Johnson's ability to motivate even far fetched ideas, guide them through research and flight-test research results has enabled this thesis to contain experimental results on a variety of aircraft. His efficient analysis of technical problems and solutions to them will always be a trait I will strive to develop. I will always be indebted to Dr. Schrage for his unfailing support for me since my first days at the institute. I have always been impressed by his character and I hope some of it has rubbed of on me during my years here. His advice and support for the UAV lab since its inception has allowed me to be involved in projects such as DARPA's Software Enabled Control, which has supported me during my graduate studies. I would like to thank Dr. Calise who in many ways has influenced this work and me through his professional advice. I have spent many hours in long discussions with Dr. Prasad and I am thankful to him for increasing my understanding of helicopter dynamics. I am indebted to Dr. Wassim M. Haddad for his excellent notes on linear and nonlinear systems. I owe much of my understanding to his books on the subject. I am grateful to Dr. Yedidia Neumeier for his support during my initial days at the department, his advice has been pivotal. I thank Dr. Naira Hovakimyan for our many discussions in the lab and elucidating many of the finer aspects of our adaptive control work. I would also like to thank Dr. Amy Pritchett for her support and timely "are-you-done-yet" to get me out of procrastination. I have enjoyed working with Dr. Vachtsevanos and value his view points on control strategies. It was a pleasure to have Dr. Eric Feron on my committee. His comments were most useful and his work on aggressive maneuvering has

been a source of inspiration for some of this work.

I am grateful to Brian Mendel and Dr. James L. Paunicka of the Boeing Phantom Works, Bill Koenig of the Air Force Research Labs and Dr. John Bay of DARPA for their support of this work. I thank Dr. Scott Clements, Dr. Graham Drozeski, Dr. Sam Sander, Cameroon Craddock, Phillip Jones and Bhaskar Saha, from ECE for collaborations on the SEC program. I thank former and current students and researchers in the group, with whom I have had numerous engaging discussions academic and otherwise, including, Drs. Mike McFarland, Rolf T. Rysdyk, Seungjae ("Franz") Lee, Manu Sharma, Flavio Nardi, Tomohisa Hayakawa, Nakwan Kim, Joe Horn, Hong Xin, Ilkay Yavrucuk, and Hungu Lee. It has also been a pleasure to work with Yoko Watanabe, Jin Cheol-Ha, Claus Christmann, Mike Curry, Jim Neidhoefer, Mike Turbe, Seung-Min Oh, Shannon Twigg, Sumit Mishra, Alison Proctor, Hesham El-Shirbiny, Aaron Kahn, and Joerg Dietrich. I would like to thank Henrik Christopherson and Wayne Pickell for their excellent work on the RMax helicopter. Their work has enabled graduate students to flight-test research on a reliable platform that is always ready to fly. Of course, I must thank Jeong Hur, the person responsible for my permanent digression into unmanned systems. His enticement of a famished graduate student with a slice of pizza for the aerial robotics competition on a cold winter day in 1996 has turned into an adventure which will continue for a lifetime. I would like to thank Dr. Eric Corban for his support of the UAV lab and our many discussions during flight tests of the R-50 helicopters. I am grateful to Dr. Jeff Jagoda for his timely answers to my questions and of course Loretta Carroll and Vivian Robinson for all their help.

I am grateful to my current contemporaries, Drs. Bong-Jun Yang, John Shin, Constantine Volyanskyy, Venky Madyshta, Ali Kutay and the soon to be "Drs.", Manuj Dhingra, Nimrod Rooz, Allen Wu, Jonathan Muse, Adrian Koller, Suraj Unnikrishnan and Ram Sattigeri. We have been comrades-in-arms for years and make

the atmosphere at the lab, light. A special thanks to Matthew Johnson, who has been my room and lab mate during my time here. I have always resorted to him first, on many things. I also thank him for proof-reading my thesis. Matt has been a constant source of support at the lab and at home with my family. Our discussions on world politics and his unique perspective on world events has left me enlightened and educated on many fronts. I would like to thank my comrade, the "Rmax", with whom I have spent many wonderful evenings, New Years, Diwali and Christmas. Time passes quickly in her company.

My wife Suzanne, has stood by me through many tribulations and triumphs. She has opened my eyes to some of the finer aspects of life. She has been subjected to my rantings on technical problems, finally ending with "there you go, I think you've fixed it now". Her constant love and support has allowed me to complete this work. She makes everything worth-wile. My sister Aarthi, has been with my parents while I have been away on this journey. Although geographically separated, she has been the link to my parents, when phone calls did not suffice. My thanks to Das Anna for his unwavering support. Of course my thanks to Andre for his support and to Mama for her prayers to the almighty. My mother and father, whose many, many, sacrifices during their life have allowed me to reach this point. Their unconditional love and support holds me in awe. From the day I was born, they have instilled in me qualities that define me. Their firm belief in me to shape my destiny and theirs, I will always treasure. Every success and achievement is theirs. Truly... I stand on the shoulders of giants. Amma, Appa, Nanri.

TABLE OF CONTENTS

LIST OF FIGURES

LIST OF SYMBOLS AND ABBREVIATIONS

$\oplus$	quaternion addition
A, B	error dynamics system matrices
$\hat{A}_1, \hat{A}_2, \hat{B}$	estimate of vehicle dynamics as a linear system
a, a	acceleration, activation potential
$a(\cdot), \hat{a}(\cdot)$	translational dynamics and its estimate
b_v, b_w	neural network (NN) biases
$\mathcal{C}$	null controllable domain
$C(l, m)$	function used to generate coordinate transformation T_{yx}
$\bar{C}_m^l$	binomial coefficient
$\mathcal{D}$	domain
E_r	PCH appears through E_r in the command tracking error dynamics
e_r, e	command tracking error, reference model tracking error respectively
$F_k^m(A)$	function to produce products of combinations of the elements of A
$f(\cdot), \hat{f}(\cdot)$	system dynamics and its estimate
$g(\cdot), \hat{g}(\cdot)$	actuator dynamics and its estimate
K, R	inner loop, outer loop gain matrices
L	transformation matrix, Lyapunov function
M_i	multipliers to incorporate non-unity saturation functions
n_1, n_2, n_3	number of NN inputs, hidden neurons, outputs
P, Q	positive definite Lyapunov equation matrices for tracking error dynamics
p	position, roll rate
q	attitude quaternion, pitch rate
r	filtered tracking error, yaw rate
$sgn(\cdot)$	function that returns the sign of its argument
T_{yx}	coordinate transformation matrix

V, W, Z	NN input, output, both weights
v_{lim}	limit on velocity in translational dynamics reference model
v	velocity
x	state vector
$x_{in}, \bar{x}$	NN input
$\breve{x}^{(i)}$	elements of the full state vector x that are not elements of the virtual control vector $x_{des}^{(i)}$
$\breve{x}^{(i)}\|x_{des}^{(i)}$	the full state vector x partitioned into states treated as virtual controls and elements that are not virtual controls
z_j	input to j^{th} hidden neuron
α	angular acceleration
$\alpha(\cdot), \hat{\alpha}(\cdot)$	attitude dynamics and its estimate
$\Delta(\cdot)$	error the NN can approximate
$\bar{\Delta}(\cdot)$	total function approximation error
$\delta, \hat{\delta}$	actuator deflections and its estimate
$\epsilon_g(\cdot), \bar{\epsilon}_g$	error NN cannot approximate and its bound
$\epsilon, \epsilon_\alpha, \epsilon_a$	NN approximation errors
ζ	error dynamics damping
η	vector of errors $e_r, e, \tilde{W}, \tilde{V}$
θ_v, θ_w	NN input-layer, output-layer thresholds
$\theta(s)$	approximate pitch dynamics transfer function
κ	e-modification gain
$\lambda_{min}(\cdot)$	minimum eigenvalue
$\lambda_{max}(\cdot)$	maximum eigenvalue
ν	total pseudo control
ν_{ad}	adaptive signal
ν_r	robustifying term

σ	sigmoidal activation function, saturation function
Ω	level of sets of Lyapunov functions
ω	angular velocity, error dynamics bandwidth
ω_{lim}	limit on angular velocity in attitude dynamics reference model

Subscripts

ad	adaptive
c	commanded
$coll, ped$	collective, pedal
cr	reference model dynamics
d	derivative
des	desired
f	force
h	hedge
i, o	inner loop, outer loop
lat, lon	lateral, longitudinal
lc	linear compensator
m	moment
p	proportional
r	robustifying term, reference model

Abbreviations

PCH	pseudocontrol hedging
IMU	inertial measurement unit
MIMO	multi-input multi-output
RPM	revolutions per minute

GTMax	refers to the Yamaha R-Max helicopter
GTSpy	refers to the 11-inch ducted fan aircraft
GTEdge	refers to the high thrust-to-weight ratio fixed-wing aircraft

SUMMARY

This thesis extends the use of neural-network-based model reference adaptive control to systems that occur as cascades. In general, these systems are not feedback linearizable. The approach taken is that of approximate feedback linearization of upper subsystems whilst treating the lower-subsystem states as virtual actuators. Similarly, lower-subsystems are also feedback linearized. Typically, approximate inverses are used for linearization purposes. Model error arising from the use of an approximate inverse is minimized using a neural-network as an adaptive element. Incorrect adaptation due to (virtual) actuator saturation and dynamics is avoided using the Pseudocontrol Hedging method. Using linear approximate inverses and linear reference models generally result in large desired pseudocontrol for large external commands. Even if the provided external command is feasible (null-controllable), there is no guarantee that the reference model trajectory is feasible. In order to mitigate this, nonlinear reference models based on nested-saturation methods are used to constrain the evolution of the reference model and thus the plant states. These reference models along with assumptions on the initial errors guarantee that the plant, reference model and neural-network states remain bounded. The method presented in this thesis lends itself to the inner-outer loop control of air vehicles, where the inner-loop controls attitude dynamics and the outer-loop controls the translational dynamics of the vehicle. The outer-loop treats the closed loop attitude dynamics as an actuator. Adaptation to uncertainty in the attitude, as well as the translational dynamics, is introduced, thus minimizing the effects of model error in all six degrees of freedom and leading to more accurate position tracking. A pole-placement approach is used to choose compensator gains for the tracking error dynamics. This alleviates

timescale separation requirements, allowing the outer loop bandwidth to be closer to that of the inner loop, thus increasing position tracking performance. A poor model of the attitude dynamics and a basic kinematics model is shown to be sufficient for accurate position tracking. In particular, the inner-outer loop method was used to control an unmanned helicopter and has subsequently been applied to a ducted-fan, a fixed-wing aircraft that transitions in and out of hover, and a full-scale rotorcraft. Experimental flight test results are also provided for a subset of these vehicles.

CHAPTER I

INTRODUCTION

1.1 Nonlinear Adaptive Control

Feedback linearization-based methods have been used extensively in the control of nonlinear systems over the past few decades. Depending on the existence of a global diffeomorphism [23], the nonlinear dynamics may be mapped onto a manifold where the system's dynamics are governed by linear equations. Differential geometry-based methods [1] have played an important role in the development of nonlinear control methods. Recent extensions include robust stabilization, nonlinear damping and others that have been developed to deal with situations where an exact diffeomorphism is not available. Parametric uncertainty in the model has been dealt with using both robust and adaptive methods. We focus on model reference direct adaptive control where the system is assumed to be feedback linearizable, and we use a single hidden layer artificial neural network to cancel model error arising from the approximate linearization [34, 9]. A single hidden layer network is nonlinearly parameterized and has the advantage of being able to approximate arbitrary unstructured parametric uncertainty to arbitrary accuracy [17]. In contrast, linearly parameterized networks require appropriate basis functions that must be correctly chosen to effectively approximate the uncertainty. Adaptive control with a single hidden layer adaptive element has been successfully used on a number of aircraft [8, 9, 29, 32].

1.2 Saturation

All systems in practice encounter saturation of plant inputs, normally in the form of magnitude saturation of actuators. The approximate model used for dynamic inversion, however, cannot contain such nonlinearities, in order to guarantee the existence of the inverse. This form of the inverse, used to approximately feedback linearize the dynamics can result in large control usage for large errors and disturbances. At high bandwidth [19] the actuators may also consistently encounter rate saturation.

With nonlinear systems, there is always a question of controllability [20, 66], especially for systems with bounded actuation. For linear systems, the Kalman controllability condition may be used to decide on the controllability of a system[13, 14]. There is no generalization of the Kalman controllability condition available for nonlinear systems. A similar concept is that of null-controllability which asks: for a system of the form $\dot{x} = f(x, u)$ and given an initial condition $x(0)$, is it possible to drive the system to the origin? In [64, 65] it is shown that deciding on the controllability for even bi-linear systems is at least NP-hard. This leads to the problem of not being able to characterize a null controllable region $\mathcal{C}_x$ (See Definitions 1 (page 34), 2 (page 35)), where there always exists a control that can drive the system to the origin. Normally, in control design for nonlinear systems, an assumption of controllability is made on the domain of interest $\mathcal{D}_x$ and the control design is such that it guarantees a domain of attraction $\Omega_x \subset \mathcal{D}_x$ which keeps all trajectories in $\mathcal{D}_x$. The assumption of controllability may however not be valid in general, especially in systems with bounded control, i.e., there is no guarantee that $\mathcal{D}_x \subset \mathcal{C}_x$. This assumption of controllability cannot be checked easily, even for systems of the form

$$\dot{x} = Ax + B\sigma(u). \tag{1}$$

Here, σ represents a vector valued magnitude saturation function (see Definition 5 on page 103). One method of guaranteeing a domain of attraction is to make sure

the control design is such that the nonlinearity $\sigma(u)$ is never active. This forms an important class of control design methods for systems with bounded actuation and include Sontag's universal formula approach using control Lyapunov functions[44] and others[4, 52]. Avoiding saturation, however, usually results in either conservative or highly complex control laws leading to possibly very conservative domains of attraction and slow convergence. See [5] and the references therein for a survey of early work on constrained control.

Another approach is to allow saturation to occur. The largest body of work with regard to bounded control has been for constrained linear systems of the form (1). It has been shown that global asymptotic stabilization for systems whose null controllable region is $\mathcal{R}^n$ (A is semi-stable) is not possible for constrained systems [71] using bounded linear feedback. It is however possible using nonlinear feedback laws (nested saturations) [73] and was fully generalized in [70, 74]. This however does not preclude semi-global stabilization using saturated linear control laws [75] for semi-stable systems including systems with rate saturation [59]. In all cases mentioned so far, static control designs are used. A whole other class of problems occurs when dynamic compensators are designed, ignoring the saturation nonlinearity. When saturation is encountered, any dynamic element is prone to windup. This same argument applies to adaptive designs (direct and indirect) which are prone to incorrect adaptation. Some of the earliest work in this direction include the "conditioning technique" [53, 15] where the mismatch between desired control and actual control is used for anti-windup. Various newer techniques to prevent incorrect adaptation have been explored including recent techniques [76, 36] and reference therein, on Anti-Windup-Bumpless-Transfer (AWBT) which involves using a dynamic anti-windup compensator to modify the feedback signal to the compensator. An important class of problems is adaptation in the presence of input constraints. In [33], an uncertain linear time-invariant plant is locally stabilized with adaptation by using a filter

driven by the mismatch in control. Related work [41] where a scaling factor called a μ-modification instead of a filter is used to ensure adaptation in the presence of input constraints, by avoiding these constraints.

Other work that deals with constrained control is that of Model Predictive Control, where optimal control inputs are calculated over a finite horizon at each sampling time by solving a trajectory optimization problem usually (usually linear or quadratic), using a plant model to predict plant outputs. MPC is able to handle input and output nonlinearities explicitly. Since this is an optimization-based approach, this process can be slow. Stability of MPC-based systems have been studied [25, 26, 56], however, results in the presence of uncertainty are lacking.

1.3 PCH

In context of the model reference adaptive control architecture presented in this thesis the Pseudocontrol Hedging [27](PCH) is used to protect any dynamic elements in the controller including an adaptive neural network. The PCH method entails removing selected input characteristics from the error dynamics by modifying the reference model, hence protecting the adaptive element from adapting incorrectly to selected input nonlinearities. In contrast to [41] or other methods that avoid saturation, the PCH method does not prevent saturation. If a desired pseudocontrol is not achieved due to actuator nonlinearity, the deficit in the pseudocontrol is used to modify the reference model dynamics by that amount. When using a linear reference model, any large commands result in saturation and large PCH signals until the reference model states are close to the plant. Although this removes the problem of incorrect adaptation from the reference model tracking error dynamics and protects the adaptive element, the reference model dynamics are now modified by a signal whose magnitude now depends on the state of the reference model and eventually depends on the external command. Closed loop stability of the plant, reference model and adaptive

element was studied by first showing ultimate boundedness of the reference model tracking error dynamics and neural network weights, then, assuming adaptation was complete, stability of the isolated non-adaptive subsystem was studied. In [27], it is shown that with a linear reference model, as long as the external command and the reference model states are close, the Lyapunov function could be shown to be negative semi-definite for certain amounts of saturation. Here there is an assumption that the plant states remain in the plant's null controllable region.

1.4 Nonlinear Reference Models

In an effort to improve upon this result, the use of a nonlinear reference model can be shown to result in better boundedness results. The reference model in model reference adaptive control is used to provide a smooth command that the tracking controller can follow. It has already been shown that the tracking error (difference between reference model and plant states) is bounded in the presence of saturation when PCH is used. One of the primary problems is dealing with large external commands, which will attempt to produce a linear response in the plant when a linear reference model is used. Since the tracking error is bounded the plant states could leave the null controllable region quickly, depending on the trajectory of the reference model. It is known that linear systems with bounded control may be stabilized on their null-controllable region using a nonlinear nested saturation-based control law [73, 74]. In much of the work on constrained control positive invariant sets have been used to place bounds on the state at any given time. Using this as a motivation, and assuming that the external command is null-controllable, boundedness of the plant states may be argued if it is assumed that there exists a region around the external command which the reference model states + tracking error are guaranteed to remain within. In this respect, artificial saturation functions are introduced in the reference model that constrain its evolution and thus the evolution of the plant states.

1.5 Systems in Cascade

Many real systems in practice appear as feedforward systems. An example is the position control of a helicopter which is an underactuated system with 6 degrees of freedom and 4 controls. Although independent controls are available for control of rotational dynamics (lateral cyclic, longitudinal cyclic, pedal), only one independent control is available for the translational dynamics (collective). Accelerations in the body x and y directions can only be generated by tilting the aircraft's thrust vector. This is an example of the feedforward nature of helicopter dynamics. In real systems, this strict feedforward structure is only approximately true. Most actuators also have secondary effects (control coupling), for example, the tail rotor thrust on a helicopter also produces translational accelerations in the body y-axis. Control of systems such as the helicopter have normally involved splitting the control task into an inner-loop that controls the attitude and an outer-loop that controls the translational dynamics along with assumptions of time scale separation between the two loops [57, 46]. Introducing adaptation in the control of the translational dynamics has advantages wherein a very simple kinematic model of the aircraft may be used for inversion purposes, leaving the adaptive element to cancel out modeling errors which include the secondary coupling effects of actuators. Although this problem could be formulated as a multi-input-multi-output adaptive control problem [18], the control allocation when designing inverse transformations for underactuated systems is not trivial. More importantly, treating it as a generic MIMO problem will result in linearizing transformations involving the independent controls only. It is not possible to incorporate information regarding the feedforward structure of the plant dynamics in the general pure MIMO setting. For example, in order to perform a coordinated turn, the bank angle required to perform the turn may be generated using a dynamic inverse of the aircraft dynamics. In a pure MIMO setting, dynamic inversion would

only allow the desired actuator deflections to be generated. Additionally, it is sometimes desirable to impose artificial limits on some of the commanded states of the system, such as the maximum attitude or velocity the aircraft may take in a given axis.

The approach of stabilizing systems in cascade adaptively and the use of PCH to protect adaptation for the upper subsystems from the nonlinearities and dynamics of the lower subsystems is unique; enabling adaption for all subsystems. Unlike other methods [45, 24] which require the plant dynamics in a feedforward form, in order to recursively stabilize plant dynamics with bounded control, we use dynamic inversion and adaptation to feedback linearize the plant into a chain of integrators and use PCH to protect the adaptive element.

1.6 Control of an Autonomous Helicopter

Unmanned helicopters are versatile machines that can perform aggressive maneuvers. This is evident from the wide range of acrobatic maneuvers executed by expert radio-control pilots. Helicopters have a distinct advantage over fixed-wing aircraft especially in an urban environment, where hover capability is helpful. There is increased interest in the deployment of autonomous helicopters for military applications, especially in urban environments[51]. These applications include reconnaissance, tracking of individuals or other objects of interest in a city, and search and rescue missions in urban areas. Autonomous helicopters must have the capability of planning routes and executing them. To be truly useful, these routes would include high-speed dashes, tight turns around buildings, avoiding dynamic obstacles and other required aggressive maneuvers. In planning [10] these routes, however, the tracking capability of the flight control system is a limiting factor because most current control systems still do not leverage the full flight envelope of small helicopters, at least, unless significant system identification and validation has been conducted.

Although stabilization and autonomous flight [60] has been achieved, the performance has generally been modest when compared to a human pilot. This may be attributed to many factors, such as parametric uncertainty (changing mass, and aerodynamic characteristics), unmodeled dynamics, actuator magnitude and rate saturation and assumptions made during control design itself. Parametric uncertainty limits the operational envelope of the vehicle to flight regimes where control designs are valid, and unmodeled dynamics and saturation can severely limit the achievable bandwidth of the system. The effects of uncertainty and unmodeled dynamics have been successfully handled using a combination of system identification [11, 37, 47] and robust control techniques [39]. Excellent flight and simulation results have been reported including acrobatic maneuvers [12] and precision maneuvers [39, 38].

A key aspect in the effective use of unmanned aerial vehicles(UAVs) for military and civil applications is their ability to accommodate changing dynamics and payload configurations automatically without having to rely on substantial system identification efforts. Variants of the Neural-Network (NN) based direct adaptive control methods have been used as enabling technologies for practical flight control systems that allow online adaptation to uncertainty. This technology has been successfully applied to the recent U.S. Air Force Reconfigurable Control for Tailless Fighter Aircraft (RESTORE) culminating in a successful flight demonstration [8, 6] of the adaptive controller on the X-36. A combined inner-outer loop architecture was also applied for guidance and control of the X-33 [28] and evaluated successfully in simulation for various failure cases.

For autonomous helicopters, a primary objective is the accurate tracking of position commands. Much adaptive control work on helicopters has concentrated on improving the tracking performance of attitude commands [35, 42, 58]. Usually a simple outer loop employing basic relationships between attitude and linear acceleration is used to control the translational dynamics. For many applications, this may

be sufficient. However, when operating in an urban environment or flying in formation with other UAVs, the high-precision position tracking ability of the controller dictates the minimum proximity between the UAV and objects in its environment. In contrast to previous attitude control-only work [19], a coupled inner-outer loop adaptive design is introduced that can handle uncertainty in all six degrees of freedom. In synthesizing a controller (Fig. 7), the conventional conceptual separation between the inner loop and outer loop is made. The inner loop controls the moments acting on the aircraft by changing the lateral stick, δ_{lat}, longitudinal stick, δ_{lon} and pedal, δ_{ped}, inputs. The outer loop controls the forces acting on the aircraft by varying the magnitude of the rotor thrust using the collective δ_{coll} input. The thrust vector is effectively oriented in the desired direction by commanding changes to the attitude of the helicopter using the inner loop. The idea of adaptation for systems in cascade is used to cancel model errors in all six degrees of freedom. Unwanted adaptation to plant input characteristics such as actuator saturation and dynamics are tackled using PCH. For example, the inner-loop attitude control sees actuator limits, rate saturation and associated dynamics. PCH [28, 27], is used to modify the inner-loop reference model dynamics in a way that allows continued adaptation in the presence of these system characteristics. This same technique, is used to prevent adaptation to inner-loop dynamics and interaction between the inner and outer loops. Without hedging of the outer loop, adaptation to uncertainty in the translational dynamics would not be possible. Additionally, nonlinear reference models are used to prescribe the aggressiveness with which external commands are achieved.

This control design was first applied to the Yamaha RMAX (GTMax) helicopter (Fig. 1) and subsequently to a 11-inch ducted fan, the GTSpy (Fig. 2), the Boeing R-22 unmanned helicopter (Fig. 3), and to a high thrust-to-weight ratio aircraft, the GTEdge (Fig. 4). The GTMax has been used to perform a mid-air launch of the GTSpy, which is perhaps the first known launch of an autonomous rotorcraft from

Figure 1: The GTMax Helicopter

Figure 2: The GTSpy Ducted Fan

Figure 3: The Boeing Unmanned Robinson-22 Helicopter

Figure 4: The GTEdge Aircraft with a high (greater than 1) thrust-to-weight ratio

another autonomous rotorcraft. Additionally, the GTEdge is capable of hovering vertically and transitioning to full aircraft mode forward flight and back to hover, all using the same adaptive control system presented in this thesis. The hover⇒forward-flight⇒hover maneuver is to the author's knowledge the first time such a maneuver has been performed by an unmanned aircraft. The only differences in control design between the various vehicles are the inverse models reflecting vehicle dynamics.

1.7 Outline of Thesis

Chapter 2 presents previous work on model reference adaptive control with input saturation and the PCH method.

Chapter 3 presents the development of the control structure for two subsystems and the more general k-subsystems in cascade with adaptation. It is also shown that the tracking error dynamics reduce to that of pre-existing work.

Chapter 4 presents the use of nonlinear reference models and boundedness theorems prescribing conditions for the boundedness of reference model, plant and neural network errors for linear and nested saturation-based reference models for k-subsystems in cascade.

In Chapter 5 an inner-outer-loop adaptive architecture is developed for trajectory control of an unmanned helicopter. Additionally, an analysis of the choice of gains that alleviates timescale separation requirements between the inner-loop and outer-loop is presented.

Chapter 6 summarizes flight test results using this control method implemented on the Yamaha Rmax helicopter and other aircraft.

Appendix A contains proofs of theorems presented in this thesis and Appendix B is a stand-alone chapter that develops results for guaranteeing real poles for the nested saturation control law.

CHAPTER II

BACKGROUND

Consider the following nonlinear system in first order form

$$\begin{aligned} \dot{x}_i &= x_{i+1} \qquad i = 1, 2, \cdots, n-1 \\ \dot{x}_n &= f(x, \delta) \\ \delta &= g(x, \delta_{des}), \end{aligned} \tag{2}$$

where $x \in \mathcal{D}_x \subset \mathcal{R}^n$, is the state of the system, $\delta \in \mathcal{R}$ is the control. The function f represents the plant dynamics and g represents a state-dependent actuation nonlinearity. Here, $\delta_{des} \in \mathcal{R}$ is the desired actuator (control) deflection while δ is the actual deflection. Typically, g represents actuator magnitude saturation.

The control objective is to synthesize a control law to track a bounded external command $x_c \in \mathcal{R}^n$ when f, g are only approximately known. It is assumed that the full state vector x is available for feedback. First, the conventional model reference adaptive control framework is presented for a single input nonlinear system. The pseudocontrol hedging method is described and used to protect the adaptive element from incorrect adaptation to input nonlinearities.

2.1 Model Reference Adaptive Control

Taking the approach of model reference adaptive control [34, 9], an approximate model for the plant dynamics $f(x, \delta)$ may be introduced as

$$\nu = \hat{f}(x, \delta_{des}), \tag{3}$$

where ν is the desired pseudocontrol. For example, in the case of second order position control of mechanical systems, ν represents desired acceleration. The function

$\hat{f}(x, \delta_{des})$ can be any available approximation of $f(x, \delta)$ with the restriction that it should invertible with respect to δ_{des}, allowing one to formulate the dynamic inverse as

$$\delta_{des} = \hat{f}^{-1}(x, \nu). \tag{4}$$

The actuator deflection δ_{des} is what is expected will achieve the desired pseudocontrol ν. In introducing these approximate models and formulation of the controller, it is assumed that the full state, x, is available for feedback. Output feedback formulations of this architecture are also available [7]. A sufficient condition for Eqn (3) to be invertible is that $\partial \hat{f}(x, \delta)/\partial \delta$ is continuous and non-zero for $(x, \delta) \in \mathcal{D}_x \times \mathcal{R}$. It is this requirement that precludes including input saturation nonlinearities as a part of the inverse.

Substituting the inverse dynamics Eqn (4) into Eqn (2) results in the following approximately linearized n-integrator system

$$\begin{aligned} \dot{x}_i &= x_{i+1} \qquad i = 1, 2, \cdots, n-1 \\ \dot{x}_n &= \nu + \bar{\Delta}(x, \delta, \hat{\delta}) - \nu_h, \end{aligned} \tag{5}$$

where $\hat{\delta}$ is the an estimate of the actuator position. An estimate needs to be used when actuator position is not readily available. If actuator position is measurable then $\hat{\delta} = \delta$. The model error is a static nonlinear function and is given by

$$\bar{\Delta}(x, \delta, \hat{\delta}) = f(x, \delta) - \hat{f}(x, \hat{\delta}).$$

The signal ν_h represents the pseudocontrol that cannot be achieved due to actuator input characteristics such as saturation and is given by

$$\begin{aligned} \nu_h &= \hat{f}(x, \delta_{des}) - \hat{f}(x, \hat{\delta}) \\ &= \nu - \hat{f}(x, \hat{\delta}). \end{aligned}$$

ν_h is also called the pseudocontrol-hedging signal or PCH signal. This leaves ν, the desired pseudocontrol that may now be designed to stabilize the linearized system

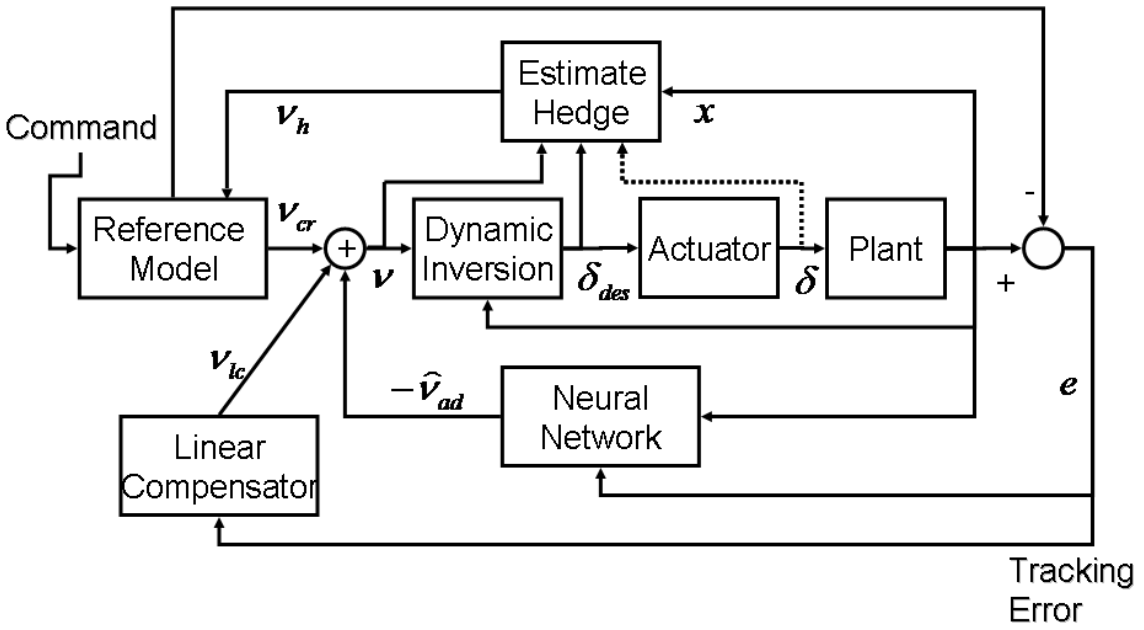

Figure 5: Model Reference Adaptive Control Architecture with PCH

and deal with canceling the model error $\bar{\Delta}$. The PCH signal, ν_h, is a disturbance and will be dealt with subsequently. Design, ν to be of the form

$$\nu = \nu_{cr} + \nu_{lc} - \bar{\nu}_{ad}, \tag{6}$$

where ν_{cr} is the output of a reference model, ν_{lc} is the output of a compensator that stabilizes the linearized dynamics and $\bar{\nu}_{ad}$, the output of an adaptive element such as a neural network that is designed to cancel the effects of model error $\bar{\Delta}$. This architecture is illustrated in Fig. 5.

2.2 Reference Model and Tracking Error

For a system in first order form, the reference model dynamics may be designed as

$$\begin{aligned} \dot{x}_{r_i} &= x_{r_{i+1}} \qquad i = 1, 2, \cdots, n-1 \\ \dot{x}_{r_n} &= \nu_{cr}(x_r, x_c), \end{aligned} \tag{7}$$

where $x_r \in \mathcal{R}^n$ are the states of the reference model and $x_c \in \mathcal{R}^n$ is a bounded external command signal. The reference model tracking error may be defined as

$$e \triangleq x_r - x. \tag{8}$$

When the tracking error dynamics are developed, the form of Eqn (7) will result in the ν_h signal appearing as a part of the error dynamics. Various methods such as anti-windup synthesis [76] and robustifying terms [16] may be used to deal with the potentially unbounded disturbance signal ν_h. However, a more critical problem is that any adaptive element (including a simple integrator) introduced to cancel the uncertainty $\Delta(\cdot)$ will be trained using the tracking error signal e, and will attempt to adapt to actuator nonlinearities due to the presence of ν_h in the tracking error dynamics. Methods such as anti-windup synthesis and robustifying terms will leave some element of the input nonlinearity in the dynamics, thus leading to some amount of incorrect adaptation.

Ultimately, the tracking error dynamics should contain no element of the saturation nonlinearity, i.e., the signal ν_h must be completely removed from $\dot{e}$. The PCH method [27] is used to protect the adaptive element from such input characteristics. This may be achieved by augmenting Eqn (7) with the hedging signal resulting in the removal of the actuator characteristic from the tracking error dynamics. The reference model dynamics are now given by

$$\begin{aligned} \dot{x}_{r_i} &= x_{r_{i+1}} \qquad i = 1, 2, \cdots, n-1 \\ \dot{x}_{r_n} &= \nu_{cr}(x_r, x_c) - \nu_h. \end{aligned} \tag{9}$$

If the actuators are saturated then the reference model will continue to demand tracking as though full authority were still available resulting in incorrect adaptation. However, the reference reference model is now "moved" in the opposite direction (hedge) by an estimate of the amount the plant did not move due to system characteristics the control designer does not want the adaptive element to see [27].

Note that the PCH signal affects the reference model output, ν_{cr}, only through changes in reference model dynamics and that the instantaneous pseudocontrol output of the reference model in not changed. The tracking error dynamics may be found by

directly differentiating Eqn (8)

$$\dot{e} = \begin{bmatrix} x_{r_2} - x_2 \\ \vdots \\ \dot{x}_{r_n} - \dot{x}_n \end{bmatrix}.$$

Considering $\dot{e}_n$,

$$\begin{aligned} \dot{e}_n &= \dot{x}_{r_n} - \dot{x}_n \\ &= \nu_{cr} - \nu_h - f(x, \delta) \\ &= \nu_{cr} - \nu + \hat{f}(x, \hat{\delta}) - f(x, \delta) \\ &= -\nu_{lc} + \bar{\nu}_{ad} + \hat{f}(x, \hat{\delta}) - f(x, \delta) \\ &= -\nu_{lc} - (\bar{\Delta}(x, \delta, \hat{\delta}) - \bar{\nu}_{ad}). \end{aligned}$$

Note that the PCH term, ν_h, in Eqn (9) cancels the PCH term in Eqn (5) thus removing it from the tracking error dynamics. If ν_{lc} is chosen to be a linear compensator of the form

$$\nu_{lc} = \begin{bmatrix} K_1 & K_2 & \cdots & K_n \end{bmatrix} e,$$

the overall tracking error dynamics may now be expressed as

$$\dot{e} = Ae + B\left[\bar{\nu}_{ad} - \bar{\Delta}(x, \delta, \hat{\delta})\right], \tag{10}$$

where,

$$A = \begin{bmatrix} 0 & 1 & 0 & \cdots & 0 \\ 0 & 0 & 1 & & 0 \\ \vdots & \vdots & & \ddots & \\ 0 & 0 & & & 1 \\ -K_1 & -K_2 & -K_3 & \cdots & -K_n \end{bmatrix}, B = \begin{bmatrix} 0 \\ 0 \\ \vdots \\ 0 \\ 1 \end{bmatrix},$$

where the compensator gains K_i, $i = 1, \cdots, n$ are chosen such that A is Hurwitz. It now remains for $\bar{\nu}_{ad}$ to be designed to cancel the model error $\bar{\Delta}(x, \delta, \hat{\delta})$ and minimize the forcing term in Eqn (10). Hence the functional form $\bar{\nu}_{ad} = \bar{\nu}_{ad}(x, \delta, \hat{\delta})$ is necessary

to effectively cancel $\bar{\Delta}$. However δ, the actuator position may not be measurable leading to the following assumption

Assumption 1. *The actual actuator position can be expressed as*

$$\delta = \delta(x, \hat{\delta}).$$

For weaker assumptions with regard to the form of the actuator dynamics see Section 3.3.

The tracking error dynamics may be represented as

$$\dot{e} = Ae + B\left[\bar{\nu}_{ad}(x, \hat{\delta}) - \bar{\Delta}(x, \hat{\delta})\right], \tag{11}$$

where $\bar{\nu}_{ad}$ is now only required to be dependent on available information.

2.3 Adaptive Element

Single hidden layer (SHL) perceptron NNs are universal approximators[17, 67, 43]. Hence, given a sufficient number of hidden layer neurons and appropriate inputs, it is possible to train the network online to cancel model error. Fig. 6 shows the structure of a generic single hidden layer network whose input-output map may be expressed as

$$\nu_{ad_k} = b_w\theta_{w_k} + \sum_{j=1}^{n_2} w_{jk}\sigma_j(z_j), \tag{12}$$

where, $k = 1, ..., n_3$, b_w is the outer layer bias, θ_{w_k} is the k^{th} threshold. w_{jk} represents the outer layer weights and the scalar σ_j is a sigmoidal activation function

$$\sigma_j(z_j) = \frac{1}{1 + e^{-az_j}}, \tag{13}$$

where, a is the so called *activation potential* and may have a distinct value for each neuron. z_j is the input to the j^{th} hidden layer neuron, and is given by

$$z_j = b_v\theta_{v_j} + \sum_{i=1}^{n_1} v_{ij}x_{in_i}, \tag{14}$$

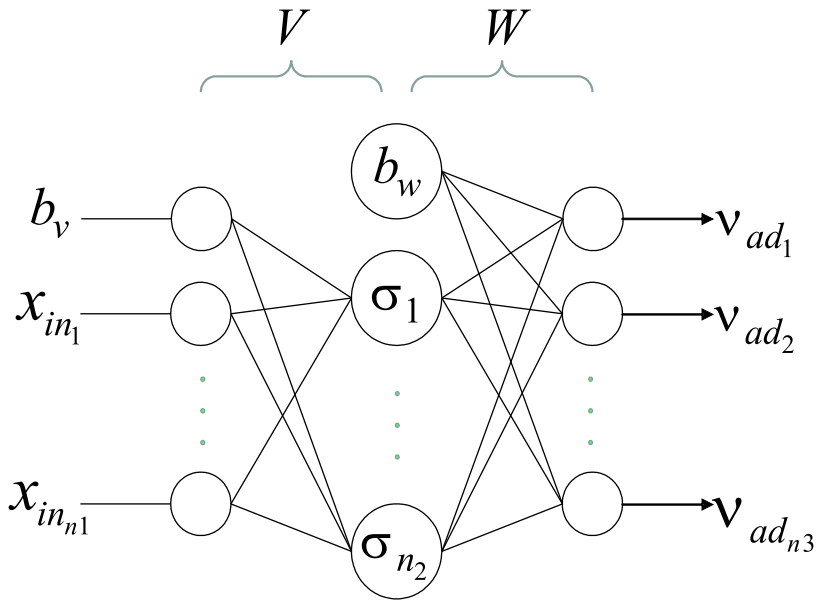

Figure 6: Neural Network with one hidden layer.

where, b_v is the inner layer bias and θ_{v_j} is the j^{th} threshold. Here, n_1, n_2 and n_3 are the number of inputs, hidden layer neurons and outputs respectively. $x_{in_i}, i = 1, ..., n_1$, denotes the inputs to the NN. For convenience, define the following weight matrices:

$$V \triangleq \begin{bmatrix} \theta_{v,1} & \cdots & \theta_{v,n_2} \\ v_{1,1} & \cdots & v_{1,n_2} \\ \vdots & \ddots & \vdots \\ v_{n_1,1} & \cdots & v_{n_1,n_2} \end{bmatrix}, \tag{15}$$

$$W \triangleq \begin{bmatrix} \theta_{w,1} & \cdots & \theta_{w,n_3} \\ w_{1,1} & \cdots & w_{1,n_3} \\ \vdots & \ddots & \vdots \\ w_{n_2,1} & \cdots & w_{n_2,n_3} \end{bmatrix}, \tag{16}$$

$$Z \triangleq \begin{bmatrix} V & 0 \\ 0 & W \end{bmatrix}. \tag{17}$$

Additionally, define the $\sigma(z)$ vector as

$$\sigma^T(z) \triangleq \begin{bmatrix} b_w & \sigma(z_1) & \cdots & \sigma(z_{n_2}), \end{bmatrix} \tag{18}$$

where $b_w > 0$ allows for the thresholds, θ_w, to be included in the weight matrix W. Also, $z = V^T \bar{x}$, where,

$$\bar{x}^T = \begin{bmatrix} b_v & x_{in}^T \end{bmatrix}, \tag{19}$$

where, $b_v > 0$, is an input bias that allows for thresholds θ_v to be included in the weight matrix V. The input-output map of the SHL network may now be written in concise form as

$$\nu_{ad} = W^T \sigma(V^T \bar{x}). \tag{20}$$

The NN may be used to approximate a nonlinear function, such as $\Delta(.)$. The universal approximation property[17] of NN's ensures that given an $\bar{\epsilon} > 0$, then $\forall\ \bar{x} \in \mathcal{D}$, where $\mathcal{D}$ is a compact set, $\exists$ an $\bar{n}_2$ and an ideal set of weights (V^*, W^*), that brings the output of the NN to within an ϵ-neighborhood of the function approximation error. This ϵ is bounded by $\bar{\epsilon}$ which is defined by

$$\bar{\epsilon} = \sup_{\bar{x} \in \mathcal{D}} \left\| W^T \sigma(V^T \bar{x}) - \Delta(\bar{x}) \right\|. \tag{21}$$

The weights, (V^*, W^*) may be viewed as optimal values of (V, W) in the sense that they minimize $\bar{\epsilon}$ on $\mathcal{D}$. These values are not necessarily unique. The universal approximation property thus implies that if the NN inputs x_{in} are chosen to reflect the functional dependency of $\Delta(\cdot)$, then $\bar{\epsilon}$ may be made arbitrarily small given a sufficient number of hidden layer neurons, n_2. The adaptive signal $\bar{\nu}_{ad}$ actually contains two terms

$$\bar{\nu}_{ad} = \nu_{ad} + \nu_r$$

where ν_{ad} is the output of the SHL NN and ν_r is a robustifying signal that arises in the proof of boundedness. The NN weight matrices may be grouped as

$$Z \triangleq \begin{bmatrix} V & 0 \\ 0 & W \end{bmatrix},$$

and the weight error is defined as

$$\tilde{W} \triangleq W^* - W, \qquad \tilde{V} \triangleq V^* - V,$$

and correspondingly

$$\tilde{Z} \triangleq Z^* - Z.$$

Theorem 1 ([27]). *Consider the system given by (2) together with the inverse law (4) and assumptions (2, 3, 4, 5, 6), with $r, \bar{\nu}_{ad}, \nu_{ad}, \nu_r$ given by equations 37, 38, 39, 40 respectively. If $K_r > 0 \in \mathcal{R}$ with lower-limit state in the proof, and where the adaptive laws $\dot{W}, \dot{V}$, satisfy 41, 42 with $\Gamma_W, \Gamma_V > 0$ and scalar $\kappa > 0$ with lower-limit state in the proof, then, the reference model tracking error, e, and NN weights $(\tilde{W}, \tilde{V})$ are uniformly ultimately bounded. Further, the plant states, x, are uniformly bounded.*

Proof. This theorem is a special case of Theorem 2 with one subsystem. Hence, the proof given in Section A.1 applies and shows boundedness of $e, \tilde{W}, \tilde{V}$. The external command and command tracking error e_r are bounded by assumption; this implies that all other states are uniformly bounded. Additionally, see [27]. □

CHAPTER III

ADAPTATION FOR SYSTEMS IN CASCADE

3.1 Adaptive Control of Two Systems in Cascade

Consider the following interconnection of two systems,

$$\begin{aligned}\dot{z}_1 &= z_2\\ \dot{z}_2 &= \phi(z,\xi,\delta_z,\delta_\xi)\\ \dot{\xi}_1 &= \dot{\xi}_2\\ \dot{\xi}_2 &= \gamma(z,\xi,\delta_z,\delta_\xi),\end{aligned} \tag{22}$$

where $\delta_z \in \mathcal{R}$ primarily affects the z-subsystem and $\delta_\xi \in \mathcal{R}$ primarily affects the ξ-subsystem. Eqn (22) represents a general interconnection; in formulating the approximate inverses however, any feedforward structure present in the plant dynamics may be leveraged. The system (22) may be approximately feedback linearized by introducing the transformation

$$\begin{bmatrix}\phi_{des}\\ \gamma_{des}\end{bmatrix} = \begin{bmatrix}\hat{\phi}(z,\breve{\xi}|\xi_{des},\delta_{z_{des}},\hat{\delta}_\xi)\\ \hat{\gamma}(z,\xi,\hat{\delta}_z,\delta_{\xi_{des}})\end{bmatrix}. \tag{23}$$

Here, ξ is partitioned into $\breve{\xi}|\xi_{des}$, such that $\xi_{des} \in \mathcal{R}^{\leq 2}$, is a subset of the ξ-subsystem states that are treated as virtual controls for the z-subsystem and $\breve{\xi}$ are the remaining ξ-subsystem states that are not treated as virtual control. The variables, ξ_{des}, $\delta_{z_{des}}$ and $\delta_{\xi_{des}}$ are the controls that are expected to achieve the desired pseudocontrol ϕ_{des} and γ_{des}. Choosing $\hat{\phi}$ and $\hat{\gamma}$ such that they are invertible, the desired control and

virtual control may be written as

$$\begin{bmatrix} \delta_{z_{des}} \\ \xi_{des} \end{bmatrix} = \begin{bmatrix} \hat{\phi}_{\delta_z}^{-1}(z, \breve{\xi}, \phi_{des_{\delta_z}}, \hat{\delta}_\xi) \\ \hat{\phi}_{\xi}^{-1}(z, \breve{\xi}, \phi_{des_{\xi}}, \hat{\delta}_\xi) \end{bmatrix},$$

$$\delta_{\xi_{des}} = \hat{\gamma}^{-1}(z, \xi, \hat{\delta}_z, \gamma_{des}),$$

with $\phi_{des_{\delta_z}} + \phi_{des_\xi} = \phi_{des}$ and $\hat{\phi}_{\delta_z}, \hat{\phi}_\xi$ formulated such that they are consistent with Eqn (23), and their inverses exist. In computing $\delta_{z_{des}}$ and $\delta_{\xi_{des}}$, any dynamics in the actuators are ignored. Additionally, the dynamics of the ξ-subsystem is ignored in computing the virtual control ξ_{des}. Defining the consolidated state vector $x = \begin{bmatrix} z^T & \xi^T \end{bmatrix}^T$ and consolidated control vector $\delta = \begin{bmatrix} \delta_z & \delta_\xi \end{bmatrix}^T$, the model error may be defined as

$$\begin{bmatrix} \bar{\Delta}_z(x, \delta, \hat{\delta}) \\ \bar{\Delta}_\xi(x, \delta, \hat{\delta}) \end{bmatrix} = \begin{bmatrix} \phi(x, \delta) - \hat{\phi}(x, \hat{\delta}) \\ \gamma(x, \delta) - \hat{\gamma}(x, \hat{\delta}) \end{bmatrix},$$

and the system dynamics of Eqn (22) may be written as

$$\begin{aligned} \dot{z}_1 &= z_2 \\ \dot{z}_2 &= \phi_{des} + \bar{\Delta}_z - \phi_h \\ \dot{\xi}_1 &= \dot{\xi}_2 \\ \dot{\xi}_2 &= \gamma_{des} + \bar{\Delta}_\xi - \gamma_h. \end{aligned} \tag{24}$$

The pseudocontrol signals ϕ_{des} and γ_{des} may now be designed to satisfy closed-loop performance and stability characteristics. Choosing,

$$\phi_{des} = \phi_{cr} + \phi_{lc} - \bar{\phi}_{ad}$$

$$\gamma_{des} = \gamma_{cr} + \gamma_{lc} - \bar{\gamma}_{ad},$$

where ϕ_{cr} and γ_{cr} are outputs of reference models for the z and ξ subsystems respectively, ϕ_{lc}, γ_{lc} are outputs of linear compensators, ϕ_h, γ_h are estimates of the deficit in pseudocontrol due to actuator nonlinearities in δ_z and δ_ξ and $\bar{\phi}_{ad}$ and $\bar{\gamma}_{ad}$ are outputs of an adaptive element designed to cancel the effects of model error.

3.1.1 Reference Model and PCH

The reference models may be designed as follows

$$\begin{aligned}
\dot{z}_{r_1} &= z_{r_2} \\
\dot{z}_{r_2} &= \phi_{cr}(z_r, z_c) - \phi_h \\
\dot{\xi}_{r_1} &= \dot{\xi}_{r_2} \\
\dot{\xi}_{r_2} &= \gamma_{cr}(\xi_r, \xi_c \oplus \xi_{des}) - \gamma_h,
\end{aligned}$$

where, $x_r = \begin{bmatrix} z_r^T & \xi_r^T \end{bmatrix}^T \in \mathcal{R}^4$ are the reference model states $x_c = \begin{bmatrix} z_c^T & \xi_c^T \end{bmatrix}^T \in \mathcal{R}^4$ represent the external command. The operator $\oplus$ represents generalized addition that augments the external command with corrections that the z-subsystem needs in order to achieve its desired pseudo-control ϕ_{des}. PCH may be used to protect the adaptation process from actuator nonlinearities in δ_ξ and δ_z. A significant difference from previous work is the inclusion of ξ_{des} in the generation of the PCH signal. Since the ξ-subsystem acts like an actuator for the z-subsystem any mismatch between ξ_{des} and ξ may be hedged out thus insulating the adaptation process from the dynamics of the ξ-subsystem. The PCH signals may now be computed as follows

$$\begin{aligned}
\phi_h &= \hat{\phi}(z, \breve{\xi} | \xi_{des}, \delta_{z_{des}}, \hat{\delta}_\xi) - \hat{\phi}(z, \xi, \hat{\delta}_z, \hat{\delta}_\xi) \\
&= \phi_{des} - \hat{\phi}(z, \xi, \hat{\delta}_z, \hat{\delta}_\xi) \\
\gamma_h &= \hat{\gamma}(z, \xi, \hat{\delta}_z, \delta_{\xi_{des}}) - \hat{\gamma}(z, \xi, \hat{\delta}_z, \hat{\delta}_\xi) \\
&= \gamma_{des} - \hat{\gamma}(z, \xi, \hat{\delta}_z, \hat{\delta}_\xi).
\end{aligned}$$

If an assumption such as Assumption 1 (pg. 18) can be made and noting that ξ is available for feedback, then

$$\bar{\Delta}(x, \delta, \hat{\delta}) = \begin{bmatrix} \bar{\Delta}_z(x, \delta, \hat{\delta}) \\ \bar{\Delta}_\xi(x, \delta, \hat{\delta}) \end{bmatrix} = \begin{bmatrix} \Delta_z(x, \hat{\delta}) \\ \Delta_\xi(x, \hat{\delta}) \end{bmatrix} = \Delta(z, \xi, \hat{\delta}_z, \hat{\delta}_\xi).$$

3.1.2 Tracking Error Dynamics

The reference model tracking error, e as follows

$$e \triangleq \begin{bmatrix} z_{r_1} - z_1 \\ z_{r_2} - z_2 \\ \xi_{r_1} - \xi_1 \\ \xi_{r_2} - \xi_2 \end{bmatrix} \qquad \dot{e} = \begin{bmatrix} z_{r_2} - z_2 \\ \dot{z}_{r_2} - \dot{z}_2 \\ \xi_{r_1} - \xi_1 \\ \dot{\xi}_{r_2} - \dot{\xi}_2 \end{bmatrix}.$$

The linear compensators may now be designed as

$$\begin{bmatrix} \phi_{lc} \\ \gamma_{lc} \end{bmatrix} = \begin{bmatrix} R_p & R_d & 0 & 0 \\ 0 & 0 & K_p & K_d \end{bmatrix} e.$$

The reference model tracking error dynamics may be evaluated as

$$\begin{aligned}
\dot{e}_2 &= \dot{z}_{r_2} - \dot{z}_2 & \dot{e}_4 &= \dot{\xi}_{r_2} - \dot{\xi}_2 \\
&= \phi_{cr} - \phi_h - \phi & &= \gamma_{cr} - \gamma_h - \gamma \\
&= \phi_{cr} - \phi_{des} + \hat{\phi} - \phi & &= \gamma_{cr} - \gamma_{des} + \hat{\gamma} - \gamma \\
&= \phi_{cr} - \phi_{lc} - \phi_{cr} + \bar{\phi}_{ad} + \hat{\phi} - \phi & &= \gamma_{cr} - \gamma_{lc} - \gamma_{cr} + \bar{\gamma}_{ad} + \hat{\gamma} - \gamma \\
&= -\phi_{lc} - (\phi - \hat{\phi} - \bar{\phi}_{ad}) & &= -\gamma_{lc} - (\gamma - \hat{\gamma} - \bar{\gamma}_{ad}) \\
&= -\phi_{lc} - (\Delta_z - \bar{\phi}_{ad}) & &= -\gamma_{lc} - (\Delta_\xi - \bar{\gamma}_{ad}),
\end{aligned}$$

The overall tracking error dynamics may be written as

$$\dot{e} = Ae + B[\bar{\nu}_{ad} - \Delta(z, \xi, \hat{\delta}_z, \hat{\delta}_\xi)], \tag{25}$$

where,

$$A = \begin{bmatrix} 0 & 1 & 0 & 0 \\ -R_p & -R_d & 0 & 0 \\ 0 & 0 & 0 & 1 \\ 0 & 0 & -K_p & -K_d \end{bmatrix}, B = \begin{bmatrix} 0 & 0 \\ 1 & 0 \\ 0 & 0 \\ 0 & 1 \end{bmatrix}, \bar{\nu}_{ad} = \begin{bmatrix} \bar{\phi}_{ad} \\ \bar{\gamma}_{ad} \end{bmatrix}, \tag{26}$$

where, $R_p, R_d, K_p, K_d \in \mathcal{R}^1_{>0}$ stabilize the z and ξ dynamics together. The general case of k-subsystems in cascade follows a similar development and is presented before boundedness theorems are stated.

3.2 Adaptive Control of k-subsystems in Cascade

Consider the following set of k-subsystems in first order form

$$\begin{aligned}
\dot{x}_{n_1}^{(1)} &= f_1(x,\delta) \\
&\vdots \\
\dot{x}_{n_i}^{(i)} &= f_i(x,\delta) \\
&\vdots \\
\dot{x}_{n_k}^{(k)} &= f_k(x,\delta),
\end{aligned} \tag{27}$$

where the superscript (i), denotes the i^{th}-subsystem which has the form

$$\begin{aligned}
\dot{x}_1^{(i)} &= x_2^{(i)} \\
\dot{x}_2^{(i)} &= x_3^{(i)} \\
&\vdots \\
\dot{x}_{n_i}^{(i)} &= f_i(x,\delta),
\end{aligned}$$

where the state vector

$$x = \left[x^{(1)T}, x^{(2)T}, \ldots, x^{(i)T}\right]^T \in \mathcal{D}_x \subset \mathcal{R}^{n_1+\cdots+n_k},$$

and the control vector is

$$\delta = [\delta_1, \delta_2, \ldots, \delta_k]^T \in \mathcal{R}^k,$$

where $x^{(i)} \in \mathcal{R}^{n_i}$ and $\delta_i \in \mathcal{R}$ for $i = 1, \ldots, k$. Noting that for each subsystem i, the primary control is δ_i and assuming a cascade structure, introduce the invertible approximations

$$\begin{aligned}
\nu_i &= \hat{f}_i(\breve{x}^{(i+1)} | x_{des}^{(i+1)}, \hat{\delta}_1, \ldots, \hat{\delta}_{i-1}, \delta_{i_{des}}, \hat{\delta}_{i+1}, \ldots, \hat{\delta}_k) \qquad \text{for } i = 1, \ldots, k-1 \\
\nu_k &= \hat{f}_k(x, \hat{\delta}_1, \ldots, \hat{\delta}_{k-1}, \delta_{k_{des}}),
\end{aligned} \tag{28}$$

resulting in the following inverse

$$\begin{aligned}
\begin{bmatrix} \delta_{1_{des}} \\ x^{(2)}_{des} \end{bmatrix} &= \begin{bmatrix} \hat{f}^{-1}_{1_{\delta_1}}(\breve{x}^{(2)}, \nu_{1_{\delta_1}}, \hat{\delta}_2, \ldots, \hat{\delta}_k) \\ \hat{f}^{-1}_{1_{x^{(2)}}}(\breve{x}^{(2)}, \nu_{1_{x^{(2)}}}, \hat{\delta}_2, \ldots, \hat{\delta}_k) \end{bmatrix}, \\
\begin{bmatrix} \delta_{i_{des}} \\ x^{(i+1)}_{des} \end{bmatrix} &= \begin{bmatrix} \hat{f}^{-1}_{i_{\delta_i}}(\breve{x}^{(i+1)}, \nu_{i_{\delta_i}}, \hat{\delta}_1, \ldots, \hat{\delta}_{i-1}, \hat{\delta}_{i+1}, \hat{\delta}_k) \\ \hat{f}^{-1}_{i_{x^{(i+1)}}}(\breve{x}^{(i+1)}, \nu_{i_{x^{(i+1)}}}, \hat{\delta}_1, \ldots, \hat{\delta}_{i-1}, \hat{\delta}_{i+1}, \hat{\delta}_k) \end{bmatrix} \qquad \text{for } i = 2, \ldots, k-1, \\
\delta_{k_{des}} &= \hat{f}^{-1}_k(x, \nu_k, \hat{\delta}_1, \ldots, \hat{\delta}_{k-1}),
\end{aligned} \tag{29}$$

where, $x^{(i)}_{des} \in \mathcal{R}^{\leq n_i}, i = 2 \cdots k$, are virtual controls, $\breve{x}^{(i)}, i = 2 \cdots k$ denotes elements of the full state vector x without the virtual controls $x^{(i)}_{des}$, $\nu_{i_{\delta_i}} + \nu_{i_{x^{(i+1)}}} = \nu_i$ and $\hat{f}_{i_{\delta_i}}, \hat{f}_{i_{x^{(i+1)}}}$ formulated such that they are consistent with Eqn (28) for $i = 1 \ldots k-1$ and their inverses exist. Substituting the inverse law of Eqn (29) into (27), the plant dynamics may be written as

$$\dot{x}^{(i)}_{n_i} = \nu_i + \bar{\Delta}_i(x, \delta, \hat{\delta}) - \nu_{h_i} \qquad \text{for } i = 1, \ldots, k.$$

Choosing the pseudocontrol as

$$\nu_i = \nu_{cr_i} + \nu_{lc_i} - \bar{\nu}_{ad_i} \qquad \text{for } i = 1, \ldots, k,$$

with reference models

$$\begin{aligned}
\dot{x}^{(1)}_{r_{n_1}} &= \nu_{cr_1}(x^{(1)}_r, x^{(1)}_c) - \nu_{h_1} \\
\dot{x}^{(i)}_{r_{n_i}} &= \nu_{cr_i}(x^{(i)}_r, x^{(i)}_c \oplus x^{(i)}_{des}) - \nu_{h_i} \quad \text{for } i = 2, \ldots, k,
\end{aligned} \tag{30}$$

where $x^{(i)}_r \in \mathcal{R}^{n_i}$ for $i = 1, \ldots, k$. The PCH signal may be computed as follows

$$\nu_{h_i} = \nu_i - \hat{f}_i(x, \hat{\delta}) \quad \text{for } i = 1, \ldots, k. \tag{31}$$

Defining the reference model tracking error as

$$e^{(i)} \triangleq x^{(i)}_r - x^{(i)} \quad \text{for } i = 1, \ldots, k, \tag{32}$$

the reference model tracking error dynamics may be written as

$$\dot{e} = Ae + B[\bar{\nu}_{ad} - \bar{\Delta}(x, \delta, \hat{\delta})], \tag{33}$$

or

$$\underbrace{\begin{bmatrix} \dot{e}^{(1)} \\ \dot{e}^{(2)} \\ \vdots \\ \dot{e}^{(k)} \end{bmatrix}}_{\dot{e}} = \underbrace{\begin{bmatrix} A^{(1)} & 0 & 0 & 0 \\ 0 & A^{(2)} & 0 & 0 \\ 0 & \cdots & \ddots & \vdots \\ 0 & 0 & 0 & A^{(k)} \end{bmatrix}}_{A} \underbrace{\begin{bmatrix} e^{(1)} \\ e^{(2)} \\ \vdots \\ e^{(k)} \end{bmatrix}}_{e} + \underbrace{\begin{bmatrix} B^{(1)} \\ B^{(2)} \\ \vdots \\ B^{(k)} \end{bmatrix}}_{B} \underbrace{\begin{bmatrix} \bar{\nu}_{ad_1} - \bar{\Delta}_1(x, \delta) \\ \bar{\nu}_{ad_2} - \bar{\Delta}_2(x, \delta) \\ \vdots \\ \bar{\nu}_{ad_k} - \bar{\Delta}_k(x, \delta) \end{bmatrix}}_{\bar{\nu}_{ad} - \bar{\Delta}(x,\delta)},$$

where $A^{(i)} \in \mathcal{R}^{n_i \times n_i}$ and has the form

$$A^{(i)} = \begin{bmatrix} 0 & 1 & 0 & \cdots & 0 \\ \vdots & & & & \vdots \\ 0 & \cdots & \cdots & \cdots & 1 \\ -K_1^{(i)} & \cdots & \cdots & \cdots & -K_{n_i}^{(i)} \end{bmatrix}_{n_i \times n_i},$$

and $B^{(i)} \in \mathcal{R}^{n_i \times k}$ has the form

$$B^{(i)}_{(\alpha,\beta)} = 0 \quad \forall\ \alpha \in \{1, \ldots, n_i\}, \forall\ \beta \in \{1, \ldots, k\}, (\alpha, \beta) \neq (n_i, i)$$
$$B^{(i)}_{(n_i,i)} = 1.$$

Associated with the reference model tracking error dynamics of Eqn (33) is the Lyapunov equation.

$$A^T P + PA + Q = 0.$$

Choosing $Q = I$, and assuming $K_j^{(i)}$ for $i = 1, \cdots, k$ and $j = 1, \cdots, n_i$, are chosen to stabilize A, it can be shown that there exists a $P > 0$ which satisfies the Lyapunov equation. For an example of choosing these gains, see Section 5.3.3.

3.3 Effect of Actuator Model on Error Dynamics

An important aspect of the PCH signal calculation given by Eqn (31) is estimation of the actual actuator position at the current instant. The assumptions and model

used to estimate the actuator positions in calculating the PCH signals play a role in what appears in the tracking error dynamics.

3.3.1 Actuator Positions are Measured

The simplest case arises when δ is measured and available for feedback. In this case, models for the actuators are not needed. In fact, when all actuator signals are known then $\bar{\Delta}(x, \delta, \hat{\delta}) = \bar{\Delta}(x, \delta) = \Delta(x, \delta)$ and the tracking error dynamics of Eqn (33) is given by

$$\dot{e} = Ae + B\left[\bar{\nu}_{ad}(x, \delta) - \Delta(x, \delta)\right]. \tag{34}$$

3.3.2 Actuator Position is a Static Function of the Model and Plant States

If it can be assumed that actuator deflections have the form $\delta = \delta(x, \hat{\delta})$, for example, saturation occurs earlier than in the model of the actuator, the discrepancy appears as model error which the NN can correct for. Thus, $\bar{\Delta}(x, \delta(x, \hat{\delta}), \hat{\delta}) = \Delta(x, \hat{\delta})$ and the error dynamics take the form

$$\dot{e} = Ae + B\left[\bar{\nu}_{ad}(x, \hat{\delta}) - \Delta(x, \hat{\delta})\right]. \tag{35}$$

3.3.3 Actuator model has error the NN cannot compensate

If actuator positions are not measured and an assumption such as $\delta = \delta(x, \hat{\delta})$ cannot be made, the uncertainty $\bar{\Delta}$ may be expressed as

$$\bar{\Delta}(x, \delta, \hat{\delta}) = \Delta(x, \hat{\delta}) + \epsilon_g(x, \delta, \hat{\delta}),$$

where $\Delta(x, \hat{\delta})$ is model error the NN can approximate and ϵ_g is the model error the NN cannot cancel when δ is not available as an input to the network and has components independent of x and $\hat{\delta}$. Errors in the actuator model that the NN can cancel include bias error in the actuator position estimate and erroneous values for when magnitude saturation occurs. Model errors that appear in ϵ_g which the neural network cannot cancel include parameters that affect the dynamics of the actuator such as actuator

time constants and rate limits. The tracking error dynamics may now be expressed as

$$\dot{e} = Ae + B\left[\bar{\nu}_{ad}(x,\hat{\delta}) - \Delta(x,\hat{\delta}) - \epsilon_g(x,\delta,\hat{\delta})\right], \tag{36}$$

where $\bar{\nu}_{ad}(x,\hat{\delta})$ is designed to cancel $\Delta(x,\hat{\delta})$ and ϵ_g appears as unmodeled input dynamics to the control system.

3.3.4 Actuator model is conservative

One way to predict actuator position accurately is to impose conservative artificial limits on the desired actuator deflections, perhaps in software and make the assumption that the real actuator tracks the conservative commands accurately. This amounts to always knowing δ, and the error dynamics take the form given by Eqn (34).

3.4 Tracking Error Boundedness

For the most general form of the tracking error dynamics given by Eqn (36), boundedness of the tracking error, e, and neural network weights, $\tilde{V}, \tilde{W}$, may be presented after the following assumptions.

Assumption 2. *The external command x_c is bounded,*

$$\|x_c\| \leq \bar{x}_c.$$

Assumption 3. *The NN approximation $\Delta(x,\hat{\delta}) = \nu_{ad}(x,\hat{\delta}) + \epsilon$ holds in a compact domain $\mathcal{D}$, which is large enough such that $\mathcal{D}_{x_c} \times \mathcal{D}_{e_r} \times \mathcal{D}_e \times \mathcal{D}_{\tilde{Z}}$ maps into $\mathcal{D}$.*

Assumption 4. *The norm of the ideal weights (V^*, W^*) is bounded by a known positive value,*

$$0 < \|Z^*\|_F \leq \bar{Z},$$

where $\|\cdot\|_F$ denotes the Frobenius norm.

Assumption 5. *Note that, Δ depends on ν_{ad} through the pseudocontrol ν, whereas $\bar{\nu}_{ad}$ has to be designed to cancel Δ. Hence the existence and uniqueness of a fixed-point-solution for $\nu_{ad} = \Delta(x, \nu_{ad})$ is assumed. Sufficient conditions[7] for this assumption are also available.*

Theorem 2. *Consider the cascade of systems (27), with the inverse law (29), a reference model consistent with (30), and assumptions (2, 3, 4, 5), where the NN training signal, r, NN output, ν_{ad}, and robustifying term, ν_r, are given by*

$$r = (e^T PB)^T \tag{37}$$

$$\bar{\nu}_{ad} = \nu_{ad} + \nu_r \tag{38}$$

$$\nu_{ad} = W^T \sigma(V^T \bar{x}) \tag{39}$$

$$\nu_r = -K_r(\|Z\|_F + \bar{Z}) r \frac{\|e\|}{\|r\|}. \tag{40}$$

If $K_r > 0 \in \mathcal{R}^{k \times k}$ is chosen sufficiently large with lower-limit stated in the proof, and NN weights W, V satisfy the adaptation laws

$$\dot{W} = -\left[(\sigma - \sigma' V^T \bar{x}) r^T + \kappa \|e\| W\right] \Gamma_W \tag{41}$$

$$\dot{V} = -\Gamma_V \left[\bar{x}(r^T W^T \sigma') + \kappa \|e\| V\right], \tag{42}$$

with $\Gamma_W, \Gamma_V > 0$ and $\kappa > 0$ with lower-limit stated in the proof, then, the reference model tracking error, (e), and NN weight errors, $(\tilde{W}, \tilde{V})$, are uniformly ultimately bounded.

Proof. See Section A.1 □

Assumption 6. *The states of the reference model, remain bounded for permissable plant and actuator dynamics. Hence,*

$$\|e_r\| \leq \bar{e}_r.$$

Corollary 1. *All system states $x^{(i)}$ for $i = 1, \ldots, k$ are uniformly ultimately bounded.*

Proof. If the ultimate boundedness of $e, \tilde{W}, \tilde{V}$ from Theorem 2 is taken together with Assumption 6, the uniform ultimate boundedness of the plant states is immediate following the definition of the reference model tracking error in Eqn (32). □

Remark 1. *Note that Theorem 2 only requires a reference model of the form (30), implying that no particular form of ν_{cr_i} is required for boundedness of the tracking error e.*

CHAPTER IV

NONLINEAR REFERENCE MODELS

This chapter presents the use of nonlinear reference models for the model reference adaptive control architecture. In chapters 2 and 3, the boundedness of the plant states depends on the boundedness of the reference model. Although the tracking error dynamics of Eqn (11) or Eqn (33) do not contain the PCH signal, it appears as a disturbance term in the reference model dynamics of Eqn (9) and Eqn (30). Theorem 1 and Theorem 2 imply that the plant states track the reference model closely even when a large magnitude of ν_h is present. Indeed, e and the neural network weight errors, $\tilde{V}, \tilde{W}$ remain bounded even when the controller is not in control of the plant. The boundedness of the reference model dynamics however, relies on an assumption. If the control law is such that no saturation takes place, i.e., $\nu_h \equiv 0, \forall t \geq 0$, then choosing ν_{cr} stable, will result in boundedness of the reference model and pertains to results presented in previous work where unbounded actuation is assumed [8, 57]. The designs in this thesis, do not in general, prevent saturation, thus it is important to choose ν_{cr} such that the reference model remains bounded and the external command is achieved without leaving the null controllable region of the plant. One may examine the effect of choosing ν_{cr} on the response of the plant by considering the isolated nonadaptive subsystem where the tracking error $e = 0$. Assuming $\bar{\nu}_{ad}^*$ is the post-adaptive output of the adaptive element ($W = W^*, V = V^*$). The closed loop system maybe written as

$$\begin{aligned}
\dot{x}_n &= f(x, \delta) \\
&= f(x, g(x, \delta_{des})) \\
&= f(x, g(x, \hat{f}^{-1}(x, \nu_{cr} + \cancel{\nu_{tc}} - \bar{\nu}_{ad}^*))),
\end{aligned}$$

which can be thought of as the zero dynamics of the system, where $\nu_{lc} = 0$ because tracking error e is assumed to be 0. If the adaptation is capable of exactly canceling the model error, the dynamics may be expressed as

$$\dot{x}_n = f(x, g(x, f^{-1}(x, \nu_{cr}))).$$

ν_{cr} could be designed so that δ and δ_{des} always match, perhaps as the output of an optimal trajectory generator that takes into account the system dynamics f and actuator input characteristics g or a conservative bounded control law. Hence, when $\delta \approx \delta_{des}$, the dynamics become

$$\dot{x}_n \approx \nu_{cr}. \tag{43}$$

Before delving into specific nonlinear reference models, the following discussion on the null controllability is useful.

4.1 Null Controllable Region

In cases of constrained control, it is not possible to stabilize the system globally unless the system itself possess this property. For example, consider an otherwise linear system of the form

$$\dot{x} = Ax + B\sigma(\delta), \tag{44}$$

with $A \in \mathcal{R}^{n\times n}$, $B \in \mathcal{R}^{n\times m}$, $\delta \in \mathcal{R}^m$. It is not possible to stabilize the system (44) globally [70] unless A has no eigenvalues in the right half plane. Additionally, even if A has no eigenvalues in the right half plane it is not possible to globally stabilize it using a linear control law [71]. It may be however be achieved using a nonlinear control law [70, 72] employing nested saturations. Semi-global results are possible for linear systems with unstable eigenvalues [20]. In the study of constrained control, the concepts of null controllability and the null controllable region are useful and are taken from [20].

Definition 1. *A state x_0 is said to be null controllable in time $T > 0$ if there exists an admissible control $\delta(t)$ such that the state trajectory $x(t)$ of the system satisfies $x(0) = x_0$ and $x(T) = 0$. The set of all states that are null controllable in time T, denoted by $\mathcal{C}(T)$, is called the null controllable region in time T.*

Definition 2. *A state x_0 is said to be null controllable if $x_0 \in \mathcal{C}(T)$ for some $T \in [0, \infty)$. The set of all null controllable states, denoted by $\mathcal{C}$, is called the null controllable region of the system.*

Determining the null controllable region of a system is not trivial. For linear systems, simple estimates may be found using the Circle and Popov criteria as described in [16, 54]. Less conservative estimates may be found as the result of an LMI optimization as described in [20]. For nonlinear systems of the form (2) and (27), there is no known method to explicitly characterize a null controllable region $\mathcal{C}_x$ where there always exists an admissible control which can bring an initial state $x(0)$ back to the origin in finite time. Although our development has been one of feedback linearization, a direct correlation between the null controllable region of a linear system[20] under bounded excitation and a nonlinear system cannot be made. However, note that the plant states are given by

$$x(t) = x_r(t) - e(t). \tag{45}$$

If the trajectory of $x_r(t)$, is governed by fast linear dynamics ($\nu_{cr} = Ke_r$), and is driven by large external commands, then some states of x_r may peak to large values and the plant states may leave the null controllable region. This problem is related to the peaking phenomenon[69] where a fast linear system (linear reference model) drives a nonlinear system. In practice, if the evolution of the reference model states x_r is constrained, using either a low gain approach or artificial saturation functions, or nonlinear damping, the likely hood of the plant states leaving the plant's null controllable region is reduced. This is evident from examining Eqn (45). Since $\|e\|$

is bounded and it is assumed that x_c is null controllable, if $x_r(t) - e(t)$ is such that it does not leave the null controllable region of the plant, then the plant states are bounded.

Assumption 7. *Noting that $\mathcal{C}_x$ is not necessarily a connected or closed set, assume that $\mathcal{D} \subseteq \mathcal{C}_x$, and that $\mathcal{D}$ in addition to being compact is also convex.*

In this chapter, three reference models are examined, the linear reference model that is commonly used in previous work, a nested saturation-based reference model and a special case of the nested saturation-based reference model which we call the constrained linear reference model.

4.2 Linear Reference Model

Consider a linear reference model for a single-subsystem of the form (2)

$$\begin{aligned} \dot{x}_{r_i} &= x_{r_{i+1}} \qquad i = 1, 2, \cdots, n-1 \\ \dot{x}_{r_n} &= \begin{bmatrix} K_1 & K_2 & \cdots & K_n \end{bmatrix} e_r - \nu_h, \end{aligned} \tag{46}$$

where the command tracking error $e_r \in \mathcal{R}^n$ is defined to be $e_r \triangleq x_c - x_r$, resulting in the command tracking error dynamics being given by

$$\dot{e}_r = A_r e_r + E_r \nu_h,$$

where

$$A_r = \begin{bmatrix} 0 & 1 & 0 & \cdots & 0 \\ 0 & 0 & 1 & & 0 \\ \vdots & \vdots & & \ddots & \\ 0 & 0 & & & 1 \\ -K_1 & -K_2 & -K_3 & \cdots & -K_n \end{bmatrix}, E_r = \begin{bmatrix} 0 \\ 0 \\ \vdots \\ 0 \\ 1 \end{bmatrix},$$

where the gains K_i are the ones used to stabilize the tracking error dynamics in Eqn (10). Similarly, the command tracking error dynamics of a linear reference model

for k-subsystems of Eqn (27) consistent with Eqn (30) may be expressed as

$$\begin{bmatrix} \dot{e}_r^{(1)} \\ \dot{e}_r^{(2)} \\ \vdots \\ \dot{e}_r^{(k)} \end{bmatrix} = \begin{bmatrix} A_r^{(1)} & 0 & 0 & 0 \\ 0 & A_r^{(2)} & 0 & 0 \\ 0 & \cdots & \ddots & \vdots \\ 0 & 0 & 0 & A_r^{(k)} \end{bmatrix} \begin{bmatrix} e_r^{(1)} \\ e_r^{(2)} \\ \vdots \\ e_r^{(k)} \end{bmatrix} + \begin{bmatrix} E_r^{(1)} \\ E_r^{(2)} \\ \vdots \\ E_r^{(k)} \end{bmatrix} \begin{bmatrix} \nu_{h_1} \\ \nu_{h_2} \\ \vdots \\ \nu_{h_k} \end{bmatrix},$$

where $A^{(i)} \in \mathcal{R}^{n_i \times n_i}$ and has the form

$$A_r^{(i)} = \begin{bmatrix} 0 & 1 & 0 & \cdots & 0 \\ \vdots & & & & \vdots \\ 0 & \cdots & \cdots & \cdots & 1 \\ -K_1^{(i)} & \cdots & \cdots & \cdots & -K_{n_i}^{(i)} \end{bmatrix}_{n_i \times n_i},$$

and $E_r^{(i)} \in \mathcal{R}^{n_i \times k}$ has the form

$$E_{r_{(\alpha,\beta)}}^{(i)} = 0 \quad \forall\ \alpha \in \{1, \ldots, n_i\}, \forall\ \beta \in \{1, \ldots, k\}, (\alpha, \beta) \neq (n_i, i)$$
$$E_{r_{(n_i,i)}}^{(i)} = 1.$$

The command tracking error of the reference model may now be written as

$$\dot{e}_r = A_r e_r + E_r \nu_h. \tag{47}$$

In the absence of the PCH signal i.e., $\nu_h \equiv 0$, the $K_j^{(i)}$ for $i = 1, \cdots, k$ and $j = 1, \cdots, n_i$, used to stabilize (33) may be used to stabilize A_r in Eqn (47) and hence there exists a $P_r > 0$ which satisfies $A_r^T P_r + P_r A_r + Q_r = 0$, for $Q_r > 0$.

Noting that $\nu_h = \nu_{cr} + \nu_{lc} - \bar{\nu}_{ad} - \hat{f}(x, \hat{\delta})$, consider now a positive definite function $L_r(e_r) = \frac{1}{2} e_r^T P_r e_r$. Then,

$$\begin{aligned} \dot{L}_r &= -\frac{1}{2} e_r^T Q_r e_r + e_r^T P_r E_r \nu_h \\ &\leq -\frac{1}{2} \lambda_{min}(Q_r) \|e_r\|^2 + \|e_r\| \|P_r E_r\| \|\nu_h\| \\ &\leq -\left(\frac{1}{2} \lambda_{min}(Q_r) - \|P_r E_r\| \|K\| \right) \|e_r\|^2 + \|\nu_{lc} + \bar{\nu}_{ad} - \hat{f}(x, \hat{\delta})\|. \end{aligned} \tag{48}$$

This bound on $\dot{L}_r$ is used in the proof of the following theorem.

Theorem 3. *Consider the cascade of systems given by (27), with the inverse law (29), a linear reference model (47) consistent with (30), where the gains are the same as those selected such that the system matrix in (33) is Hurwitz and assumptions (2, 3, 4, 5, 7), where the NN training signal, r, NN output, ν_{ad}, and robustifying term, ν_r, are given by*

$$
\begin{aligned}
r &= (e^T P B)^T \\
\bar{\nu}_{ad} &= \nu_{ad} + \nu_r \\
\nu_{ad} &= W^T \sigma(V^T \bar{x}) \\
\nu_r &= -K_r(\|Z\|_F + \bar{Z}) r \frac{\|e\|}{\|r\|}.
\end{aligned}
$$

If $K_r > 0 \in \mathcal{R}^{k \times k}$ is chosen sufficiently large with lower-limit stated in the proof, and NN weights W, V satisfy the adaptation laws

$$
\begin{aligned}
\dot{W} &= -\left[(\sigma - \sigma' V^T \bar{x}) r^T + \kappa \|e\| W\right] \Gamma_W \\
\dot{V} &= -\Gamma_V \left[\bar{x}(r^T W^T \sigma') + \kappa \|e\| V\right],
\end{aligned}
$$

with, $\Gamma_W, \Gamma_V > 0$ and $\kappa > 0$ with lower-limit stated in the proof, then, the command tracking error, e_r, reference model tracking error, e, and NN weight errors $(\tilde{W}, \tilde{V})$ are uniformly ultimately bounded. Further, the plant states, x, are ultimately bounded.

Proof. See Section A.2 □

4.3 Nested Saturation-Based Reference Model

An alternative to the linear reference model is one containing nested-saturations and is based on the work by Teel[73, 72, 74]. This form allows one to restrict the evolution of states in a prescribable manner.

4.3.1 Single Subsystem

Consider a nested saturation-based reference model for a single subsystem of the form (9),

$$\dot{x}_{r_i} = x_{r_{i+1}} \qquad i = 1, 2, \cdots, n-1$$
$$\dot{x}_{r_n} = M_n \sigma_n \left[\frac{K_n}{M_n} e_r + M_{n-1}\sigma_{n-1} \left(\frac{K_{n-1}}{M_n M_{n-1}} e_r \ldots + M_1 \sigma_1 \left(\frac{K_1}{M_n \cdots M_1} e_r \right) \right) \right] - \nu_h.$$

For the single-input case, the gains are row vectors, $K_i \in \mathcal{R}^{1\times n}$ for $i = 1, \cdots, n$ and the functions $\sigma_i : \mathcal{R} \to \mathcal{R}$ and are unity saturation functions, where

$$\sigma(s) = sgn(s) min(1, |s|).$$

Non-unity limits may be incorporated using the multipliers $M_i \in \mathcal{R} > 0$ for $i = 1, \cdots, n$. The command tracking error dynamics may now be expressed as

$$\dot{e}_r = A_r e_r + B_r M_n \sigma_n \left(\frac{K_n}{M_n} e_r + \cdots + M_1 \sigma_1 \left(\frac{K_1}{M_n \cdots M_1} e_r \right) \right) + E_r \nu_h, \tag{49}$$

where,

$$A_r = \begin{bmatrix} 0 & 1 & 0 & \cdots & 0 \\ 0 & 0 & 1 & & 0 \\ \vdots & \vdots & & \ddots & \\ 0 & 0 & & & 1 \\ 0 & 0 & 0 & \cdots & 0 \end{bmatrix}, B_r = \begin{bmatrix} 0 \\ 0 \\ \vdots \\ 0 \\ -1 \end{bmatrix}, E_r = \begin{bmatrix} 0 \\ 0 \\ \vdots \\ 0 \\ 1 \end{bmatrix},$$

4.3.2 k-subsystems

The command tracking error dynamics of a nested saturation-based reference model for k-subsystems of Eqn (27) consistent with Eqn (30) may be expressed as

$$\begin{bmatrix} \dot{e}_r^{(1)} \\ \dot{e}_r^{(2)} \\ \vdots \\ \dot{e}_r^{(k)} \end{bmatrix} = \begin{bmatrix} A^{(1)} & 0 & 0 & 0 \\ 0 & A^{(2)} & 0 & 0 \\ 0 & \cdots & \ddots & \vdots \\ 0 & 0 & 0 & A^{(k)} \end{bmatrix} \begin{bmatrix} e_r^{(1)} \\ e_r^{(2)} \\ \vdots \\ e_r^{(k)} \end{bmatrix} + \begin{bmatrix} B_r^{(1)} \\ B_r^{(2)} \\ \vdots \\ B_r^{(k)} \end{bmatrix} M_n \sigma(\cdots) + \begin{bmatrix} E_r^{(1)} \\ E_r^{(2)} \\ \vdots \\ E_r^{(k)} \end{bmatrix} \begin{bmatrix} \nu_{h_1} \\ \nu_{h_2} \\ \vdots \\ \nu_{h_k} \end{bmatrix}, \tag{50}$$

with $\sigma(\cdots)$ given by

$$\sigma(\cdots) = \sigma_n \left[M_n^{-1} K_n e_r + M_{n-1}\sigma_{n-1}\left(M_{n-1}^{-1} M_n^{-1} K_{n-1} e_r \ldots + M_1 \sigma_1 \left(M_1^{-1} \cdots M_n^{-1} K_1 e_r \right) \right) \right], \tag{51}$$

where $A_r^{(i)} \in \mathcal{R}^{n_i \times n_i}$ and has the form

$$A_r^{(i)} = \begin{bmatrix} 0 & 1 & 0 & \cdots & 0 \\ 0 & 0 & 1 & & 0 \\ \vdots & \vdots & & \ddots & \\ 0 & 0 & & & 1 \\ 0 & 0 & 0 & \cdots & 0 \end{bmatrix}_{n_i \times n_i},$$

and $E_r^{(i)} \in \mathcal{R}^{n_i \times k}$ has the form

$$E^{(i)}_{r_{(\alpha,\beta)}} = 0 \quad \forall\ \alpha \in \{1, \ldots, n_i\}, \forall\ \beta \in \{1, \ldots, k\}, (\alpha, \beta) \neq (n_i, i)$$
$$E^{(i)}_{r_{(n_i,i)}} = 1,$$

and $B_r^{(i)} \in \mathcal{R}^{n_i \times k}$ has the form

$$B^{(i)}_{r_{(\alpha,\beta)}} = 0 \quad \forall\ \alpha \in \{1, \ldots, n_i\}, \forall\ \beta \in \{1, \ldots, k\}, (\alpha, \beta) \neq (n_i, i)$$
$$B^{(i)}_{r_{(n_i,i)}} = -1.$$

Here, $K_i \in \mathcal{R}^{k \times n_1 + n_2 + \ldots + n_k}$, are such that $A_r + B_r \left[K_n + K_{n-1} + \cdots + K_1 \right]$ is Hurwitz. The vector valued saturation function is given by $\sigma : \mathcal{R}^k \to \mathcal{R}^k$ with

$$\sigma(u) = \begin{bmatrix} \sigma(u_1) & \sigma(u_2) & \cdots & \sigma(u_k) \end{bmatrix}^T,$$

with $\sigma(u_i) = sgn(u_i) min(1, |u_i|)$. The saturation limits are incorporated into the diagonal matrices $M_i \in \mathcal{R}^{k \times k}$, with each entry being strictly positive. An important aspect of the nested saturation-based reference model is that if the limits and gains are chosen appropriately [70, 73, 71, 74], the true domain of attraction of the isolated reference model ($\nu_h \equiv 0$), is $\mathcal{R}^{n_1 + \cdots + n_k}$. An estimate of this system's domain of attraction (with $\nu_h \equiv 0$) may be found by using the procedure in [3] and related results

in [20, 22]. For a given initial condition $e_r(0) \in \mathcal{R}^{n_1+\cdots+n_k}$, if the state trajectory of the system (50) is denoted by $\psi(t, e_r(0))$, then the domain of attraction of the origin is defined as the set of all initial conditions which can be brought back to the origin asymptotically.

$$\mathcal{D}_{e_r} \triangleq \left\{ e_r(0) \in \mathcal{R}^{n_1+\cdots+n_k} : \lim_{t\to\infty} \psi(t, e_r(0)) = 0 \right\}.$$

Let $P_r \in \mathcal{R}^{n_1+\cdots+n_k \times n_1+\cdots+n_k}$ be a positive definite matrix used to define an ellipsoid

$$\Omega(P_r, \rho) = \left\{ e_r \in \mathcal{R}^{n_1+\cdots+n_k} : e_r^T P_r e_r \leq \rho \right\}.$$

Consider the positive definite function $L_r(e_r) = e_r^T P_r e_r$ and this time including the PCH signal in our analysis,

$$\begin{aligned}\dot{L}_r(e_r) &= 2e_r^T P_r \left(A_r e_r + B_r M_n \sigma(\cdots) \right) + e_r^T P_r E_r \nu_h \\ &\leq -\gamma(e_r) + \|e_r\|\|P_r E_r\|\alpha_1 \lambda_{max}(M_n) + \|e_r\|\|P_r E_r\|\|\nu_{lc} + \bar{\nu}_{ad} - \hat{f}(x, \hat{\delta})\|\end{aligned}$$

where $\sigma(\cdots)$ is given by Eqn (51), and it is now guaranteed that,

$$-\gamma(e_r) < 0 \quad \forall e_r \in \Omega(P_r, \rho) \backslash \{0\}.$$

This is in contrast to Eqn (48) because $\|P_r E_r\|\|K\|\|e_r\|^2$, now does not appear in $\dot{L}_r$. This is because, $\|\nu_{cr}\|$ using a nested saturation reference model is bounded by a known value $\|\nu_{cr}\| \leq \alpha_1 \lambda_{max}(M_n)$ as opposed to $\|\nu_{cr}\| \leq \|K\|\|e_r\|$ for the linear reference model.

4.3.3 Checking Invariance

Given a set $\Omega(P_r, \rho)$ one may explicitly verify that $-\gamma(e_r) < 0 \ \forall e_r \in \Omega(P_r, \rho)$. For the general case of k-subsystems, a sufficient condition to ascertain this is; given an

ellipsoid $\Omega(P_r, \rho)$, if there exists gains $H_1, H_2, \cdots, H_{N_k} \in \mathcal{R}^{k \times N_k}$ such that $\forall \theta \in \Theta$

$$
\begin{aligned}
&P_r(A_r + B_r M_n \beta(\theta, H_1, F_1 + D_2 H_2, \\
&\qquad F_1 + D_2 F_2 + D_2 D_3 H_3, \\
&\qquad \vdots \\
&\qquad F_1 + D_2 F_2 + D_2 D_3 F_3 + \cdots + D_2 \cdots D_{N_k - 1} H_{N_k - 1}, \\
&\qquad F_1 + D_2 F_2 + D_2 D_3 F_3 + \cdots + \cdots + D_2 \cdots D_{N_k} H_{N_k}, \\
&\qquad F_1 + D_2 F_2 + D_2 D_3 F_3 + \cdots + \cdots + D_2 \cdots D_{N_k} F_{N_k})) \\
&+(A_r + B_r M_n \beta(\theta, H_1, F_1 + D_2 H_2, \\
&\qquad F_1 + D_2 F_2 + D_2 D_3 H_3, \\
&\qquad \vdots \\
&\qquad F_1 + D_2 F_2 + D_2 D_3 F_3 + \cdots + D_2 \cdots D_{N_k - 1} H_{N_k - 1}, \\
&\qquad F_1 + D_2 F_2 + D_2 D_3 F_3 + \cdots + \cdots + D_2 \cdots D_{N_k} H_{N_k}, \\
&\qquad F_1 + D_2 F_2 + D_2 D_3 F_3 + \cdots + \cdots + D_2 \cdots D_{N_k} F_{N_k}))^T P < 0,
\end{aligned}
\tag{52}
$$

and $\Omega(P_r, \rho) \in \bigcap_{i=1}^{N_k} \mathcal{L}(H_i)$, then $\Omega(P_r, \rho)$ is a contractively invariant set of the system (50) with $\nu_h \equiv 0$. The set $\mathcal{L}(H_i)$ is defined as

$$
\mathcal{L}(H_i) \triangleq \left\{ e_r \in \mathcal{R}^{N_k} : |H_i e_r| \leq 1 \right\}. \tag{53}
$$

Here, for conciseness and clarity, $N_k \triangleq n_1 + \ldots + n_k$, $F_i \triangleq M_{N_k - i + 1}^{-1} K_{N_k - i + 1}$, $D_i \triangleq M_{N_k - i + 1}$ for $i = 1, \cdots, N_k$. The set $\Theta = \{\theta \in \mathcal{R}^k : \theta_i \in [1, N_k + 1]\}$. The vector θ is essentially used to choose from among the rows of matrices that are arguments to the function β. The set Θ represents all such combinations. The structure of the matrix $\beta(\theta, \cdots, \cdots)$ and a description on generating Θ is given in [3]. The domain of attraction may be estimated by maximizing the size of an assumed reference set over $H_1, \cdots, H_{N_k}, P_r > 0$, subject to the above invariance conditions. For details see [20, 22, 3].

Remark 2. *Note that Eqn (52) essentially verifies that for every possible combination of saturation that occurs, there exists a control law (of possibly very low gain) that can de-saturate all the saturation functions and stabilize the system at the same time.*

Theorem 4. *Consider the cascade of systems given by (27), with the inverse law (29), reference model (50) which is consistent with (30), where the gains are the same as those selected such that the system matrix in (33) is Hurwitz and assumptions (2, 3, 4, 5, 7), where the NN training signal, r, NN output, ν_{ad}, and robustifying term, ν_r, are given by*

$$r = (e^T PB)^T$$

$$\bar{\nu}_{ad} = \nu_{ad} + \nu_r$$

$$\nu_{ad} = W^T \sigma(V^T \bar{x})$$

$$\nu_r = -K_r(\|Z\|_F + \bar{Z}) r \frac{\|e\|}{\|r\|}.$$

If $K_r > 0 \in \mathcal{R}^{k \times k}$ is chosen sufficiently large with lower-limit stated in the proof, and NN weights W, V satisfy the adaptation laws

$$\dot{W} = -\left[(\sigma - \sigma' V^T \bar{x}) r^T + \kappa \|e\| W\right] \Gamma_W$$

$$\dot{V} = -\Gamma_V \left[\bar{x}(r^T W^T \sigma') + \kappa \|e\| V\right],$$

with, $\Gamma_W, \Gamma_V > 0$, $\kappa > 0$ with lower-limit stated in the proof, and the external command $x_c(t)$ is such that $e_r(t) \in \Omega(P_r, \rho)$, for some $\rho > 0$, then, the command tracking error, e_r, the reference model tracking error, e, and NN weights $(\tilde{W}, \tilde{V})$ are uniformly ultimately bounded. Further, the plant states, x, are ultimately bounded.

Proof. See Section A.3 □

4.4 Constrained Linear Model

A special case of the nested saturation reference model is given by Eqn (55) which allows one to impose prescribable limits on the evolution of the error states. For example, consider the following reference model for the second order position dynamics

of a system, where a given large position command is at a maximum speed of v_{max} and a maximum acceleration of a_{max}.

$$\begin{aligned}\dot{x}_{r_1} &= x_{r_2} \\ \dot{x}_{r_2} &= \nu_{cr} = M_2\sigma_2\left(\frac{K_2}{M_2}\left(e_{r_2} + M_1\sigma_1\left(\frac{K_1}{M_1K_2}e_{r_1}\right)\right)\right),\end{aligned} \tag{54}$$

where $M_2 = a_{max}$ and $M_1 = v_{max}$. For large position errors and a zero commanded velocity, σ_1 is saturated and the dynamics are governed by $\dot{x}_{r_2} = K_2(e_{r_2} \pm M_1)$. An equilibrium point for this system is when $x_{r_2} = M_1 = v_{max}$. A similar analysis can be made for when σ_2 is saturated. Consider the single subsystem case with n states and PCH signal.

$$\begin{aligned}\dot{x}_{r_i} &= x_{r_{i+1}} \qquad i = 1, 2, \cdots, n-1 \\ \dot{x}_{r_n} &= M_n\sigma_n\left[\frac{K_n}{M_n}\left(e_{r_n} + M_{n-1}\sigma_{n-1}\left(\frac{K_{n-1}}{M_{n-1}K_n}\left(e_{r_{n-1}}\ldots + M_1\sigma_1\left(\frac{K_1}{M_1K_2}e_{r_1}\right)\right)\right)\right)\right] \\ &\quad - \nu_h,\end{aligned} \tag{55}$$

When none of the limit functions σ_i are active, Eqn (55) is the same as Eqn (46). The functions σ_i are unity saturation functions. These limits (multipliers) may be chosen such that PCH signal activity is reduced. It is possible that these parameters may be derived from practical limits such as speed, attitude, angular rate and angular acceleration limits that may be prescribed for an air vehicle[30]. Theorem 4 is also applicable to ascertain boundedness of this reference model.

Nested saturation-based reference models including the constrained linear model however have certain properties that must be recognized. For example, consider the second order reference model (ignoring PCH) of Eqn (54) with desired real poles at $-a_1, -a_2 \in \mathcal{R} < 0$. Based on this desired behavior in the linear region, the constrained linear model has the following dynamics.

with $K_1 = a_1 a_2, K_2 = (a_1 + a_2)$. When neither σ_1 or σ_2 is saturated, the characteristic equation becomes

$$s^2 + K_2 s + K_1 = s^2 + (a_1 + a_2)s + a_1 a_2,$$

which has roots at $-a_1, -a_2$. Now assume that σ_1 becomes saturated, then the system becomes

$$\dot{x}_{r_n} = K_2 e_{r_2} \pm M_1,$$

where M_1 is the saturation limit for $\sigma_1(\cdot)$. This system has the characteristic equation

$$s(s + K_2) = s(s + a_1 + a_2),$$

where one of the poles has moved to the origin and the second pole has become faster (assuming both $a_1, a_2 > 0$ which is required for stability). This shifting of poles as different elements of the nonlinear reference model saturate is undesirable because these faster poles can lead to excitation of higher-order dynamics. Such problems may be avoided by choosing gains as described in Appendix B.

CHAPTER V

APPLICATION TO THE RMAX HELICOPTER

This chapter is concerned with the development of an adaptive controller for an autonomous helicopter using a neural network as the adaptive element. The attitude and translational dynamics are input-state feedback linearized separately using dynamic inversion and linear controllers are designed for the linearized dynamics. The effect of nonlinear parametric uncertainty arising due to approximate inversion is minimized using an adaptive element. A nonlinearly parameterized NN will be used to provide on-line adaptation. The design is such that actuator saturation limits are not avoided or prevented. A common assumption when designing control systems for air vehicles is the timescale separation [57] between the inner-loop attitude control and outer-loop trajectory control systems. The assumption allows the inner loop and outer loop to be designed separately but requires the outer-loop bandwidth to be much lower than that of the inner loop. Selecting linear compensator gains through a combined analysis of the two loops places the closed loop position response poles at desired locations. This allows the outer-loop bandwidth to be closer to that of the inner loop, thus increasing position tracking performance. PCH is used to protect outer-loop adaptation from inner-loop dynamics and inner-loop adaptation from actuator dynamics. Additionally, the flight results presented in this chapter are the first where adaptation is used to compensate for modeling errors in all six degrees of freedom. We first develop the adaptive controller architecture for a generic six-degree-of-freedom air vehicle, followed by a description of the NN and selection of linear compensator gains. The controller is then applied to the trajectory and attitude control of an unmanned helicopter. The framework of chapters 3 and 4 are used

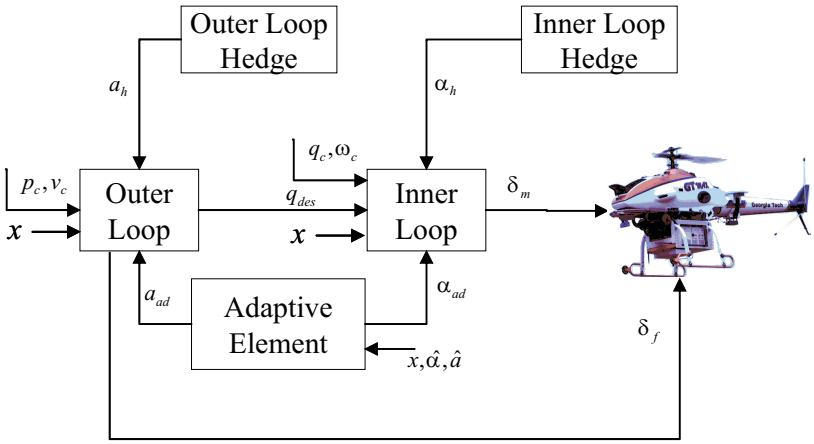

Figure 7: Overall Inner and Outerloop with Adaptation and Hedging.

to show boundedness. Practical discussions on the choice of parameters and reference model dynamics are provided. Finally, flight test results are presented.

5.1 Controller Development

Consider an air vehicle modeled as a nonlinear system of the form

$$\dot{p} = v \tag{56}$$

$$\dot{v} = a(p, v, q, \omega, \delta_f, \delta_m) \tag{57}$$

$$\dot{q} = \dot{q}(q, \omega) \tag{58}$$

$$\dot{\omega} = \alpha(p, v, q, \omega, \delta_f, \delta_m), \tag{59}$$

where, $p \in \mathcal{R}^3$ is the position vector, $v \in \mathcal{R}^3$ is the velocity of the vehicle, $q \in \mathcal{R}^4$ is the attitude quaternion and $\omega \in \mathcal{R}^3$ is the angular velocity. Eqn (57) represents translational dynamics and Eqn (59) represents the attitude dynamics. Eqn (58) represents the quaternion propagation equations [68]. The use of quaternions, though not a minimal representation of attitude, avoids numerical and singularity problems that Euler-angles-based representations have. This enables the control system to be all attitude capable as required for aggressive maneuvering. The state vector x may now be defined as $x \triangleq \begin{bmatrix} p^T & v^T & q^T & \omega^T \end{bmatrix}^T$.

The control vectors are denoted by δ_f and δ_m and represent actual physical actuators on the aircraft, where δ_f denotes the primary force generating actuators and δ_m denotes the primary moment generating actuators. For a helicopter, the main force effector is the rotor thrust which is controlled by changing main rotor collective δ_{coll}. Hence $\delta_f \in \mathcal{R} = \delta_{coll}$. There are three primary moment control surfaces, the lateral cyclic δ_{lat}, longitudinal cyclic δ_{lon}, and tail rotor pitch, also called the pedal input δ_{ped}. Hence, $\delta_m \in \mathcal{R}^3 = \begin{bmatrix} \delta_{lat} & \delta_{lon} & \delta_{ped} \end{bmatrix}^T$. This classification of the controls as moment and force generating, is an artefact of the inner-loop–outer-loop control design strategy. In general, both control inputs, δ_f and δ_m, may each produce forces and moments. The helicopter is an under-actuated system, and hence, the aircraft attitude, q, is treated like a virtual actuator used to tilt the main rotor thrust in order to produce desired accelerations. Defining the consolidated control vector δ as

$$\delta \triangleq \begin{bmatrix} \delta_f^T & \delta_m^T \end{bmatrix}^T,$$

the actuators themselves may have dynamics represented by

$$\dot{\delta} = \begin{bmatrix} \dot{\delta}_m \\ \dot{\delta}_f \end{bmatrix} = \begin{bmatrix} g_m(x, \delta_m, \delta_{m_{des}}) \\ g_f(x, \delta_f, \delta_{f_{des}}) \end{bmatrix} = g(x, \delta, \delta_{des}), \tag{60}$$

where $g(\cdot)$ is assumed to be asymptotically stable but perhaps unknown.

When any actuator dynamics and nonlinearities are ignored, approximate feedback linearization of the system represented by (56, 57, 58, 59) is achieved by introducing the following transformation:

$$\begin{bmatrix} a_{des} \\ \alpha_{des} \end{bmatrix} = \begin{bmatrix} \hat{a}(p, v, q_{des}, \omega, \delta_{f_{des}}, \hat{\delta}_m) \\ \hat{\alpha}(p, v, q, \omega, \hat{\delta}_f, \delta_{m_{des}}) \end{bmatrix},$$

where, a_{des}, α_{des} are commonly referred to as the pseudocontrol and represent desired accelerations. Here, $\hat{a}$, $\hat{\alpha}$ represent an available approximation of $a(\cdot)$ and $\alpha(\cdot)$. Additionally, $\delta_{f_{des}}, \delta_{m_{des}}, q_{des}$ are the control inputs and attitude that are predicted to

achieve the desired pseudo-control. This form assumes that translational dynamics are coupled strongly with attitude dynamics, as is the case for a helicopter. From the outer-loop's point of view, q (attitude), is like an actuator that generates translational accelerations and q_{des} is the desired attitude that the outer-loop inversion expects will contribute towards achieving the desired translational acceleration, a_{des}. The dynamics of q appears like actuator dynamics to the outer loop. The attitude quaternion q_{des} will be used to augment the externally commanded attitude q_c to achieve the desired translational accelerations. Because actuator positions are often not measured on small helicopters, estimates of the actuator positions $\hat{\delta}_m, \hat{\delta}_f$ are used. For cases where the actuator positions are directly measured, they may be regarded as known $\hat{\delta}_m = \delta_m$ and $\hat{\delta}_f = \delta_f$. In fact, in the outer loop's case, the attitude q is measured using inertial sensors. When $\hat{a}$ and $\hat{\alpha}$ are chosen such that they are invertible, the desired control and attitude may be written as

$$\begin{bmatrix} \delta_{f_{des}} \\ q_{des} \end{bmatrix} = \begin{bmatrix} \hat{a}_{\delta_f}^{-1}(p, v, a_{des_{\delta_f}}, \omega, \hat{\delta}_m) \\ \hat{a}_q^{-1}(p, v, a_{des_q}, \omega, \hat{\delta}_m) \end{bmatrix} \tag{61}$$
$$\delta_{m_{des}} = \hat{\alpha}^{-1}(p, v, q, \omega, \hat{\delta}_f, \alpha_{des}),$$

with $a_{des_{\delta_f}} + a_{des_q} = a_{des}$, $\hat{a}_{\delta_f}, \hat{a}_q$ formulated to be consistent with Eqn (61) and where actuator estimates are given by actuator models

$$\dot{\hat{\delta}} = \begin{bmatrix} \dot{\hat{\delta}}_f \\ \dot{\hat{\delta}}_m \end{bmatrix} = \begin{bmatrix} \hat{g}_f(x, \hat{\delta}_f, \delta_{f_{des}}) \\ \hat{g}_m(x, \hat{\delta}_m, \delta_{m_{des}}) \end{bmatrix} = \hat{g}(x, \hat{\delta}, \delta_{des}). \tag{62}$$

In later sections, it will be shown that $\hat{\alpha}$, can just be an approximate linear model of vehicle attitude dynamics and $\hat{a}$ a set of simple equations relating translational accelerations to the attitude of the vehicle. Introducing the inverse control law Eqn (61) into Eqn (57) and Eqn (59) results in the following closed-loop translational and

attitude dynamics

$$\begin{aligned}\dot{v} &= a_{des} + \bar{\Delta}_a(x, \delta, \hat{\delta}) - a_h \\ \dot{\omega} &= \alpha_{des} + \bar{\Delta}_\alpha(x, \delta, \hat{\delta}) - \alpha_h,\end{aligned} \tag{63}$$

where

$$\bar{\Delta}(x, \delta, \hat{\delta}) = \begin{bmatrix} \bar{\Delta}_a(x, \delta, \hat{\delta}) \\ \bar{\Delta}_\alpha(x, \delta, \hat{\delta}) \end{bmatrix} = \begin{bmatrix} a(x, \delta) - \hat{a}(x, \hat{\delta}) \\ \alpha(x, \delta) - \hat{\alpha}(x, \hat{\delta}) \end{bmatrix}, \tag{64}$$

are static nonlinear functions (model error) that arise due to imperfect model inversion and errors in the actuator model $\hat{g}$. The signals, a_h and α_h, represent the pseudocontrol that cannot be achieved due to actuator input characteristics such as saturation. If the model inversion were perfect and no saturation were to occur, $\bar{\Delta}, a_h$ and α_h would vanish leaving only the pseudocontrols a_{des} and α_{des}. One may address model error and stabilize the linearized system by designing the pseudocontrols as

$$\begin{aligned}a_{des} &= a_{cr} + a_{pd} - \bar{a}_{ad} \\ \alpha_{des} &= \alpha_{cr} + \alpha_{pd} - \bar{\alpha}_{ad},\end{aligned} \tag{65}$$

where a_{cr} and α_{cr} are outputs of reference models for the translational and attitude dynamics respectively. a_{pd} and α_{pd} are outputs of proportional-derivative (PD) compensators; and finally, $\bar{a}_{ad}$ and $\bar{\alpha}_{ad}$ are the outputs of an adaptive element (an NN) designed to cancel model error $\bar{\Delta}$. The effects of input dynamics, represented by a_h, α_h will first be addressed in the following section by designing the reference model dynamics such that they do not appear in the tracking error dynamics. The reference model, tracking error dynamics and adaptive element are discussed in the following sections.

5.1.1 Reference Model and PCH

Any dynamics and nonlinearities associated with the actuators δ_m, δ_f have not yet been considered in the design. If they become saturated (position or rate), the reference models will continue to demand tracking as though full authority were still

available. Furthermore, the inner loop appears like an actuator with dynamics to the outer loop. Practical operational limits on the maximum attitude of the aircraft may have also been imposed in the inner-loop reference model. This implies that the outer-loop desired attitude augmentation q_{des} may not actually be achievable, or at the very least is subject to the inner-loop dynamics. When an adaptive element such as a neural network is introduced, these input dynamics and nonlinearities will appear in the tracking error dynamics resulting in the adaptive element attempting to correct for them and is undesirable. PCH may be used to prevent the adaptive element from attempting to adapt to these input characteristics. The reference model dynamics may be redesigned to include PCH as follows

$$\dot{v}_r = a_{cr}(p_r, v_r, p_c, v_c) - a_h \tag{66}$$

$$\dot{\omega}_r = \alpha_{cr}(q_r, \omega_r, q_c \oplus q_{des}, \omega_c) - \alpha_h, \tag{67}$$

where p_r and v_r are the outer-loop reference model states whereas q_r, ω_r, are the inner-loop reference model states, a_h and α_h are the difference between commanded pseudocontrol and achieved pseudocontrol. The external command signal is $x_c = \begin{bmatrix} p_c^T & v_c^T & q_c^T & \omega_c^T \end{bmatrix}^T$. Note that the attitude desired by the outer loop is now added to the commands for the inner loop controller. Here, $q_c \oplus q_{des}$ denotes quaternion addition[68]. The PCH signals are given by

$$\begin{aligned} a_h &= \hat{a}(p, v, q_{des}, \omega, \delta_{f_{des}}, \hat{\delta}_m) - \hat{a}(p, v, q, \omega, \hat{\delta}_f, \hat{\delta}_m) \\ &= a_{des} - \hat{a}(p, v, q, \omega, \hat{\delta}_f, \hat{\delta}_m) \end{aligned} \tag{68}$$

$$\begin{aligned} \alpha_h &= \hat{\alpha}(p, v, q, \omega, \hat{\delta}_f, \delta_{m_{des}}) - \hat{\alpha}(p, v, q, \omega, \hat{\delta}_f, \hat{\delta}_m) \\ &= \alpha_{des} - \hat{\alpha}(p, v, q, \omega, \hat{\delta}_f, \hat{\delta}_m). \end{aligned} \tag{69}$$

Note that the hedge signals a_h, α_h, do not directly affect the reference model output a_{cr}, α_{cr}, but do so only through subsequent changes in the reference model states.

5.1.2 Tracking error dynamics

One may define the tracking error vector, e, as

$$e \triangleq \begin{bmatrix} p_r - p \\ v_r - v \\ \tilde{Q}(q_r, q) \\ \omega_r - \omega \end{bmatrix}, \tag{70}$$

where, $\tilde{Q} : \mathcal{R}^4 \times \mathcal{R}^4 \mapsto \mathcal{R}^3$, is a function[27] that, given two quaternions results in an error angle vector with three components. An expression for $\tilde{\boldsymbol{Q}}$ is given by

$$\begin{aligned} \tilde{Q}(p, q) = 2sgn(q_1 p_1 + q_2 p_2 + q_3 p_3 + q_4 p_4) \times \\ \begin{bmatrix} -q_1 p_2 + q_2 p_1 + q_3 p_4 - q_4 p_3 \\ -q_1 p_3 - q_2 p_4 + q_3 p_1 + q_4 p_2 \\ -q_1 p_4 + q_2 p_3 - q_3 p_2 + q_4 p_1 \end{bmatrix}. \end{aligned} \tag{71}$$

The output of the PD compensators may be written as

$$\begin{bmatrix} a_{pd} \\ \alpha_{pd} \end{bmatrix} = \begin{bmatrix} R_p & R_d & 0 & 0 \\ 0 & 0 & K_p & K_d \end{bmatrix} e, \tag{72}$$

where, $R_p, R_d \in \mathcal{R}^{3\times3}$, $K_p, K_d \in \mathcal{R}^{3\times3}$ are linear gain positive definite matrices whose choice is discussed below. The tracking error dynamics may be found by directly differentiating Eqn (70)

$$\dot{e} = \begin{bmatrix} v_r - v \\ \dot{v}_r - \dot{v} \\ \omega_r - \omega \\ \dot{\omega}_r - \dot{\omega} \end{bmatrix}.$$

Considering $\dot{e}_2$,

$$\begin{aligned}
\dot{e}_2 &= \dot{v}_r - \dot{v} \\
&= a_{cr} - a_h - a(x,\delta) \\
&= a_{cr} - a_{des} + \hat{a}(x,\hat{\delta}) - a(x,\delta) \\
&= a_{cr} - a_{pd} - a_{cr} + \bar{a}_{ad} + \hat{a}(x,\hat{\delta}) - a(x,\delta) \\
&= -a_{pd} - (a(x,\delta) - \hat{a}(x,\hat{\delta}) - \bar{a}_{ad}) \\
&= -a_{pd} - (\bar{\Delta}_a(x,\delta,\hat{\delta}) - \bar{a}_{ad}),
\end{aligned}$$

$\dot{e}_4$ may be found similarly. Then, the overall tracking error dynamics may now be expressed as

$$\dot{e} = Ae + B\left[\bar{\nu}_{ad} - \bar{\Delta}(x,\delta,\hat{\delta})\right], \tag{73}$$

where, $\bar{\Delta}$ is given by Eqn (64),

$$\bar{\nu}_{ad} = \begin{bmatrix} \bar{a}_{ad} \\ \bar{\alpha}_{ad} \end{bmatrix}, A = \begin{bmatrix} 0 & I & 0 & 0 \\ -R_p & -R_d & 0 & 0 \\ 0 & 0 & 0 & I \\ 0 & 0 & -K_p & -K_d \end{bmatrix}, B = \begin{bmatrix} 0 & 0 \\ I & 0 \\ 0 & 0 \\ 0 & I \end{bmatrix}. \tag{74}$$

and so the linear gain matrices must be chosen such that A is Hurwitz. Now, $\bar{\nu}_{ad}$ remains to be designed in order to cancel the effect of $\bar{\Delta}$.

Remark 3. *(a) Note that commands, $\delta_{m_{des}}, \delta_{f_{des}}, q_{des}$, do not appear in the tracking error dynamics. PCH allows adaptation to continue when the actual control signal has been replaced by any arbitrary signal and thus allows switching between manual and automatic flight during flight tests. (b) If the actuator is considered ideal and the actual position and the commanded position are equal, addition of the PCH signal a_h, α_h has no effect on any system signal.*

The adaptive signal $\bar{\nu}_{ad}$ contains two terms

$$\bar{\nu}_{ad} = \nu_{ad} + \nu_r = \begin{bmatrix} a_{ad} + a_r \\ \alpha_{ad} + \alpha_r \end{bmatrix},$$

where ν_{ad} is the output of the SHL NN described in Section 2.3. For an air vehicle with adaptation in all degrees of freedom, $\nu_{ad} \in \mathcal{R}^6$, where the first three outputs, a_{ad}, approximates Δ_a and the last three outputs, α_{ad}, approximate Δ_α and is consistent with the definition of the error in Eqn (70). The term, $\nu_r = [a_r^T, \alpha_r^T]^T \in \mathcal{R}^6$ is a robustifying signal that arises in the proof of boundedness.

5.2 Boundedness

Associated with the tracking error dynamics given in Eqn (73), is the Lyapunov function

$$A^T P + PA + Q = 0. \tag{75}$$

Choosing positive definite [27]

$$\begin{aligned} Q &= \begin{bmatrix} Q_1 & 0 \\ 0 & Q_2 \end{bmatrix} \frac{1}{\frac{1}{4}n_2 + b_w^2} \\ Q_1 &= \begin{bmatrix} R_d R_p^2 & 0 \\ 0 & R_d R_p \end{bmatrix} > 0 \\ Q_2 &= \begin{bmatrix} K_d K_p^2 & 0 \\ 0 & K_d K_p \end{bmatrix} > 0. \end{aligned} \tag{76}$$

Making use of the property that $R_p, R_d, K_p, K_d > 0$ and diagonal, results in a positive definite solution for P. Hence,

$$\begin{aligned} P &= \begin{bmatrix} P_1 & 0 \\ 0 & P_2 \end{bmatrix} \frac{1}{\frac{1}{4}n_2 + b_w^2} \\ P_1 &= \begin{bmatrix} R_p^2 + \frac{1}{2}R_p R_d^2 & \frac{1}{2}R_p R_d \\ \frac{1}{2}R_p R_d & R_p \end{bmatrix} > 0 \\ P_2 &= \begin{bmatrix} K_p^2 + \frac{1}{2}K_p K_d^2 & \frac{1}{2}K_p K_d \\ \frac{1}{2}K_p K_d & K_p \end{bmatrix} > 0. \end{aligned} \tag{77}$$

The inputs to the NN have to be chosen to satisfy the functional dependence of $\Delta(x, \hat{\delta})$ and may be specified as

$$\begin{aligned} \bar{x}^T &= \begin{bmatrix} b_v & x_{in}^T \end{bmatrix} \\ x_{in}^T &= \begin{bmatrix} x_c^T & e_r^T & e^T & \nu_{ad}^T & \|Z\|_F \end{bmatrix}. \end{aligned} \tag{78}$$

Note that with regard to the outer loop, the inner loop acts like an actuator with dynamics, at least with respect to achieving the desired attitude q_{des}. The actual attitude quaternion, q, is available and appears as a part of the state measurement. Hence, it is always available as an input to the adaptive element as well as in the calculation of the hedge signal.

Theorem 5. *Consider the system given by (56, 57, 58, 59), with the inverse law (61), constrained-linear reference models consistent with (66, 67), and assumptions (2, 3, 4, 5, 7), with $r, \bar{\nu}_{ad}, \nu_{ad}, \nu_r$ given by equations 37, 38, 39, 40 respectively. If $K_r > 0 \in \mathcal{R}^{6\times 6}$ is chosen sufficiently large, the adaptive laws $\dot{W}, \dot{V}$, satisfy 41, 42 with $\Gamma_W, \Gamma_V > 0$ and $\kappa > 0$ is sufficiently large, and the external command $x_c(t)$ is such that $e_r(t) \in \Omega(P_r, \rho)$, for some $\rho > 0$, then, the command tracking error, e_r, the reference model tracking error e, and NN weights $(\tilde{W}, \tilde{V})$ are uniformly ultimately bounded. Further, the plant states are ultimately bounded.*

Proof. Theorem 4 applies. □

5.3 Helicopter Specific Design

Consider the application of the combined inner-outer-loop adaptive architecture to the trajectory control of a helicopter. The dynamics [48, 47, 11] of the helicopter may be modeled in the same form as Eqns. (56-59). Most small helicopters include a Bell-Hiller stabilizer bar, which provides provide lagged rate feedback, and is a source of unmodeled dynamics. The nonlinear model used for simulation in this work included

the stabilizer bar dynamics. Additionally, blade flapping and other aspects such as gear and engine dynamics were also modeled.

5.3.1 Approximate Model

An approximate model for the attitude dynamics of the helicopter was generated by linearizing the nonlinear model around hover and neglecting coupling between the attitude and translational dynamics as well as the stabilizer bar

$$\alpha_{des} = \hat{A}_1 \begin{bmatrix} p \\ q \\ r \end{bmatrix} + \hat{A}_2 \begin{bmatrix} u \\ v \\ w \end{bmatrix} + \hat{B} \left(\underbrace{\begin{bmatrix} \delta_{lat} \\ \delta_{lon} \\ \delta_{ped} \end{bmatrix}}_{des} - \underbrace{\begin{bmatrix} \delta_{lat} \\ \delta_{lon} \\ \delta_{ped} \end{bmatrix}}_{trim} \right), \tag{79}$$

or,

$$\alpha_{des} = \hat{A}_1 \omega_B + \hat{A}_2 v_B + \hat{B}(\delta_{m_{des}} - \delta_{m_{trim}}).$$

where, $\hat{A}_1$ and $\hat{A}_2$ represent the attitude and translational dynamics respectively, ω_B represents the angular velocity of the body with respect to the earth expressed in the body frame. The body velocity velocity vector with respect to the earth expressed in the body frame is given by v_B and $\delta_{m_{trim}}$ is the trim control vector that is consistent with the linear model. Choosing the control matrix $\hat{B}$ such that it is invertible, the moment controls may be evaluated as

$$\delta_{m_{des}} = \hat{B}^{-1}(\alpha_{des} - \hat{A}_1 \omega_B - \hat{A}_2 v_B) + \delta_{m_{trim}}.$$

The translational dynamics may be modeled as a point mass with a thrust vector that may be oriented in a given direction as illustrated in Fig. 8. More involved inverses [55] may be used, but the simple relationships between thrust, attitude and accelerations suffice when used with adaptation

$$a_{des} = \begin{bmatrix} 0 \\ 0 \\ Z_{\delta_{coll}} \end{bmatrix} (\delta_{coll_{des}} - \delta_{coll_{trim}}) + L_{bv} g, \tag{80}$$

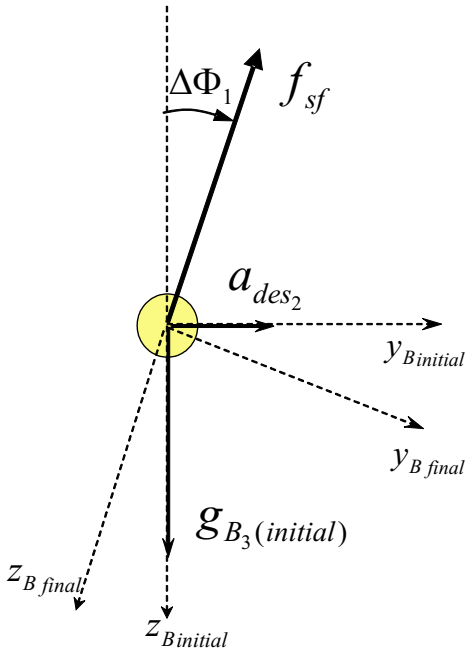

Figure 8: Point mass model for outerloop inversion.

where, $Z_{\delta_{coll}}$ is the control derivative for acceleration in the vertical axis. L_{bv} is the direction cosine matrix that transforms a vector from the vehicle (or local) frame to the body frame and g is an assumed gravity vector. The desired specific force along the body z axis may be evaluated as

$$f_{sf} = (a_{des} - L_{bv}g)_3.$$

The required collective input may be evaluated as

$$\delta_{coll_{des}} = \frac{f_{sf}}{Z_{\delta_{coll}}} + \delta_{coll_{trim}}.$$

The attitude augmentation required in order to orient the thrust vector to attain the desired translational accelerations are given by the following small angle corrections from the current reference body attitude and attitude command

$$\Delta\Phi_1 = \frac{a_{des_2}}{f_{sf}}, \quad \Delta\Phi_2 = -\frac{a_{des_1}}{f_{sf}}, \quad \Delta\Phi_3 = 0, \tag{81}$$

For this simplified helicopter model, heading change has no effect on accelerations in the x, y plane and hence $\Delta\Phi_3 = 0$. These three correction angles may now be used

to generate the attitude quaternion correction desired by the outer loop. Thus,

$$q_{des} = q(\Delta\Phi_1, \Delta\Phi_2, \Delta\Phi_3), \tag{82}$$

where, $q(.)$ is a function[68] that expresses an euler-angles-based rotation as a quaternion. The overall detailed controller architecture is shown in Fig. 9.

Remark 4. *If the desired specific force f_{sf} is close to zero, which occurs when the desired acceleration in the body z axis is the same as the component of gravity vector along that axis, then, Equation (81) is undefined. To overcome this problem, one can impose a restriction where (81) is only computed if $|f_{sf}| > \bar{f}_{sf}$, where $\bar{f}_{sf} > 0$ and is a lower limit. Essentially it means, do not bother using attitude unless the desired specific force is greater than $\bar{f}_{sf}$.*

5.3.2 Reference Model

A reasonable choice for the reference model dynamics is given by

$$\dot{v}_r = R_p(p_c - p_r) + R_d(v_c - v_r) - a_h$$
$$\dot{\omega}_r = K_p(\tilde{Q}(q_c \oplus q_{des}, q_r)) + K_d(\omega_c - \omega_r) - \alpha_h,$$

where, R_p, R_d, K_p, K_d are the same gains used for the PD compensator in Eqn (72). If limits on the angular rate or translational velocities are to be imposed, then they may be easily included in the reference model dynamics as follows

$$a_{cr} = R_d[v_c - v_r + \sigma(R_d^{-1}R_p(p_c - p_r), v_{lim})] - a_h \tag{83}$$
$$\alpha_{cr} = K_d[\omega_c - \omega_r + \sigma(K_d^{-1}K_p\tilde{Q}(q_c \oplus q_{des}, q_r), \omega_{lim})] - \alpha_h. \tag{84}$$

The function $\sigma(\cdot)$ is the saturation function and v_{lim}, ω_{lim} are the translational and angular rate limits respectively.

Remark 5. *Note that there are no limits placed on the externally commanded position, velocity, angular rate or attitude. For example, in the translational reference model, if a large position step is commanded, $p_c = [1000, 0, 0]^T ft$ and $v_c =$*

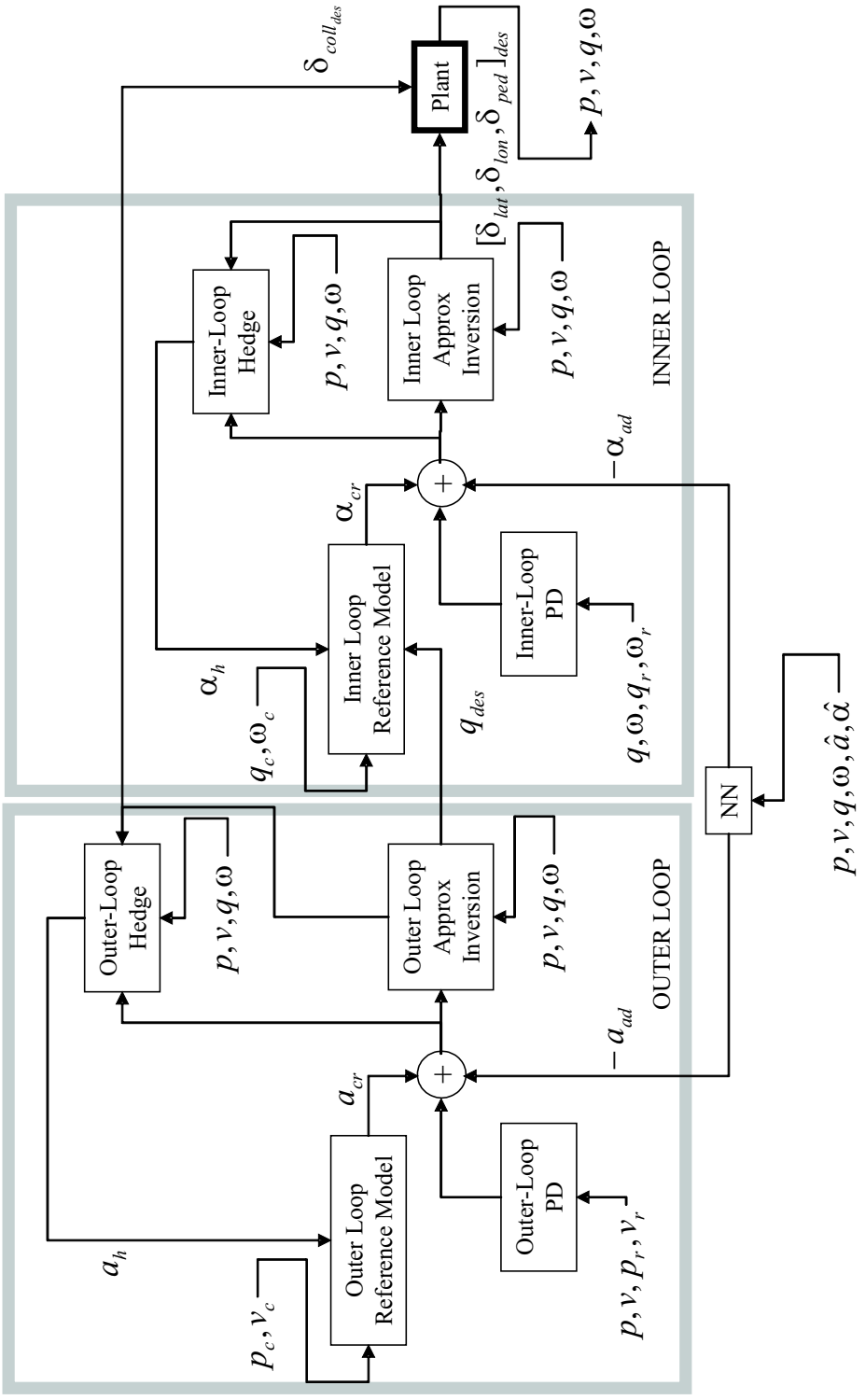

Figure 9: Detailed inner and outer loop controller architecture for an autonomous helicopter.

$[0,0,0]^T ft/s$, *the speed at which this large step will be achieved is* v_{lim}. *On the other hand if* $p_c = \int v_c dt$ *and* $v_c = [60,0,0]^T ft/s$, *the speed of the vehicle will be* $60 ft/s$. *Similarly,* ω_{lim} *dictates how fast large attitude errors will be corrected. Additionally, aggressiveness with which translational accelerations will be pursued by tilting the body may be governed by limiting the magnitude of* q_{des} *to the scalar limit* q_{lim}.

5.3.3 Choice of Gains Linear Dynamics

When the combined adaptive inner-outer-loop controller for position and attitude control is implemented, the poles for the combined error dynamics must be selected appropriately. The following analysis applies to the situation where inversion model error is compensated for accurately by the NN and we assume that the system is exactly feedback linearized. The inner loop and outer loop each represent a second order system and the resulting position dynamics $p(s)/p_c(s)$ are fourth order in directions perpendicular to the rotor spin axis.

When the closed-loop longitudinal dynamics, near hover, are considered, and with an acknowledgment of an abuse of notation, it may be written as

$$\ddot{x} = a_{des} = \ddot{x}_c + R_d(\dot{x}_c - \dot{x}) + R_p(x_c - x) \tag{85}$$

$$\ddot{\theta} = \alpha_{des} = \ddot{\theta}_g + K_d(\dot{\theta}_g - \dot{\theta}) + K_p(\theta_g - \theta), \tag{86}$$

where, R_p, R_d, K_p and K_d are the PD compensator gains for the inner loop (pitch angle) and outer loop (fore-aft position). Now x is now the position, θ the attitude and θ_g the attitude command. Normally, $\theta_g = \theta_c + \theta_{des}$ where θ_c is the external command and θ_{des} the outer-loop-generated attitude command. Here, we assume that the external attitude command and its derivatives are zero; hence, $\theta_g = \theta_{des}$. In the following development, the transfer function $x(s)/x_c(s)$ is found and used to place the poles of the combined inner-outer loop system in terms of the PD compensator gains.

When contributions of $\dot{\theta}_g(s)$ and $\ddot{\theta}_g(s)$, are ignored, the pitch dynamics Eqn (86) may be rewritten in the form of a transfer function as

$$\theta(s) = \frac{\theta(s)}{\theta_g(s)}\theta_g(s) = \frac{K_p}{s^2 + K_d s + K_p}\theta_g(s). \tag{87}$$

If the outer-loop linearizing transformation used to arrive at Eqn (85) has the form $\ddot{x} = f\theta$, where $f = -g$ and g is gravity, it may be written as

$$s^2 x(s) = f\theta(s). \tag{88}$$

The outer-loop attitude command may be generated as

$$\theta_{des} = \frac{\ddot{x}_{des}}{f} = \frac{a_{des}}{f}. \tag{89}$$

Note that $\theta_g = \theta_{des}$; if $\theta_c = 0$,

$$\theta_g = \theta_{des} = \frac{1}{f}\left[\ddot{x}_c + R_d(\dot{x}_c - \dot{x}) + R_p(x_c - x)\right]. \tag{90}$$

When Eqn (87) and Eqn (90) are used in Eqn (88)

$$s^2 x(s) = \frac{K_p\left[s^2 x_c + R_d s(x_c - x) + R_p(x_c - x)\right]}{s^2 + K_d s + K_p}, \tag{91}$$

Rearranging the above equation results in the following transfer function

$$\frac{x(s)}{x_c(s)} = \frac{K_p s^2 + K_p R_d s + K_p R_p}{s^4 + K_d s^3 + K_p s^2 + K_p R_d s + K_p R_p}. \tag{92}$$

One way to choose the gains is by examining a fourth-order characteristic polynomial written as the product of two second order systems

$$\begin{aligned}
\Upsilon(s) &= (s^2 + 2\zeta_o\omega_o + \omega_o^2)(s^2 + 2\zeta_i\omega_i + \omega_i^2) \\
&= s^4 + (2\zeta_i\omega_i + 2\zeta_o\omega_o)s^3 \\
&+ (\omega_i^2 + 4\zeta_o\omega_o\zeta_i\omega_i + \omega_o^2)s^2 \\
&+ (2\zeta_o\omega_o\omega_i^2 + 2\omega_o^2\zeta_i\omega_i)s + \omega_o^2\omega_i^2,
\end{aligned} \tag{93}$$

where, the subscripts i, o, represent the inner and outerloop values respectively.

Comparing the coefficients of the poles of Eqn (92) and Eqn (93) allows the gains to be expressed as a function of the desired pole locations for each axis in turn

$$\begin{aligned} R_p &= \frac{\omega_o^2 \omega_i^2}{\omega_i^2 + 4\zeta_o\omega_o\zeta_i\omega_i + \omega_o^2} \\ R_d &= 2\frac{\omega_o\omega_i(\zeta_o\omega_i + \omega_o\zeta_i)}{\omega_i^2 + 4\zeta_o\omega_o\zeta_i\omega_i + \omega_o^2} \\ K_p &= \omega_i^2 + 4\zeta_o\omega_o\zeta_i\omega_i + \omega_o^2 \\ K_d &= 2\zeta_i\omega_i + 2\zeta_o\omega_o. \end{aligned} \tag{94}$$

Additionally, the zeros of the transfer function given by Eqn (92) affect the transient response. Thus, $\omega_i, \zeta_i, \omega_o, \zeta_o$ must be selected such that performance is acceptable.

5.3.4 Imposing Response Characteristics

The methods presented in this thesis do not contain assumptions that limit its application to unmanned helicopters. Manned rotorcraft normally have to meet standards, such as those specified in the Aeronautical Design Standard-33 [2] handling qualities specifications. Control system performance[39, 58] may be evaluated by imposing response requirements and computing metrics prescribed in the ADS-33. When there is no saturation, the hedging signals a_h, α_h are zero. When it is assumed that the adaptation has reached its ideal values of (V^*, W^*), then

$$\begin{aligned} \dot{v} &= a_{cr} + a_{pd} + \epsilon_a \\ \dot{\omega} &= \alpha_{cr} + \alpha_{pd} + \epsilon_\alpha, \end{aligned}$$

where ϵ_a and ϵ_α are bounded by $\bar{\epsilon}$. Additionally, the Lyapunov analysis provides guaranteed model following, which implies a_{pd} and α_{pd} are small. Thus, $\dot{v} \approx a_{cr}$ and $\dot{\omega} \approx \alpha_{cr}$. Hence, as long as the preceding assumptions are valid over the bandwidth of interest, the desired response characteristics may be encoded into the reference model a_{cr} and α_{cr}.

CHAPTER VI

EXPERIMENTAL RESULTS

The proposed guidance and control architecture was applied to the Georgia Institute of Technology Yamaha R-Max helicopter (GTMax) shown in Fig. 1. The GTMax helicopter weighs about $157lb$ and has a main rotor radius of $5.05ft$. Nominal rotor speed is 850 revolutions per minute. Its practical payload capability is about $66lbs$ with a flight endurance of greater than 60 minutes. It is also equipped with a Bell-Hillier stabilizer bar. Its avionics package includes a Pentium 266 flight control computer, an inertial measurement unit (IMU), a global positioning system, a 3-axis magnetometer and a sonar altimeter. The control laws presented in this chapter were first implemented in simulation[30] using a nonlinear helicopter model that included flapping and stabilizer bar dynamics. Wind and gust models were also included. Additionally, models of sensors with associated noise characteristics were implemented. Many aspects of hardware such as the output of sensor model data as serial packets was simulated. This introduced digitization errors as would exist in real-life and also allowed testing of many flight specific components such as sensor drivers[31]. The navigation system consists of a 17-state Kalman filter to estimate variables such as attitude, and terrain altitude. The navigation filter was executed at $100Hz$ and corresponds to the highest rate at which the IMU is able to provide data. Controller calculations occurred at $50Hz$. The control laws were first implemented as C-code and tested in simulation. Because almost all aspects specific to flight-testing were included in the simulation environment, a subset of the code from the simulation environment was implemented on the main flight computer. During flight, ethernet

and serial-based data links provided a link to the ground station computer that allowed monitoring and uploading of way-points. A simple kinematics-based trajectory generator (with limits on accelerations) was used to generate smooth consistent trajectories $(p_c, v_c, q_c, \omega_c)$ for the controller. Various moderately aggressive maneuvers were performed during flight to test the performance of the trajectory-tracking controller. Controller testing began with simple hover followed by step responses and way-point navigation. Following initial flight tests, aggressiveness of the trajectory was increased by relaxing acceleration limits in the trajectory generator and relaxing ω_{lim} and v_{lim} in the reference models. Tracking error performance was increased by increasing the desired bandwidth of the controllers. Selected results from these flight tests are provided in the following sections.

6.1 Parameter Selections

The controller parameters for the inner loop involved choosing K_p, K_d based on a natural frequency of $2.5, 2, 3\ rad/s$ for the roll, pitch and yaw channels respectively and damping ratio of 1.0. For the outer loop, R_p, R_d were chosen based on a natural frequency of $2, 2.5, 3\ rad/s$ for the x, y and z body axis all with a damping ratio of unity. The NN was chosen to have 5 hidden layer neurons. The inputs to the network included body axis velocities and rates as well as the estimated pseudocontrols i.e, $x_{in} = [v_B^T, \omega_B^T, \hat{a}^T, \hat{\alpha}^T]$. The output layer learning rates[27] Γ_W were set to unity for all channels and a learning rate of $\Gamma_V = 10$ was set for all inputs. Limits on maximum translation rate and angular rate in the reference model dynamics were set to $v_{lim} = 10\ ft/s$ and $\omega_{lim} = 2\ rad/s$. Additionally, attitude corrections from the outer loop, q_{des} were limited to 30 degrees.

With regard to actuator magnitude limits, the helicopter has a radio-control transmitter that the pilot may use to fly the vehicle manually. The full deflections available on the transmitter sticks in each of the channels were mapped as $\delta_{lat}, \delta_{lon}, \delta_{ped} \in [-1, 1]$

corresponding to the full range of lateral tilt and longitudinal tilt of the swash plate and full range of tail rotor blade pitch. The collective was mapped as $\delta_{coll} \in [-2.5, 1]$, corresponding to the full range of main rotor blade pitch available to the human pilot. The dynamic characteristics of the actuators were not investigated in detail. Instead, conservative rate limits were artificially imposed in software. Noting that $\delta = [\delta_{coll}, \delta_{lat}, \delta_{lon}, \delta_{ped}]^T$, the actuator model used for PCH purposes as well as artificially limiting the controller output has form

$$\dot{\hat{\delta}} = \lim_{\lambda \to +\infty} \sigma \left(\lambda(\sigma(\delta_{des}, \delta_{min}, \delta_{max}) - \hat{\delta}), \dot{\delta}_{min}, \dot{\delta}_{max} \right), \tag{95}$$

where $\hat{\delta}$ is limited to lie in the interval $[\delta_{min}, \delta_{max}]$. The discrete implementation has the form

$$\hat{\delta}[k+1] = \sigma \left(\hat{\delta}[k] + \sigma \left(\sigma(\delta_{des}, \delta_{min}, \delta_{max}) - \hat{\delta}[k], \Delta T \dot{\delta}_{min}, \Delta T \dot{\delta}_{max} \right), \delta_{min}, \delta_{max} \right), \tag{96}$$

where ΔT is the sampling time. The magnitude limits were set to

$$\begin{aligned} \delta_{min} &= [-2.5, -1, -1, -1]^T \\ \delta_{max} &= [1, 1, 1, 1]^T \end{aligned} \tag{97}$$

units, and the rate limits were set to

$$\begin{aligned} \dot{\delta}_{min} &= [-4, -2, -2, -2]^T \\ \dot{\delta}_{max} &= [4, 2, 2, 2]^T \end{aligned} \tag{98}$$

units per second.

6.2 Flight Test

Finally, the controller was flight tested on the GTMax helicopter shown in Fig. 1. A lateral position step[1] response is shown in Fig. 10. The vehicle heading was regulated

[1]During flight tests, variables were sampled at varying rates in order to conserve memory and datalink bandwidth. The trajectory commands p_c, v_c, q_c, ω_c were sampled at $1Hz$, actuator deflections $\delta_{coll}, \delta_{lon}, \delta_{lat}$ and δ_{ped} were sampled at $50Hz$, vehicle position and speed was sampled at $50Hz$.

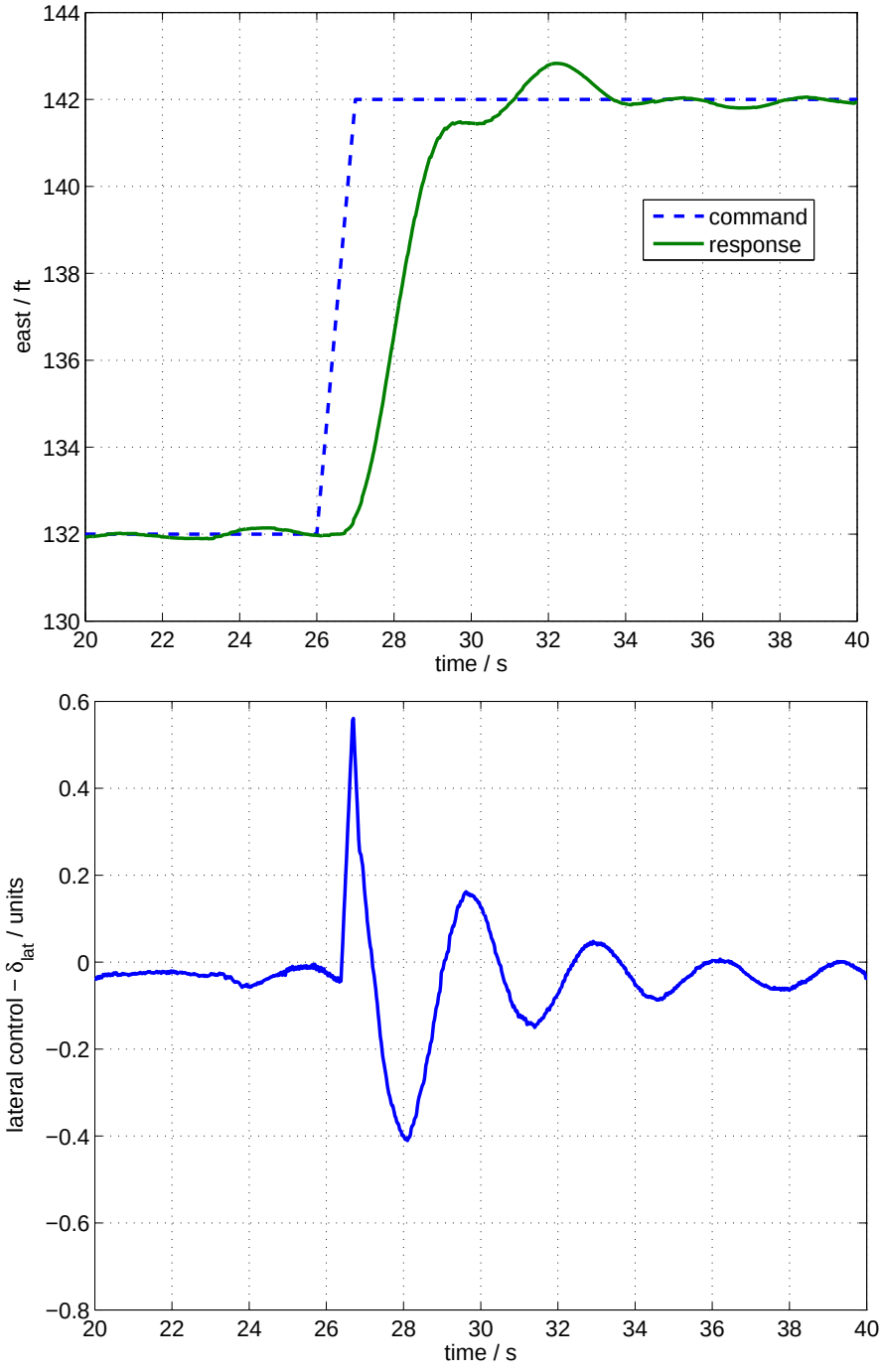

Figure 10: Response to a $20ft$ step in the lateral direction.

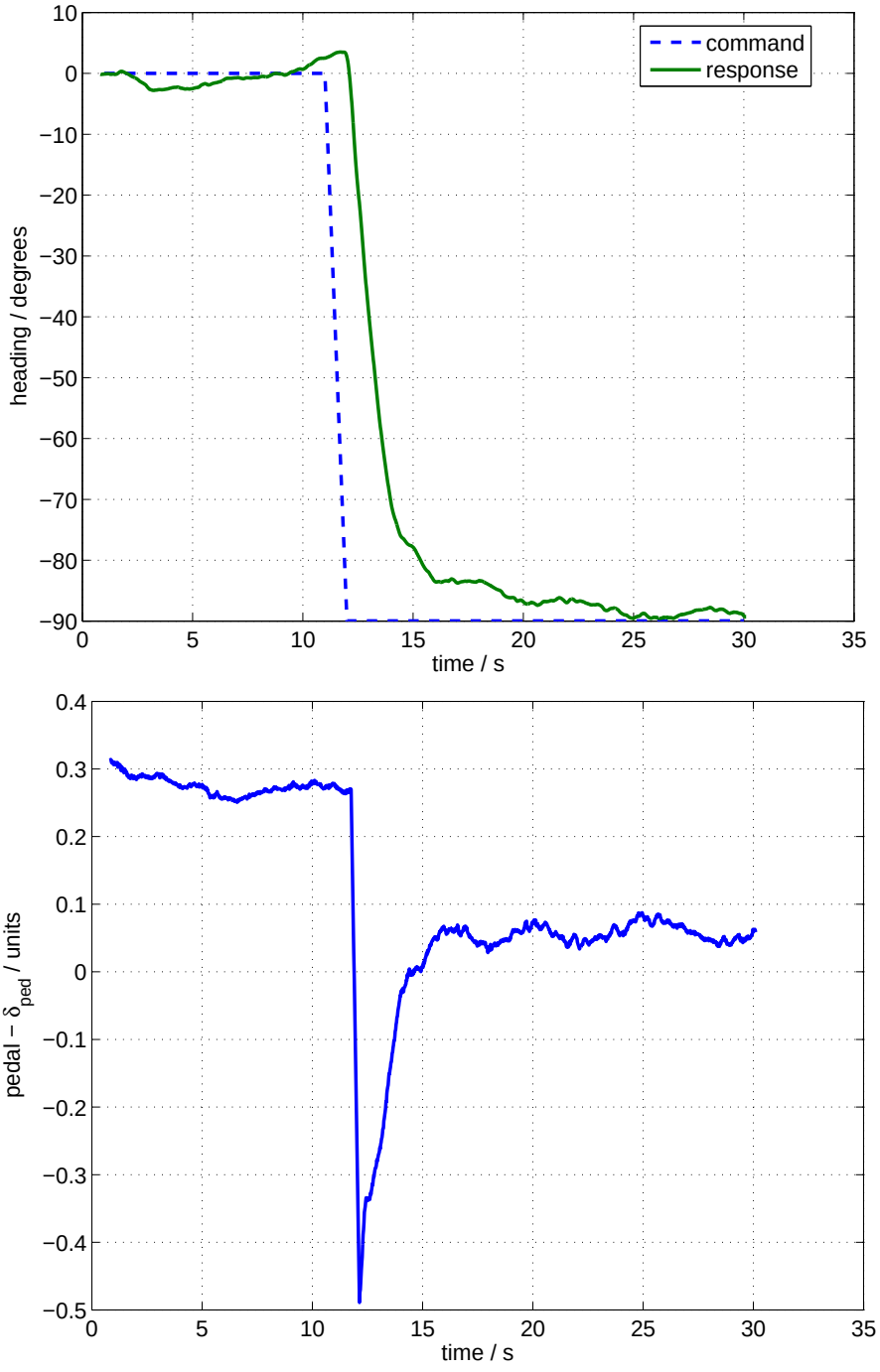

Figure 11: Response to a 90 degree heading command.

due-north during this maneuver. Lateral control deflections during the maneuver were recorded and are also shown. A step heading command response and pedal control history is shown in Fig. 11.

During takeoff and landing phases a range sensor (sonar) is used to maintain and update the estimated local terrain altitude in the navigation system. The sonar is valid up to $8ft$ above the terrain, sufficient for landing and takeoff purposes. Fig. 12 illustrates the altitude and collective profile during a landing. The vehicle starts at an initial hover at $300ft$, followed by a descent at $7ft/s$ until the vehicle is $15ft$ above the estimated terrain. The vehicle then descends at $0.5ft/s$ until weight-on-skids is automatically detected at which point the collective is slowly ramped down. Automatic takeoff (Fig. 13) is similar where the collective is slowly ramped up until weight-on-skids is no longer detected. It should be noted that NN adaptation is active at all times except when weight-on-skids is active. Additionally, when weight is on skids, the collective ramp-up during takeoff and ramp-down during landing is open-loop.

The approximate model used to compute the dynamic inverse (Eqn (80) and Eqn (79)) is based on a linear model of the dynamics in hover. To evaluate controller performance at different points of the envelope, the vehicle was commanded to track a trajectory that accelerated up to a speed of $100ft/s$. To account for wind, an upwind and downwind leg were flown. In the upwind leg the vehicle accelerated up to $80ft/s$ and during the downwind leg the vehicle accelerated up to a speed of $97ft/s$ as shown in Fig. 14. Collective and longitudinal control deflections are also shown. In the upwind leg, the collective is saturated and the vehicle is unable to accelerate further. The longitudinal control deflections behave nominally as the vehicle accelerates and decelerates through a wide range of the envelope. The NN is able to adapt to rapidly

Since the command vector is sampled at a low rate ($1Hz$), a step command appears as a fast ramp in figures.

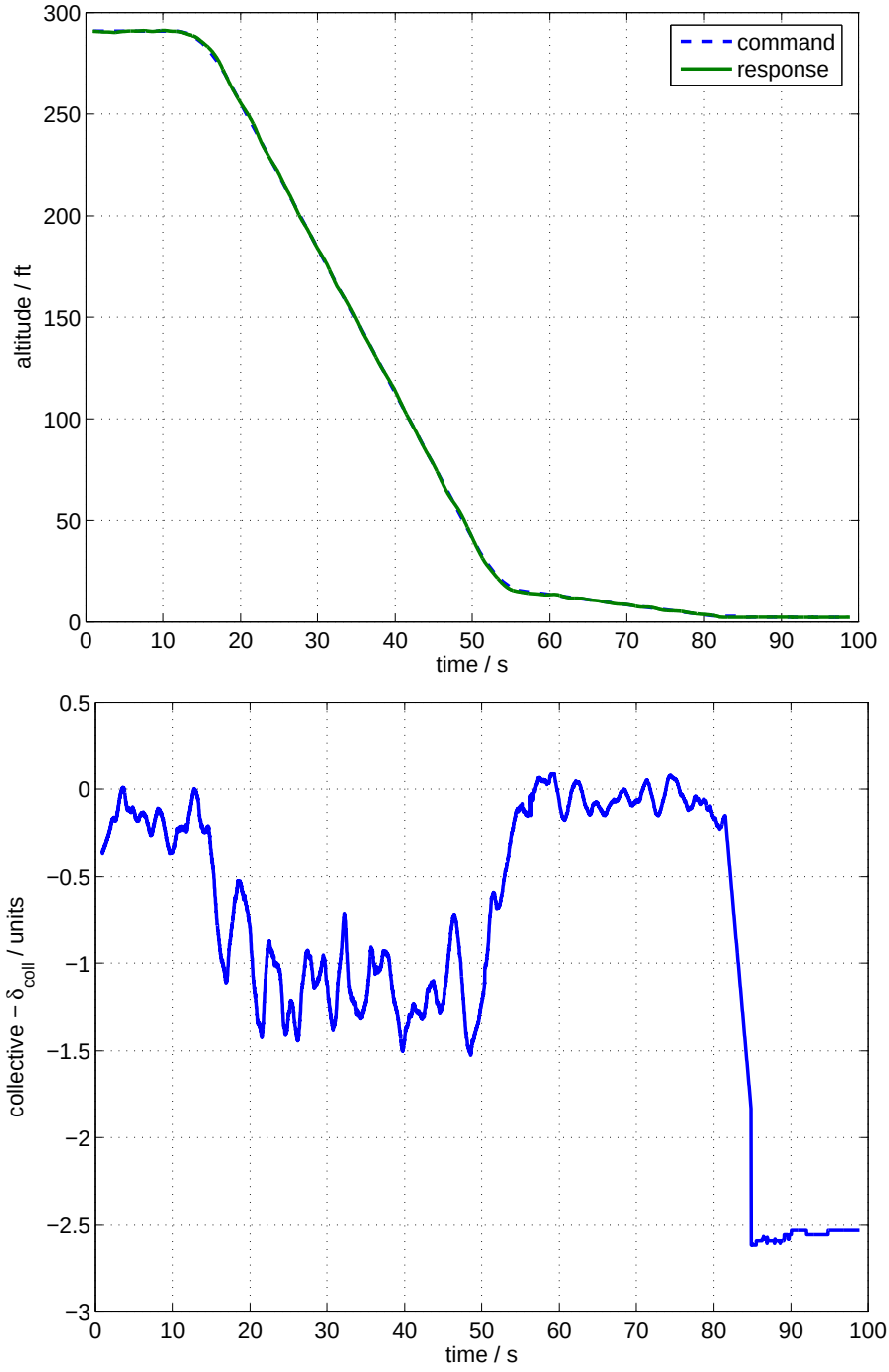

Figure 12: Automatic landing maneuver.

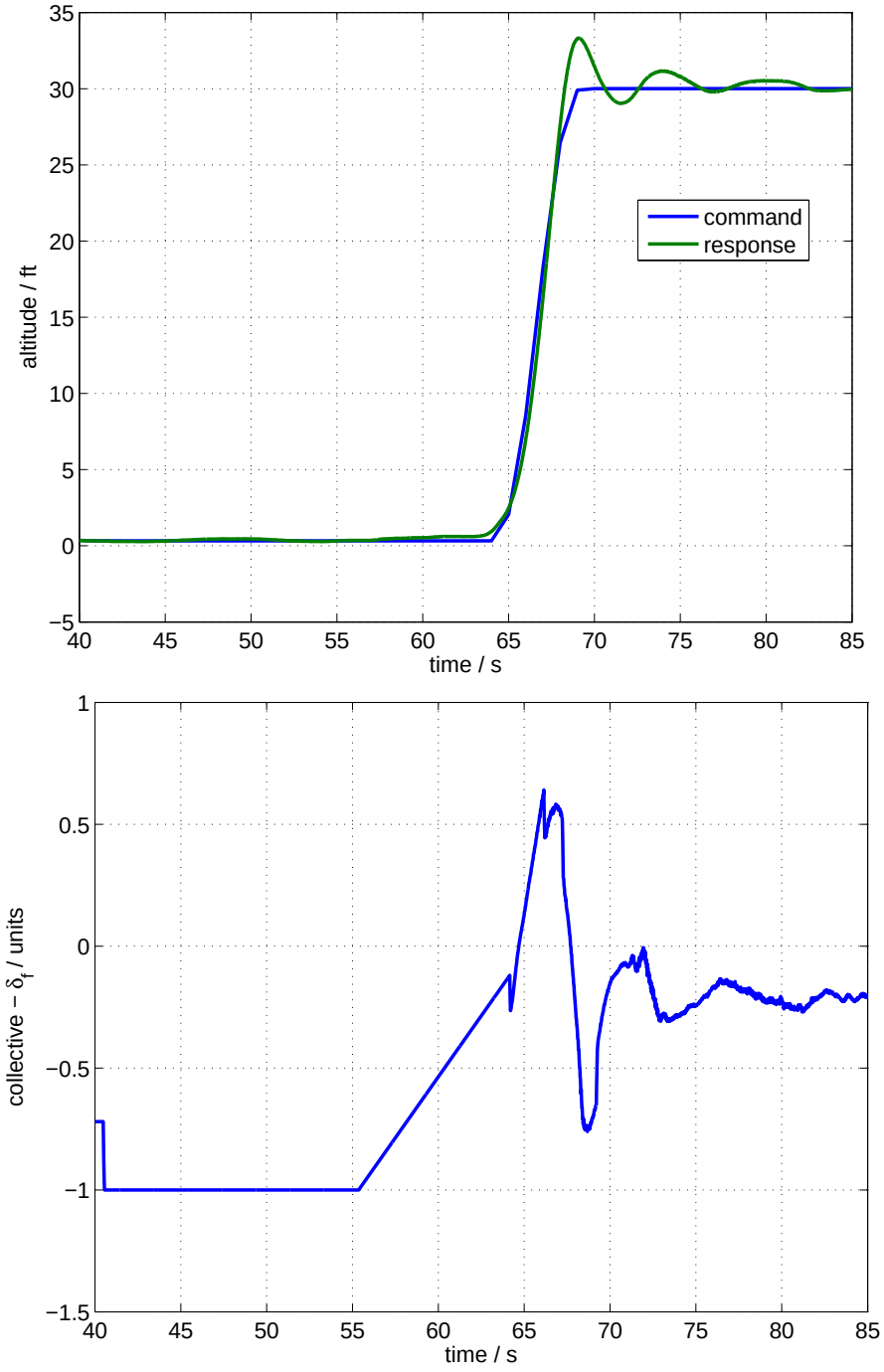

Figure 13: Automatic take-off maneuver.

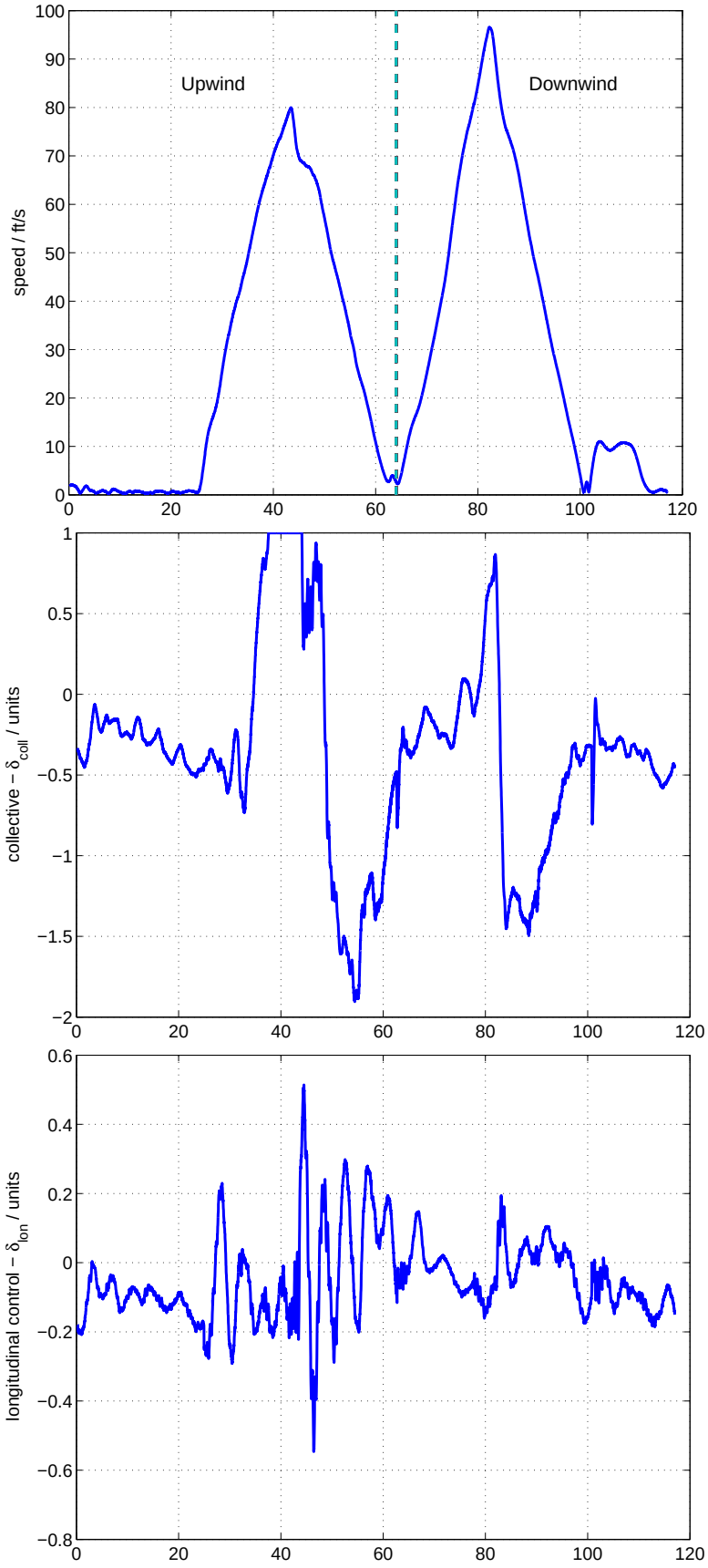

Figure 14: High speed forward flight up to $97 ft/s$.

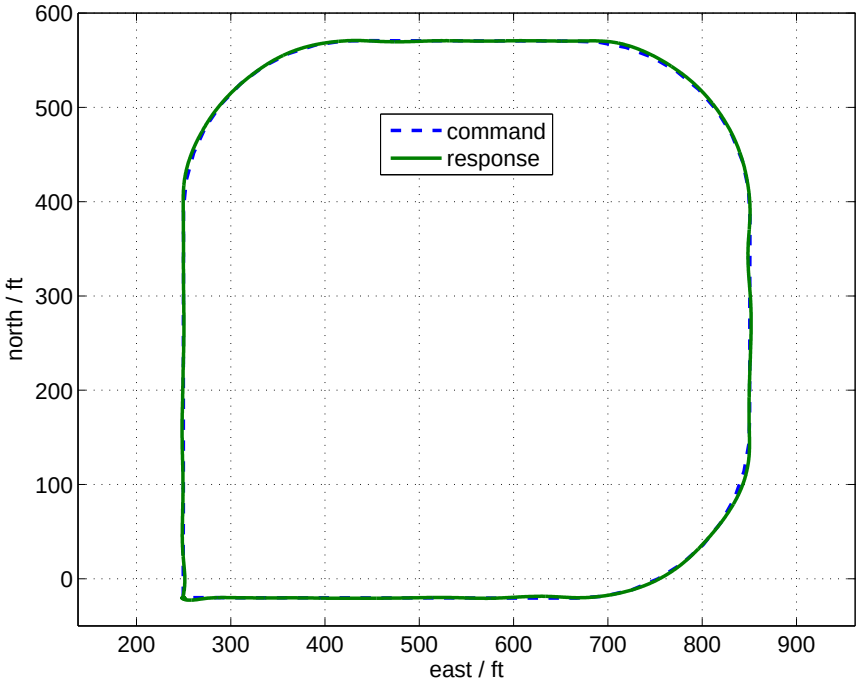

Figure 15: Flying a square pattern at $30ft/s$.

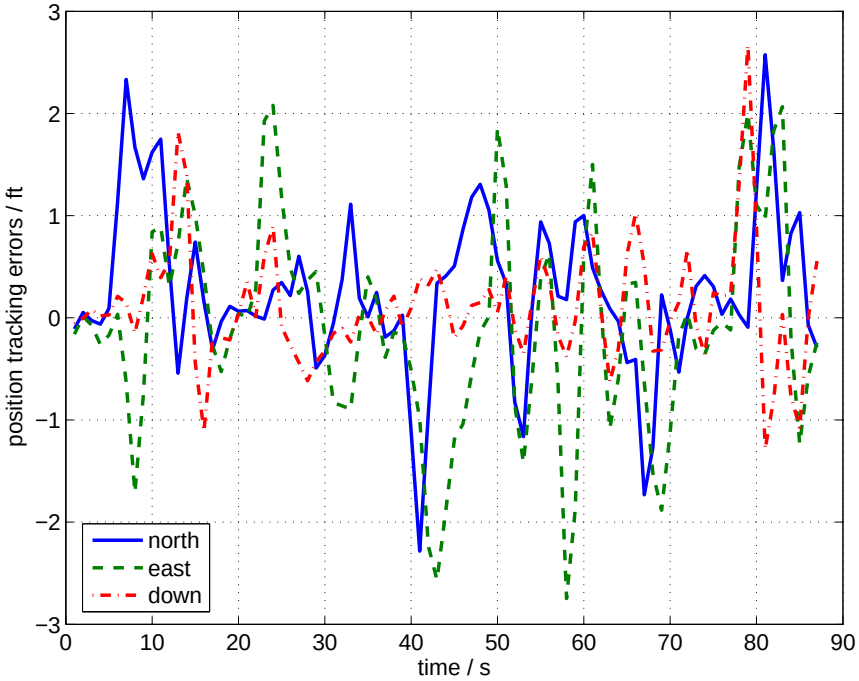

Figure 16: Command tracking errors while flying a square pattern at $30ft/s$.

changing flight conditions, from the baseline inverting design at hover through to the maximum speed of the aircraft. A conventional proportional-integral-derivative design would have required scheduling of gains throughout the speed range. More significantly, classical design would require accurate models at each point, unlike this design which does not. In addition to flight at high speeds, tracking performance was evaluated at moderate speeds, where a square pattern was flown at $30ft/s$ for which position tracking is shown in Fig. 15. External command position tracking errors are shown in Fig. 16 with a peak total position error $3.3ft$ and standard deviation of $0.8ft$.

Many maneuvers such as high-speed flight are quasi steady, in the sense that once in the maneuver, control deflection changes are only necessary for disturbance rejection. To evaluate performance where the controls have to vary significantly in order to track the commanded trajectory, the helicopter was commanded to perform a circular maneuver in the north-east plane with constant altitude and a constantly changing heading. The trajectory equations for this maneuver are given by

$$p_c = \begin{bmatrix} \frac{V}{\omega}\cos(\omega t) \\ \frac{V}{\omega}\sin(\omega t) \\ -h \end{bmatrix}, \qquad v_c = \begin{bmatrix} -V\sin(\omega t) \\ V\cos(\omega t) \\ 0 \end{bmatrix},$$

$$\psi_c = \omega t f,$$

where, t is current time and h is a constant altitude command. V is speed of the maneuver, ω is angular speed of the helicopter around the maneuver origin, and f is number of 360° changes in heading to be performed per circuit. If $\omega = \pi/2 rad/s$, the helicopter will complete the circular circuit once every 4 seconds. If $f = 1$, the helicopter will rotate anticlockwise 360° once per circuit. Fig. 17 shows the response to such a trajectory with parameters $\omega = 0.5 rad/s$, $f = 1$, $V = 10ft/s$. After the initial transition into the circular maneuver, the tracking is seen to be within 5 ft. To visualize the maneuver easily, superimposed still images of the vehicle during the

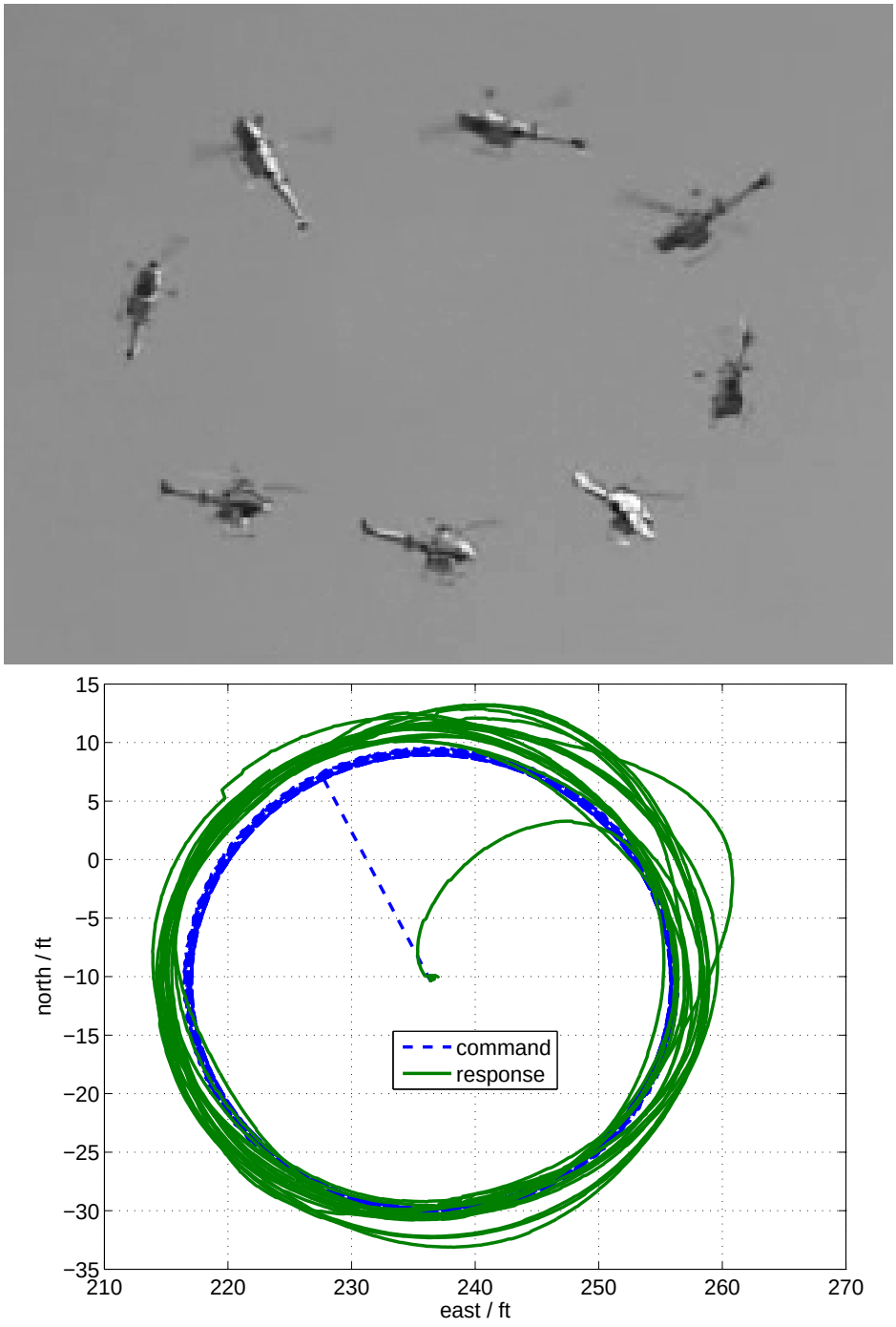

Figure 17: Circular maneuver, with 360° heading changes during the circuit.

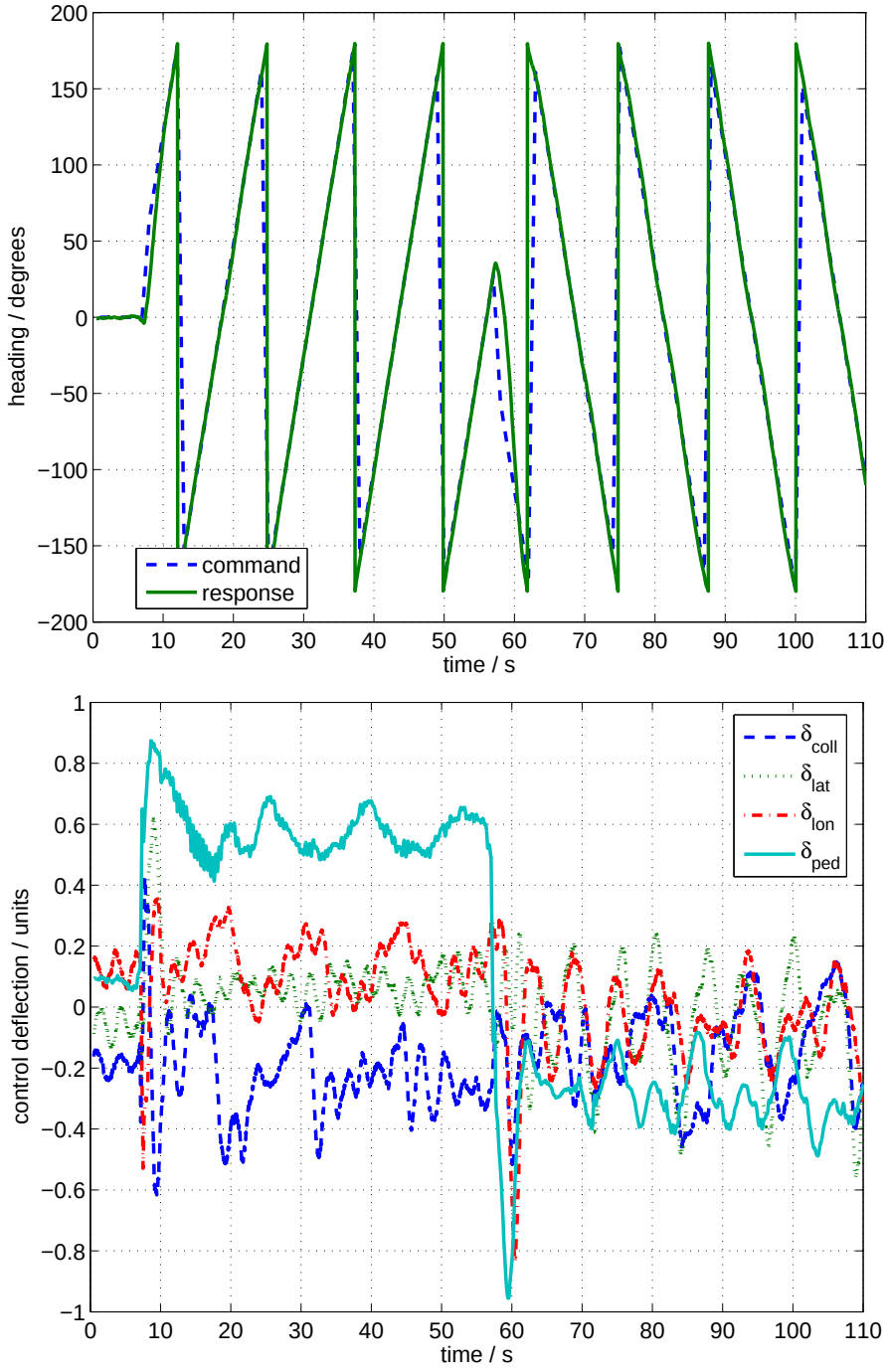

Figure 18: Heading tracking during circular maneuver and control time history.

circular maneuver are shown. Both anticlockwise and clockwise heading changes during the maneuver were tested by changing the parameter from $f = 1$ (anticlockwise) to $f = -1$ (clockwise) at $t = 55s$. Fig. 18 shows that heading tracking is good in both cases. The time history of the pedal input δ_{ped} and all other controls during the maneuver is also shown and illustrates how the vehicle has to exercise all of its controls during this maneuver.

Next, the ability of the controller to track a previous manually-flown maneuver was tested. First, a human pilot flew a figure eight, 3-dimensional pattern with the vehicle. Vehicle state was recorded and was then played back as commands to the adaptive controller. A 3D plot of the pilot and controller flown trajectories are shown in Fig. 19 along with projected ground track. Overall, the tracking in position was measured to be within $11.3ft$ of the desired pilot flown trajectory with a standard deviation of $4.7ft$.

Finally, a tactically useful maneuver was flown to test controller performance at high speeds and pitch attitudes. The objective of the maneuver is to make a 180-degree velocity change from a forward flight condition of $70ft/s$ north to a $70ft/s$ forward flight going south. The trajectory command and response in the north-altitude plane is shown in Fig. 20 along with the pitch angle. A time history of the altitude and the collective control deflection is shown in Fig. 21. During the maneuver the helicopter is commanded to increase altitude by up to $50ft$ in order to minimize saturation of the down collective. In the deceleration phase the vehicle is able to track the command trajectory well; however in accelerating to $70ft/s$ going south, tracking performance suffers. In both the acceleration and deceleration phases, poor tracking corresponds with saturation of the collective control. The oscillations in altitude in Fig. 21 are expected and are due to control saturation which limits the vehicle's descent rate. The large pitch attitudes experienced are what the outer-loop inversion evaluates as being required to perform such rapid decelerations and accelerations.

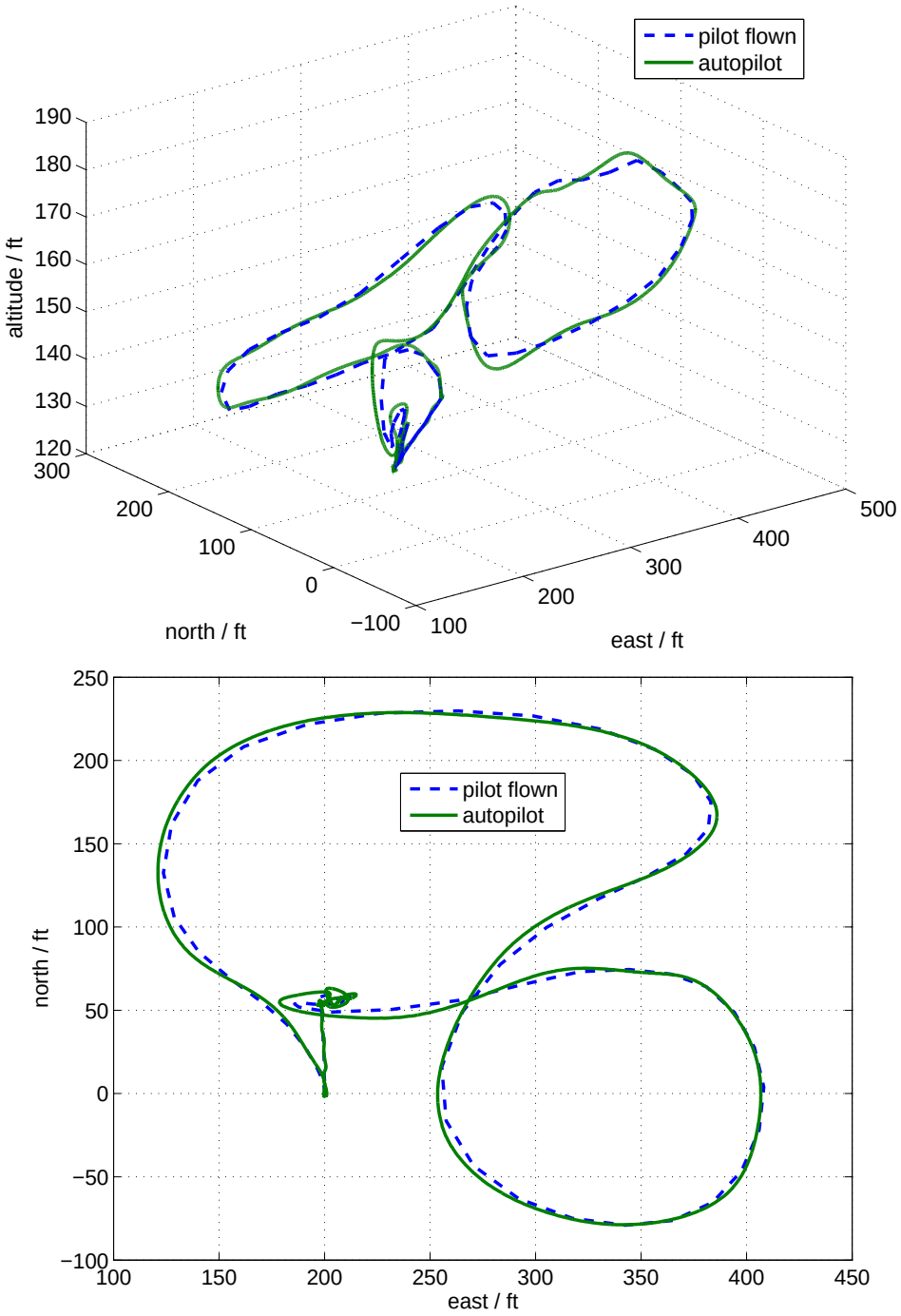

Figure 19: A 3D view and ground track view, of a trajectory initially flown manually by a pilot and then tracked by the controller.

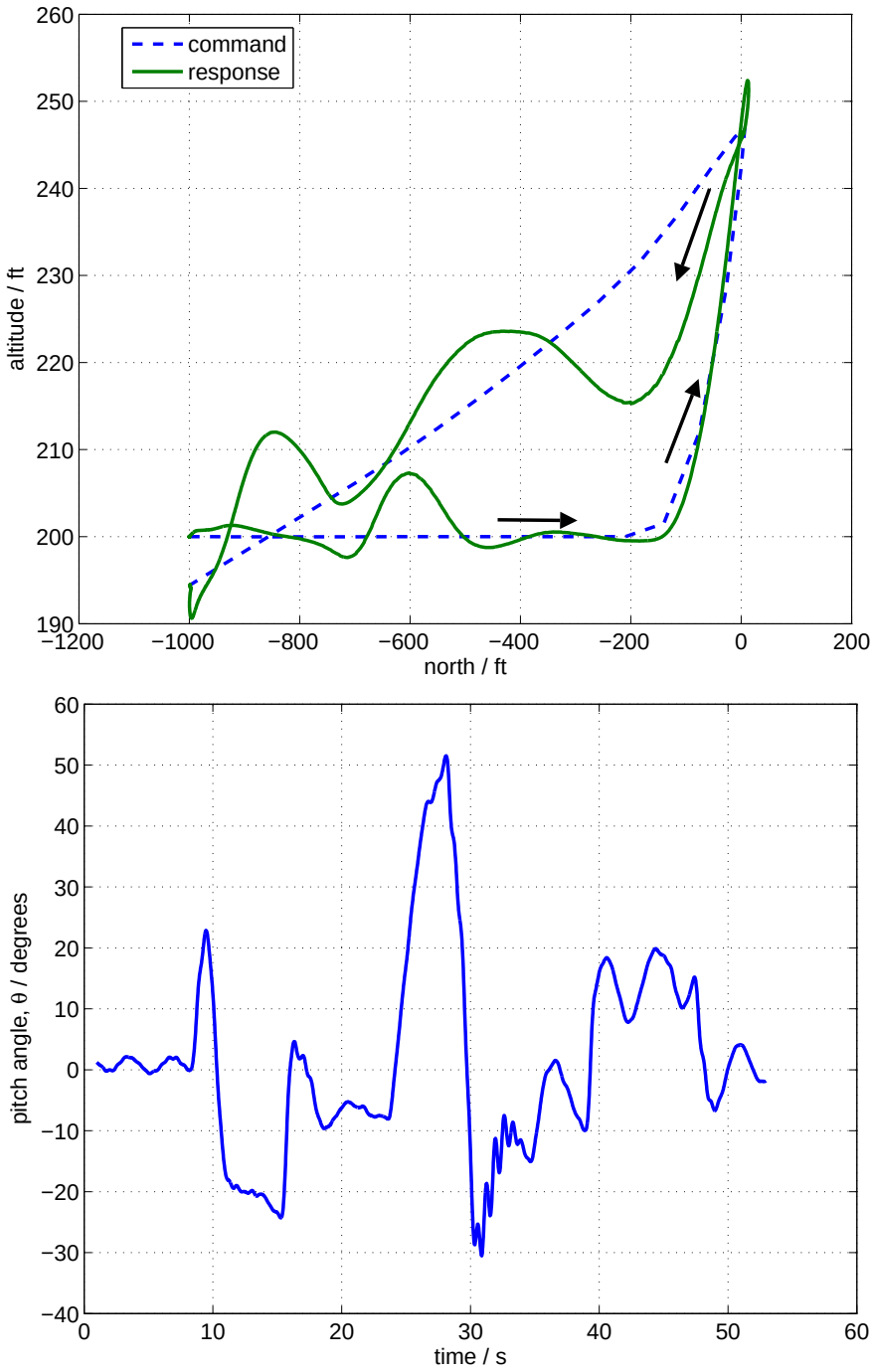

Figure 20: North-Altitude and pitch angle profile during a 180° velocity change maneuver. *Note: North axis and Altitude axis scales are not equal.*

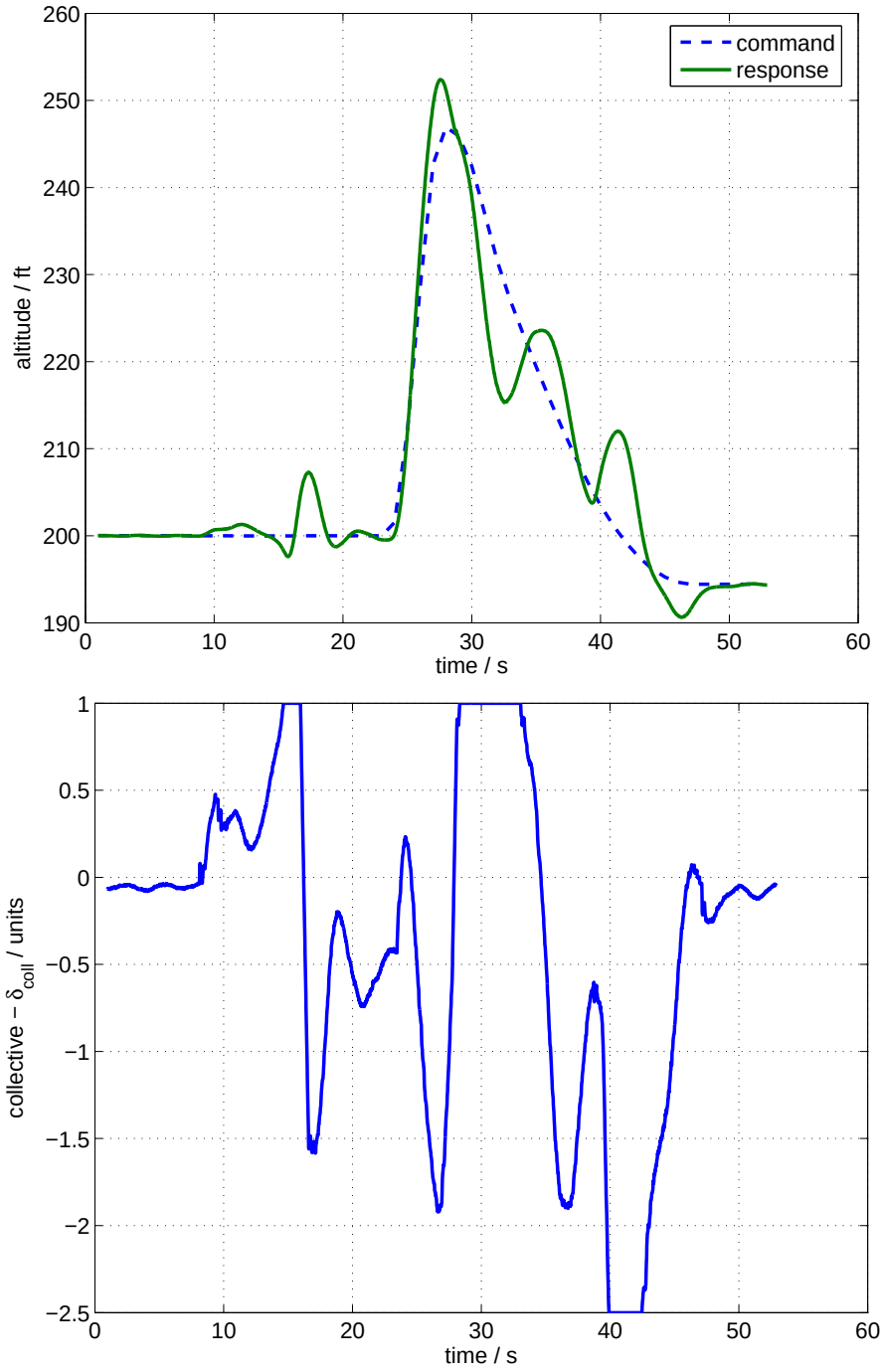

Figure 21: Altitude and collective control history during a 180° velocity change maneuver.

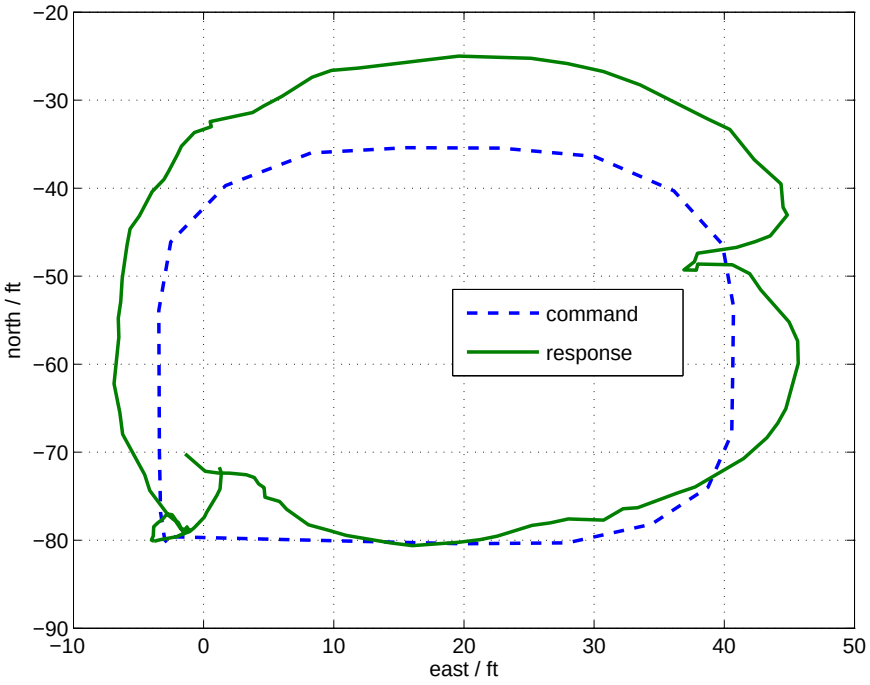

Figure 22: The GTSpy performing a box maneuver

This experiment is an example of maneuvering where the commanded trajectory is more aggressive than the capability of the vehicle and is reflected by the extended periods of saturation. It is possible to operate at the limits of the vehicle primarily due to PCH which protects the adaptation process.

6.3 Application to a Ducted Fan

Following tests on the GTMax helicopter, the control method presented in this thesis was applied to other smaller aircraft. The algorithms were ported to a custom DSP/FPGA hardware device (the FCS20) along with a small sensor board that contained gyroscopes and accelerometers for inertial sensing and a GPS. The avionics package weighed less than $1lb$ and fell within the payload capacity of the 11-inch ducted fan (GTSpy). The GTSpy has a maximum take-off weight of $5.5lbs$ and is driven by a two-bladed fixed-pitch propeller. The propeller is enclosed in an annular wing duct with an outer diameter of $11inches$. Vanes located directly beneath the

Figure 23: Deployment of the GTSpy ducted fan from the GTMax helicopter

propeller move in order to provide yaw control about the propeller axis. Two sets of control surfaces located further below the propeller move in order to provide pitch and roll moments. Maneuvering is accomplished by tilting the thrust vector with the control surfaces relying primarily on inflow for dynamic pressure during hover. Following satisfactory tethered tests, the vehicle was untethered and allowed to fly simple missions. Fig. 22 shows a plan view of a small $50ft$ box maneuver and the GTSpy's tracking. The large deviation on the eastern side of the box is most likely due to a wind gust. Another maneuver performed was the mid-air deployment of the GTSpy. The GTSpy was mounted on the GTMax helicopter with its engine on and then deployed from a safe altitude. The GTSpy was able to recover from the initial deployment transient and maintain attitude and position within 5 seconds of launch. Fig. 23 shows the GTSpy and GTMax during the deployment transient. Both the GTMax and GTSpy were under computer control during this maneuver and is the first known deployment of a rotorcraft from another rotorcraft.

6.4 Application to a Fixed Wing Aircraft

The control method presented in this thesis was further applied to a high-thrust-to-weight ratio fixed wing aircraft with conventional aircraft controls and a fixed pitch two-bladed propeller. The dynamic inverse used for control purposes approximated the aircraft in hover mode where the body axis was defined as

$$x_{heli} = L_2(-\pi/2)x_{airplane}$$

where L_2 is a rotation matrix around the airplane's body y-axis. Hence the ailerons control helicopter-yaw, the rudder controls helicopter-roll and the elevators continue to control pitch. The external commands provided to the control algorithm contains a commanded pitch angle as a function of speed. Inner-loop gains were based on $2.5, 1.5, 2.5 rad/s$ for the (helicopter) roll, pitch and yaw axis respectively. Outer-loop gains were based on $1.5, 1.0, 0.7 rad/s$ for the x, y and z helicopter-body-axis respectively. The output-layer learning rates Γ_W was set to unity on all channels and a learning rate of Γ_V was set for all inputs. Reference model parameters were set to $v_{lim} = 10 ft/s$ and $\omega_{lim} = 1.0 rad/s$. The control effectiveness B was scaled based on speed in order to reflect the reduced control authority of the control surfaces in hover. Flight tests were initiated with the airplane performing circular orbits and gradually lowering airspeed until hover. The reverse, transition to forward flight was accomplished by a more aggressive command into forward flight.

The following figures illustrate the response of the aircraft during transitions between hover and forward flight. Fig. 24 shows the vehicle in forward flight at $80 ft/s$ performing a circular orbit. At $t = 26s$ a transition to hover is initiated by supplying external trajectory commands that lower the vehicle's speed. Transition is completed at $t = 35s$ with a low residual speed of approximately $5 ft/s$. At $t = 55s$ a transition back to forward flight at $80 ft/s$ is initiated and completed at $t = 65s$. During hover, $t \in [35, 55]$, the control deflections are seen to be significantly higher due to the lower

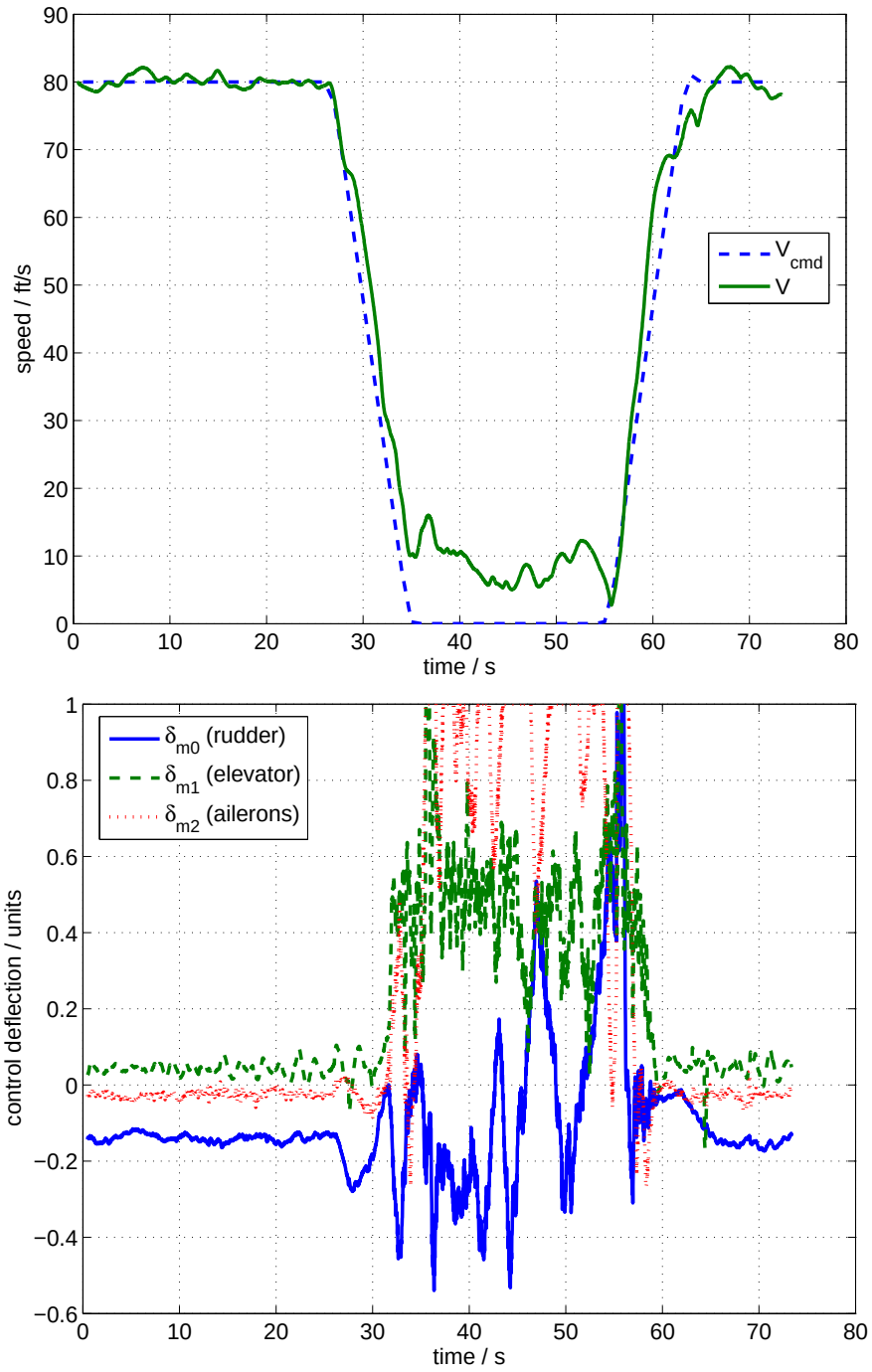

Figure 24: GTEdge speed profile and control deflections during transitions between hover and forward flight

effectiveness at lower speeds. The ailerons are saturated for significant intervals in a particular direction in order to counteract engine torque.

Fig. 25 illustrates the (helicopter) pitch angle during transitions as well as the throttle control deflections. In forward flight, the pitch angle is approximately $-75deg$ and varies in hover due to reduced control effectiveness and the presence of a steady wind. Additionally, Fig. 26 shows the position trajectory during transitions whereas Fig. 27 is a snapshot of the aircraft during the maneuver.

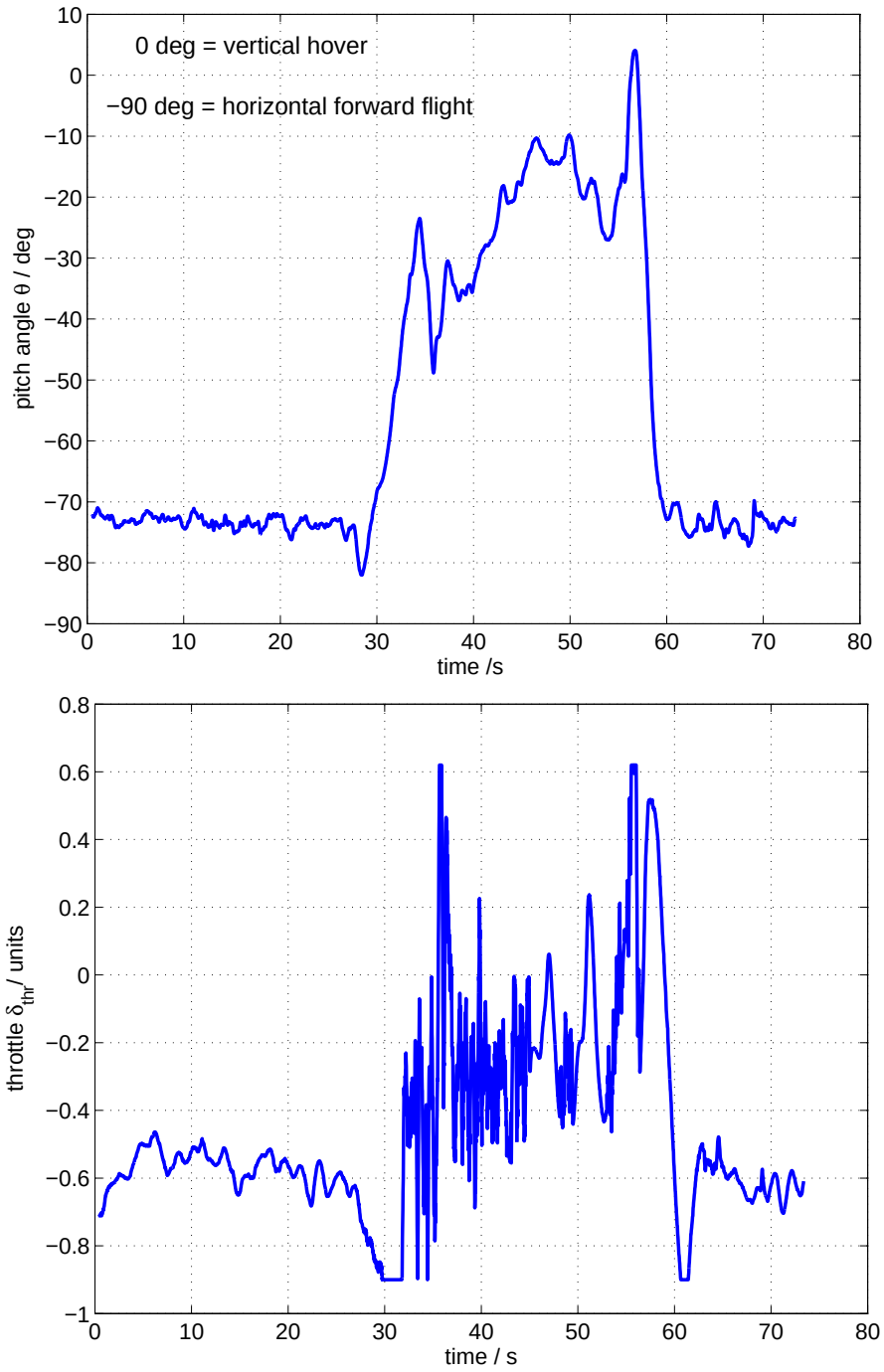

Figure 25: GTEdge pitch angle, throttle profile during transitions between hover and forward flight

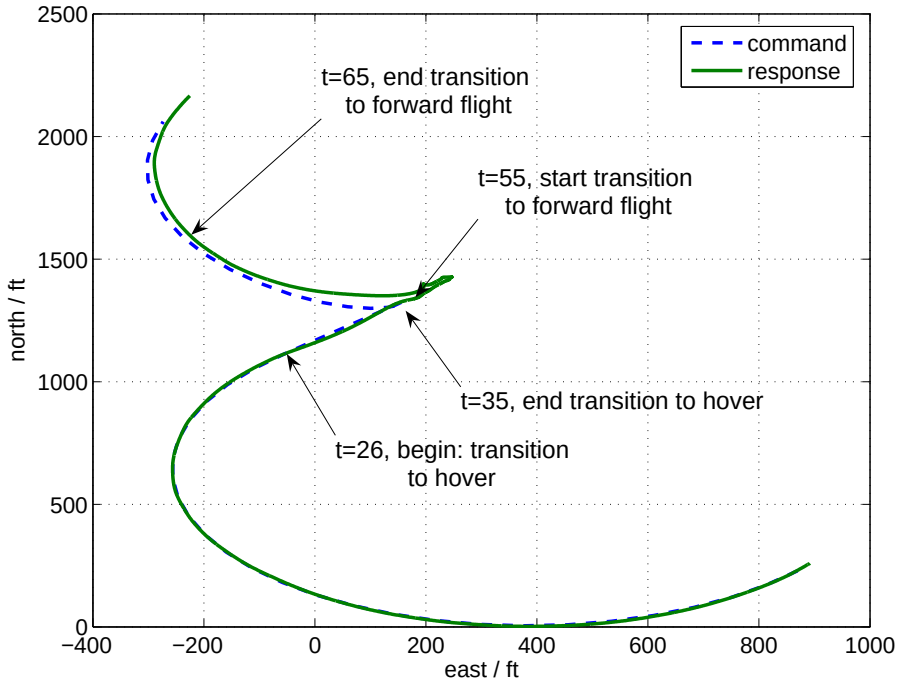

Figure 26: GTEdge trajectory during transitions

Figure 27: GTEdge during a transition

CHAPTER VII

CONCLUSIONS AND FUTURE WORK

7.1 Conclusions

This contributions of this thesis include a framework for the adaptive control of systems in cascade with saturation using the concept of virtual controls. It is shown that in addition to using PCH to protect adaptation from input nonlinearities, PCH may also be used to protect adaptation from the inherent dynamics present in the virtual controls. Additionally, the tracking error dynamics is shown to reduce to a form used in prior work and is thus a generalization of previous work. When the dynamic inverses used to generate desired virtual controls are not present, the problem reduces to that of a multi-input case where only independent actuators are used to control the plant.

Although the null controllable region for general nonlinear plants may not be easily determined, the thesis presents the use of a nested saturation-based reference model that restricts the evolution of the plant states making it less likely to leave the null controllable region and limits may be chosen based on the plant structure. This improves on previous work where linear reference models and large external commands produced a linear responses which could cause the plant to leave its null controllable region. In introducing saturation functions in the reference model, the global asymptotic stability property for stable linear plants is no longer valid. Even though the null controllable region for semi-stable linear reference models is the whole state-space; for a given set of gains, and a nested saturation-based law, it might not be possible to stabilize the reference model on $\mathcal{R}^n$. To overcome this problem, for a given nested saturation-based law, gains, the reference model's domain of attraction

may be characterized as an invariant ellipsoid using linear matrix inequalities leading to restrictions on the applied external command. Additionally a method of choosing gains which guarantees the location of poles when different saturation elements of the nested saturation law saturate mitigates interactions with unmodeled higher order dynamics.

Results using a combination of systems in cascade and nested saturation-based laws applied to the control of an autonomous helicopter provides adaptation in all six degrees of freedom resulting in a full flight envelope controller requiring no scheduling of gains. A method of choosing gains that stabilize the linearized dynamics for maximum position tracking performance provides good tracking results in flight. The versatility of the adaptive control method presented in this thesis is also demonstrated by the application of the same controller with modified dynamic inverses to the flight of a small 11-inch ducted fan (GTSpy), which in many ways is much more challenging. Flight on the GTEdge aircraft illustrates the ability to deal with an aircraft that hovers like a helicopter and then transitions through a high-angle-of-attack regime into full forward flight in aircraft mode. The controller's implementation on the Boeing R-22 illustrates this control method's ability to fly on full-scale aircraft. The full-envelope flight of the GTMax with various payload configurations and mid-air deployment of the GTSpy illustrates this control method's ability to deal with uncertainty effectively.

7.2 Recommended Future Work

Short-term extensions could include the following

- An immediate extension could be the use of composite Lyapunov functions [21] for describing the null controllable region of reference models under nested saturation. The level set of these composite Lyapunov functions can be shown to

be the convex hull of a set of invariant ellipsoids, resulting in a better characterization of bounds and better bounds in the proof of Theorem 4.

- Characterize the trajectory of $x_r(t)$ and the requirements of the set $\mathcal{D}_x \subset \mathcal{C}_x$ based on the parameters of the nested saturation reference model in Assumption 7.

- In the proof of Theorem 4 in Section A.3, in computing a bound on ν_h, conditions that retain the negative sign on $\hat{f}(x, \hat{\delta})$ need to be developed for the single input and the multi-input case. This will correctly indicate the benefits of larger actuator limits.

- The LMI-based estimate of the domain of attraction of the nested saturation reference models are ellipsoids, it would be beneficial if the domain of attraction can be increased arbitrarily (semi-globally) in a certain direction of the state space.

- Investigate whether Lemma 1 can be generalized to guarantee the movement of complex poles.

- Investigate whether the development of adaptive control for systems in cascade may be generalized to arbitrarily interconnected systems.

Long-term extensions include the possibility of adaptive gains in linear reference models or adaptive gains and limits in the nested saturation-based reference model. Consider an alternative to using saturation functions to restrict the evolution of the reference model where the gains are scaled depending on various factors. Consider a system

$$\dot{x}_n = f(x, \sigma(\delta)).$$

The control law δ may be designed of the form

$$\delta = -\frac{k_1}{\lambda^n}x_1 - \frac{k_2}{\lambda^{n-1}}x_2 - \cdots - \frac{k_n}{\lambda}x_n.$$

Assuming, k_i is stabilizing, this form of the scaling preserves damping while all the poles are moved closer to the origin when λ is increased, effectively reducing the bandwidth of the system. This type control law is parameterized using one parameter, λ. Assume that on the on the null controllable region there always exists a $\lambda \in (0, \infty]$, that will stabilize the system or provide conditions for such an assertion. One can get arbitrarily close to the null controllable boundary (if it location is known) by choosing one parameter, λ. Instead of the LMI-based optimization scheme used in this thesis where the null controllable region is estimated through an optimization process, the control law simplifies to a one parameter family of control laws. See [49] for a motivating example. The question remains on how to choose λ. A simple choice of λ is

$$\lambda = 1 + \|x\|^p,$$

for some $p > 0$. This scaling results in large domains of attraction, but has poor performance for large initial conditions (or commands). Another method is to increase λ when saturation is encountered, using an adaptive law such as

$$\begin{aligned} \dot{\lambda} &= -\frac{\alpha}{N}(\lambda - 1) \text{ for } \|\nu_h\| = 0 \\ &= \alpha \qquad\qquad\quad \text{for } \|\nu_h\| \neq 0, \end{aligned}$$

where $\alpha, N > 0$ and control the rate at which λ is increased when $\nu_h \neq 0$ and the recovery when $\nu_h = 0$. An immediate problem with this approach is that even though the gains are scaled down in the presence of saturation, the adaptation is carried out with ν_h as the activating signal for reducing gains. The magnitude of ν_h is irrelevant once saturated, because, the response is open loop. To illustrate this consider the

reference model dynamics from Chapter 2 when saturation occurs.

$$\begin{aligned}\dot{x}_n &= \nu_{cr} - \nu_h \\ &= \nu_{cr} - \nu_{cr} - \nu_{lc} + \bar{\nu}_{ad} + \hat{f}(x, \hat{\delta}) \\ &= -Ke + f(x, \delta).\end{aligned}$$

The PCH signal contains no information on how close the plant states are to the null controllable boundary, just that the gains are too high. The above adaptive law reduces gains until the actuators are unsaturated. This will result in a smaller PCH signal (post saturation) but will not effectively change when the system comes out of saturation. This problem is easily visible in the *mu*-modification approach of [41]. A degree of hysteresis in the choice of λ would be more useful and will also avoid chattering on the saturation boundary. Another way to look at the null controllable region boundary is to assume that the system leaves the null controllable region once saturation has occurred for a certain period of time. This assumption is a good measure of the null controllable region boundary for linear systems, as shown in [40], which also presents a gain scheduled control law with hysteresis. This assumption however, is probably not applicable to nonlinear systems in general.

Another promising approach is one that allows saturation to occur but uses adaptation to compensate so that saturation is avoided in future. The PCH signal is essentially treated as a nonlinear function and a neural network is used to approximate and compensate for saturation [62, 61].

APPENDIX A

PROOFS OF BOUNDEDNESS

In the following set of proofs a '*' represents ideal values, where the following variables, $\tilde{W} \triangleq W^* - W, \tilde{V} \triangleq V^* - V, z = V^T\bar{x}, \tilde{z} = z^* - z$ hold. The arguments to the sigmoidal activation function $\sigma(\cdot)$ are dropped for clarity and conciseness. Noting that the sigmoidal functions are bounded, the NN output may be bounded as

$$\begin{aligned} \nu_{ad} &= W^T\sigma(z) \\ &= (W^{*T} - \tilde{W}^T)\sigma(V^T\bar{x}) \\ \|\nu_{ad}\| &\leq \alpha_0(\bar{Z} + \|\tilde{Z}\|_F) \end{aligned}$$

for some constant α_0.

An expansion of $\sigma(z)$ around the estimated weights is given by

$$\sigma(z^*) = \sigma(z) + \left.\frac{\partial\sigma(s)}{\partial s}\right|_{s=z}(z^* - z) + \mathcal{O}^2(\tilde{z}).$$

By the substitution of $\bar{\nu}_{ad} = \nu_{ad} + \nu_r$, and $\bar{\Delta} = \Delta + \epsilon_g = \nu^*_{ad} + \epsilon + \epsilon_g$, the tracking error dynamics may be expressed as

$$\dot{e} = Ae + B[\nu_{ad} - (\nu^*_{ad} + \epsilon + \epsilon_g) + \nu_r].$$

Now,

$$\begin{aligned} \nu^*_{ad} + \epsilon + \epsilon_g - \nu_{ad} &= W^{*T}\sigma^* - W^T\sigma + \epsilon + \epsilon_g \\ &= W^{*T}\left[\sigma(z) + \sigma'\tilde{z} + \mathcal{O}^2(\tilde{z})\right] - W^T\sigma + \epsilon + \epsilon_g. \end{aligned}$$

Adding and subtracting $W^T\sigma' z$ and $W^T\sigma' z^*$

$$\nu^*_{ad} + \epsilon + \epsilon_g - \nu_{ad} = \tilde{W}^T(\sigma - \sigma' z) + W^T\sigma'\tilde{z} + w,$$

where,

$$w = \tilde{W}^T \sigma' z^* + W^{*T} \mathcal{O}^2(\tilde{z}) + \epsilon + \epsilon_g.$$

The tracking error dynamics may finally be written as

$$\dot{e} = Ae + B\left\{ -\left[\tilde{W}^T(\sigma - \sigma' z) + W^T \sigma' \tilde{z} + w \right] + \nu_r \right\}.$$

Assuming $\|e_r\| < \bar{e}_r$, the inputs to the network may be bounded as

$$\begin{aligned} \bar{x} &= \begin{bmatrix} b_v & x_c^T & e_r^T & e^T & \nu_{ad}^T & \|Z\|_F \end{bmatrix} \\ \|\bar{x}\| &\leq b_v + \bar{x}_c + \bar{e}_r + \|e\| + \alpha_0(\bar{Z} + \|\tilde{Z}\|_F) + \bar{Z} + \|\tilde{Z}\|_F \\ &= k_0 + k_1 \|\tilde{Z}\|_F + \|e\|, \end{aligned}$$

where $k_1 = (1 + \alpha_0)$, $k_0 \triangleq b_v + \bar{x}_c + \bar{e}_r + k_1 \bar{Z}$. Additionally, the higher order terms of $\mathcal{O}^2(\tilde{z})$ may be bounded as

$$\begin{aligned} \|\mathcal{O}^2(\tilde{z})\| &\leq 2\alpha_0 + \alpha_1 \|\tilde{V}^T\|_F \|\bar{x}\| \\ &\leq 2\alpha_0 + \alpha_1 k_1 \|\tilde{Z}\|_F^2 + \alpha_1 k_0 \|\tilde{Z}\|_F + \alpha_1 \|\tilde{Z}\|_F \|e\|. \end{aligned}$$

Otherwise, the inputs to the network are bounded as

$$\begin{aligned} \bar{x} &= \begin{bmatrix} b_v & x_c^T & e_r^T & e^T & \nu_{ad}^T & \|Z\|_F \end{bmatrix} \\ \|\bar{x}\| &\leq b_v + \bar{x}_c + \bar{e}_r + \|e\| + \alpha_0(\bar{Z} + \|\tilde{Z}\|_F) + \bar{Z} + \|\tilde{Z}\|_F \\ &= k_0 + k_1 \|\tilde{Z}\|_F + \|e\| + \|e_r\|, \end{aligned}$$

where $k_1 = (1 + \alpha_0)$, $k_0 \triangleq b_v + \bar{x}_c + k_1 \bar{Z}$, and the higher order terms of $\mathcal{O}^2(\tilde{z})$ may be bounded as follows

$$\begin{aligned} \|\mathcal{O}^2(\tilde{z})\| &\leq 2\alpha_0 + \alpha_1 \|\tilde{V}^T\|_F \|\bar{x}\| \\ &\leq 2\alpha_0 + \alpha_1 k_1 \|\tilde{Z}\|_F^2 + \alpha_1 k_0 \|\tilde{Z}\|_F + \alpha_1 \|\tilde{Z}\|_F \left(\|e\| + \|e_r\| \right). \end{aligned}$$

Depending on whether a bound on e_r is assumed, the disturbance term w may be bounded as

$$\|w\| = c_0 + c_1 \|\tilde{Z}\|_F + c_2 \|e\| \|\tilde{Z}\|_F + c_3 \|\tilde{Z}\|_F^2, \tag{99}$$

or

$$\|w\| = c_0 + c_1\|\tilde{Z}\|_F + c_2(\|e\| + \|e_r\|)\|\tilde{Z}\|_F + c_3\|\tilde{Z}\|_F^2, \tag{100}$$

where, c_0, c_1, c_2, c_3 are computable constants given by

$$c_0 = 2\alpha_0\bar{Z} + \bar{\epsilon} + \bar{\epsilon}_g$$

$$c_1 = 2\alpha_1 k_0 \bar{Z}$$

$$c_2 = 2\alpha_1 \bar{Z}$$

$$c_3 = 2\alpha_1 k_1 \bar{Z}$$

A.1 Proof of Theorem 2

Proof. A Lyapunov candidate function is

$$L(e, \tilde{W}, \tilde{V}) = \frac{1}{2}\left[e^T P e + tr\left(\tilde{W}\Gamma_W^{-1}\tilde{W}^T\right) + tr\left(\tilde{V}^T\Gamma_V^{-1}\tilde{V}\right)\right]. \tag{101}$$

When the weight update equations of Eqn (41) and Eqn (42) are used, the time derivative of L along trajectories can be expressed as

$$\dot{L} = -\frac{1}{2}e^T Q e + r^T(-w + \nu_r) + \kappa\|e\| tr\left(\tilde{Z}^T Z\right).$$

When $Z = Z^* - \tilde{Z}$ and $\|Z\|_F \geq \|\tilde{Z}\|_F - \bar{Z}$ and the robustifying term of Eqn (40) are used

$$\dot{L} = -\frac{1}{2}e^T Q e - r^T w - r^T K_r r\left(\|Z\|_F + \bar{Z}\right)\frac{\|e\|}{\|r\|} + \kappa\bar{Z}\|e\|\|\tilde{Z}\|_F - \kappa\|e\|\|\tilde{Z}\|_F^2.$$

Using Eqn (99),

$$\begin{aligned}
\dot{L} \leq & -\frac{1}{2}\lambda_{min}(Q)\|e\|^2 + \|e\|\|PB\|\left(c_0 + c_1\|\tilde{Z}\|_F + c_2\|e\|\|\tilde{Z}\|_F + c_3\|\tilde{Z}\|_F^2\right) \\
& - \lambda_{min}K_r\|e\|\|PB\|\|\tilde{Z}\|_F\|e\| + \kappa\bar{Z}\|\tilde{Z}\|_F - \kappa\|e\|\|\tilde{Z}\|_F^2 \\
= & -\frac{1}{2}\lambda_{min}(Q)\|e\|^2 \\
& + c_0\|PB\|\|e\| \\
& + \left(c_1\|PB\| + \kappa\bar{Z}\right)\|e\|\|\tilde{Z}\|_F \\
& - \left(\kappa - c_3\|PB\|\right)\|e\|\|\tilde{Z}\|_F^2 \\
& - \left(\lambda_{min}(K_r)\|PB\| - c_2\|PB\|\right)\|e\|^2\|\tilde{Z}\|_F \\
= & -a_{22}\|e\|^2 + a_2\|e\| + a_{23}\|e\|\|\tilde{Z}\|_F - a_{233}\|e\|\|\tilde{Z}\|_F^2 - a_{223}\|e\|^2\|\tilde{Z}\|_F,
\end{aligned} \tag{102}$$

where the subscripts $\{2, 3\}$ of the coefficients a_{ijk} correspond to the variables $\|e\|$, $\|\tilde{Z}\|_F$ respectively. After ignoring the trivial solution $\|e\| = 0$, and selecting $\lambda_{min}(K_r) > c_2$, $\kappa > c_3\|PB\|$, it can be shown that $\dot{L} \leq 0$ when one of the following conditions holds

$$\|e\| \geq \frac{a_2 + a_{23}\|\tilde{Z}\|_F}{a_{22}},$$

or,

$$\|\tilde{Z}\|_F \geq \frac{a_{23} + \sqrt{a_{23}^2 + 4a_{233}a_2}}{2a_{233}}.$$

By selecting $\lambda_{min}(Q), \kappa$ and learning rates (Γ_W and Γ_V), $\dot{L} \leq 0$ everywhere outside a compact set $\Omega_\beta \subset \Omega_\alpha$ where Ω_α is the largest level set of L that is completely within $\mathcal{D}$. Ultimate boundedness may be concluded from a Lyapunov extension in [50]. □

A.2 Proof of Theorem 3

A Lyapunov candidate function is

$$L(e_r, e, \tilde{W}, \tilde{V}) = \frac{1}{2}\left[e_r^T P e_r + e^T P e + tr\left(\tilde{W}\Gamma_W^{-1}\tilde{W}^T\right) + tr\left(\tilde{V}^T\Gamma_V^{-1}\tilde{V}\right)\right].$$

When the weight update equations of Eqn (41) and Eqn (42) are used, the time derivative of L along trajectories can be expressed as

$$\dot{L} = -\frac{1}{2}e_r^T Q_r e_r + e_r^T P_r E_r \nu_h - \frac{1}{2}e^T Q e + r^T(-w + \nu_r) + \kappa\|e\| tr\left(\tilde{Z}^T Z\right).$$

Noting that

$$\nu_h = \nu_{cr} + \nu_{lc} + \bar{\nu}_{ad} - \hat{f}(x, \hat{\delta}),$$

with the bounds

$$\begin{aligned}
\|\nu_{cr}\| &\leq \|K\|\|e_r\| \\
\|\nu_{lc}\| &\leq \|K\|\|e\| \\
\|\bar{\nu}_{ad}\| &\leq \alpha_0 \left(\bar{Z} + \|\tilde{Z}\|_F\right) + \lambda_{max}(K_r)\|\tilde{Z}\|_F\|e\|.
\end{aligned}$$

Hence,

$$\begin{aligned}
\dot{L} \leq & -\frac{1}{2}\lambda_{min}(Q_r)\|e_r\|^2 \\
& + \|e_r\|\|P_rE_r\| \left(\|K\|(\|e_r\| + \|e\|) + \alpha_0\bar{Z} + \alpha_0\|\tilde{Z}\|_F + \lambda_{max}(K_r)\|\tilde{Z}\|_F\|e\| + \|\hat{f}(x, \hat{\delta})\|\right) \\
& - \frac{1}{2}\lambda_{min}(Q)\|e\|^2 + \|e\|\|PB\| \left(c_0 + c_1\|\tilde{Z}\|_F + c_2(\|e_r\| + \|e\|)\|\tilde{Z}\|_F + c_3\|\tilde{Z}\|_F^2\right) \\
& - \lambda_{min}K_r\|e\|\|PB\|\|\tilde{Z}\|_F\|e\| + \kappa\bar{Z}\|\tilde{Z}\|_F - \kappa\|e\|\|\tilde{Z}\|_F^2 \\
= & \quad - \left(\frac{1}{2}\lambda_{min}(Q_r) - \|K\|\|P_rE_r\|\right)\|e_r\|^2 \\
& \quad - \frac{1}{2}\lambda_{min}(Q)\|e\|^2 \\
& \quad - (\kappa - c_3\|PB\|)\|e\|\|\tilde{Z}\|_F^2 \\
& \quad - (\lambda_{min}(K_r) - c_2)\|PB\|\|e\|^2\|\tilde{Z}\|_F \\
& \quad + c_0\|PB\|\|e\| \\
& \quad + \left(c_1\|PB\| + \kappa\bar{Z}\right)\|e\|\|\tilde{Z}\|_F \\
& \quad + \|K\|\|P_rE_r\|\|e_r\|\|e\| \\
& \quad + \left(\alpha_0\bar{Z} + \|\hat{f}(x, \hat{\delta})\|\right)\|P_rE_r\|\|e_r\| \\
& \quad + \alpha_0\|P_rE_r\|\|e_r\|\|\tilde{Z}\|_F \\
& \quad + (c_2\|PB\| + \lambda_{max}(K_r)\|P_rE_r\|)\|e_r\|\|e\|\|\tilde{Z}\|_F \\
= & -a_{11}\|e_r\|^2 - a_{22}\|e\|^2 - a_{233}\|e\|\|\tilde{Z}\|_F^2 - a_{223}\|e\|^2\|\tilde{Z}\|_F + a_2\|e\| \\
& \quad + a_{23}\|e\|\|\tilde{Z}\|_F + a_{12}\|e_r\|\|e\| + a_1\|e_r\| + a_{13}\|e_r\|\|\tilde{Z}\|_F + a_{123}\|e_r\|\|e\|\|\tilde{Z}\|_F,
\end{aligned}$$

where the subscripts $\{1,2,3\}$ of the coefficients a_{ijk} correspond to the variables $\|e_r\|, \|e\|, \|\tilde{Z}\|_F$ respectively. Assuming, $\kappa > c_3\|PB\|$ and $\lambda_{min}(K_r) > c_2$, it can be shown that $\dot{L} \leq 0$ when one of the following conditions is true,

$$
\begin{aligned}
&-a_{11}\|e_r\|^2 + b_{11}\|e_r\| + b_{10} \leq 0 \\
\text{or} \; &-a_{22}\|e\|^2 + b_{21}\|e\| + b_{20} \leq 0 \\
\text{or} \; &-a_{233}\|e\|\|\tilde{Z}\|_F^2 + b_{31}\|\tilde{Z}\|_F + b_{30} \leq 0,
\end{aligned}
$$

and

$$
\begin{aligned}
b_{10} &= a_2\|e\| + a_{23}\|e\|\|\tilde{Z}\|_F \\
b_{11} &= a_1 + a_{12}\|e\| + a_{13}\|\tilde{Z}\|_F + a_{123}\|e\|\|\tilde{Z}\|_F \\
b_{20} &= a_1\|e_r\| + a_{13}\|e_r\|\|\tilde{Z}\|_F \\
b_{21} &= a_2 + a_{23}\|\tilde{Z}\|_F + a_{12}\|e_r\| + a_{123}\|e_r\|\|\tilde{Z}\|_F \\
b_{30} &= a_2\|e\| + a_{12}\|e_r\|\|e\| + a_1\|e_r\| \\
b_{31} &= a_{23}\|e\| + a_{13}\|e_r\| + a_{123}\|e_r\|\|e\|,
\end{aligned}
$$

which corresponds to the following restrictions on the error variables

$$
\begin{aligned}
\|e_r\| &\geq \frac{b_{11} + \sqrt{b_{11}^2 + 4a_{11}b_{10}}}{2a_{11}} \\
\|e\| &\geq \frac{b_{21} + \sqrt{b_{21}^2 + 4a_{22}b_{20}}}{2a_{22}} \\
\|\tilde{Z}\|_F &\geq \frac{b_{31} + \sqrt{b_{31}^2 + 4a_{233}\|e\|b_{30}}}{2a_{233}\|e\|}.
\end{aligned}
$$

By selecting $\lambda_{min}(Q), \kappa$ and learning rates (Γ_W and Γ_V), $\dot{L} \leq 0$ everywhere outside a compact set $\Omega_\beta \subset \Omega_\alpha$ where Ω_α is the largest level set of L that is completely within $\mathcal{D}$. Ultimate boundedness may be concluded from a Lyapunov extension in [50].

A.3 Proof of Theorem 4

A Lyapunov candidate function is

$$
L(e_r, e, \tilde{W}, \tilde{V}) = \frac{1}{2}\left[e_r^T P e_r + e^T P e + tr\left(\tilde{W}\Gamma_W^{-1}\tilde{W}^T\right) + tr\left(\tilde{V}^T\Gamma_V^{-1}\tilde{V}\right)\right].
$$

When the weight update equations of Eqn (41) and Eqn (42) are used, the time derivative of L along trajectories can be expressed as

$$\dot{L} = e_r^T P_r \left(A_r e_r + B_r M_n \sigma_n(\cdots)\right) + e_r^T P_r E_r \nu_h - \frac{1}{2} e^T Q e + r^T(-w + \nu_r) + \kappa \|e\| tr\left(\tilde{Z}^T Z\right).$$

Noting that $\nu_h = \nu_{cr} + \nu_{lc} + \bar{\nu}_{ad} - \hat{f}(x, \hat{\delta})$ with the bounds

$$\begin{aligned}
\|\nu_{cr}\| &\leq \alpha_1 \lambda_{max}(M_n) \\
\|\nu_{lc}\| &\leq \|K\| \|e\| \\
\|\bar{\nu}_{ad}\| &\leq \alpha_0 \left(\bar{Z} + \|\tilde{Z}\|_F\right) + \lambda_{max}(K_r) \|\tilde{Z}\|_F \|e\|,
\end{aligned}$$

for some constant α_1, hence,

$$\begin{aligned}
\dot{L} \leq & -\gamma(e_r) \\
& + \|e_r\| \|P_r E_r\| \left(\alpha_1 \lambda_{max}(M_n) + \|K\| \|e\| + \alpha_0 \bar{Z} + \alpha_0 \|\tilde{Z}\|_F + \lambda_{max}(K_r) \|\tilde{Z}\|_F \|e\| + \|\hat{f}(x, \hat{\delta})\|\right) \\
& - \frac{1}{2} \lambda_{min}(Q) \|e\|^2 + \|e\| \|PB\| \left(c_0 + c_1 \|\tilde{Z}\|_F + c_2 (\|e_r\| + \|e\|) \|\tilde{Z}\|_F + c_3 \|\tilde{Z}\|_F^2\right) \\
& - \lambda_{min} K_r \|e\| \|PB\| \|\tilde{Z}\|_F \|e\| + \kappa \bar{Z} \|\tilde{Z}\|_F - \kappa \|e\| \|\tilde{Z}\|_F^2 \\
= \quad & -\gamma(e_r) \\
& - \frac{1}{2} \lambda_{min}(Q) \|e\|^2 \\
& - (\kappa - c_3 \|PB\|) \|e\| \|\tilde{Z}\|_F^2 \\
& - (\lambda_{min}(K_r) - c_2) \|PB\| \|e\|^2 \|\tilde{Z}\|_F \\
& + c_0 \|PB\| \|e\| \\
& + \left(c_1 \|PB\| + \kappa \bar{Z}\right) \|e\| \|\tilde{Z}\|_F \\
& + \|K\| \|P_r E_r\| \|e_r\| \|e\| \\
& + \left(\alpha_1 \lambda_{max}(M_n) + \alpha_0 \bar{Z} + \|\hat{f}(x, \hat{\delta})\|\right) \|P_r E_r\| \|e_r\| \\
& + \alpha_0 \|P_r E_r\| \|e_r\| \|\tilde{Z}\|_F \\
& + (c_2 \|PB\| + \lambda_{max}(K_r) \|P_r E_r\|) \|e_r\| \|e\| \|\tilde{Z}\|_F \\
= & -\gamma(e_r) - a_{22} \|e\|^2 - a_{233} \|e\| \|\tilde{Z}\|_F^2 - a_{223} \|e\|^2 \|\tilde{Z}\|_F + a_2 \|e\| + a_{23} \|e\| \|\tilde{Z}\|_F \\
& + a_{12} \|e_r\| \|e\| + a_1 \|e_r\| + a_{13} \|e_r\| \|\tilde{Z}\|_F + a_{123} \|e_r\| \|e\| \|\tilde{Z}\|_F.
\end{aligned}$$

Assuming, $\kappa > c_3\|PB\|$, $\lambda_{min}(K_r) > c_2$ and $e_r \in \Omega(P_r, \rho)$, it can be shown that $\dot{L} \leq 0$ when one of the following conditions is true

$$
\begin{aligned}
&-\gamma(e_r) + b_{11}\|e_r\| + a_2\|e\| + a_{23}\|e\|\|\tilde{Z}\|_F \leq 0 \\
&\text{or} -a_{22}\|e\|^2 + b_{21}\|e\| + b_{20} \leq 0 \\
&\text{or} -a_{233}\|e\|\|\tilde{Z}\|_F^2 + b_{31}\|\tilde{Z}\|_F + b_{30} \leq 0,
\end{aligned}
$$

where the subscripts $\{1, 2, 3\}$ of the coefficients a_{ijk} correspond to the variables $\|e_r\|, \|e\|, \|\tilde{Z}\|_F$ respectively and

$$
\begin{aligned}
b_{11} &= (a_1 + a_{12}\|e\| + a_{13}\|\tilde{Z}\|_F + a_{123}\|e\|\|\tilde{Z}\|_F) \\
b_{20} &= a_1\|e_r\| + a_{13}\|e_r\|\|\tilde{Z}\|_F \\
b_{21} &= a_2 + a_{23}\|\tilde{Z}\|_F + a_{12}\|e_r\| + a_{123}\|e_r\|\|\tilde{Z}\|_F \\
b_{30} &= a_2\|e\| + a_{12}\|e_r\|\|e\| + a_1\|e_r\| \\
b_{31} &= a_{23}\|e\| + a_{13}\|e_r\| + a_{123}\|e_r\|\|e\|,
\end{aligned}
$$

which corresponds to the following restrictions on the error variables.

$$
\begin{aligned}
\|e_r\| &\leq \frac{\gamma(e_r) - \left(a_2\|e\| + a_{23}\|e\|\|\tilde{Z}\|_F\right)}{b_{11}} \\
\|e\| &\geq \frac{b_{21} + \sqrt{b_{21}^2 + 4a_{22}b_{20}}}{2a_{22}} \\
\|\tilde{Z}\|_F &\geq \frac{b_{31} + \sqrt{b_{31}^2 + 4a_{233}\|e\|b_{30}}}{2a_{233}\|e\|}.
\end{aligned}
$$

Here the function $\gamma(e_r) > 0$ and imposes an upper limit on the size of external command x_c. By selecting $\lambda_{min}(Q), \kappa$ and learning rates (Γ_W and Γ_V), $\dot{L} \leq 0$ everywhere outside a compact set $\Omega_\beta \subset \Omega_\alpha$ where Ω_α is the largest level set of L that is completely within $\mathcal{D}$. Ultimate boundedness may be concluded from a Lyapunov extension in [50].

Remark 6. *Defining the vector of error variables as*

$$\eta \triangleq \begin{bmatrix} e_r \\ e \\ vec\tilde{W} \\ vec\tilde{V} \end{bmatrix},$$

Assumption 7 implicitly guarantees that the external command $x_c(t)$ is feasible. The ultimate boundedness of Theorem 3 and Theorem 4 ensure that as long as the initial condition of the errors $\eta(0) \in \Omega_\alpha$, then there exists a time $T(\eta(0))$ such that $\eta(t)$ will enter the set Ω_β and remain inside it for all $t > T(\eta(0))$.

Remark 7. *In the case of Theorem 2, with $\eta = [e^T vec\tilde{W}^T vec\tilde{V}^T]$ and $\eta(0) \in \Omega_\alpha$, then there exists a time $T(\eta(0))$ such that $\eta(t)$ will enter the set Ω_β and remain inside it for all $t > T(\eta(0))$. However, $e_r(t)$ is assumed to be bounded.*

APPENDIX B

NESTED SATURATION WITH GUARANTEED REAL POLES

B.1 Motivation

The problem addressed involves the global stabilization of a chain of integrators

$$\dot{x}_1 = x_2, \cdots, \dot{x}_n = u. \tag{103}$$

The system given by (103) is a subset of a class of systems that are said to be *asymptotically null-controllable with bounded controls* [70, 20]. This property was shown in [63] to be equivalent to the system being stabilizable and having all open-loop poles in the closed left-half plane.

It was shown in [71] that it is not possible to globally stabilize integrator chains of order $n > 2$ using a bounded *linear* feedback law. However, it was shown by Teel in [73] that a nonlinear law consisting of nested saturators can guarantee global asymptotic stability for integrator chains of any order n. This control law may be expressed as

$$u = -\sigma_n(h_n(x) + \sigma_{n-1}(h_{n-1}(x) + \cdots + \sigma_1(h_1(x)))),$$

where h_i are linear combinations of the state (feedback) and the saturation functions σ_i satisfy certain properties. The existence of such a globally stabilizing control law was established in [73] by choosing *one* set of h_i's such that global asymptotic stability could be proven. The choice of h_i is a design degree of freedom and may be exercised to prescribe pole locations and the linear dynamics when different elements of the control law are saturated.

We observed that the h_i chosen by Teel with *conventional saturation* functions (see Definition 4) results in all the poles of the closed loop system residing at -1 when none of the saturation elements in the control law are saturated. If the k^{th} saturator is the outermost element to be saturated, then the resulting closed loop system has poles at -1 with multiplicity $n-k$ and poles at 0 with multiplicity k, at least until the element comes out of saturation. A discussion on the prescription of performance by pole placement (both real and complex) is provided in [72], however no explicit transformation is provided. Another aspect is the behavior of these poles as different elements of the control law saturate. Ideally, these poles should not change when saturation occurs. Both these properties (pole placement and movement when saturated) are useful if the nested saturation control law is to be employed in practice.

The simple and elegant nested saturation law can benefit greatly from these properties. Hence, the effort here is to develop a transformation, i.e., a way to select h_i such that closed loop poles for the unsaturated system may be prescribed as $\{-a_1, -a_2, \cdots - a_n\}$, where $a_i \in \mathcal{R}\backslash 0$ and $a_i > 0$ for stability. Additionally, it will be shown that when the outermost saturated element is σ_k, the poles of resulting linear system reside at $\{-a_1, -a_2, \cdots - a_{n-k}, 0_1, 0_2, \cdots 0_k\}$.

B.2 Guaranteed Real Poles

Definition 3 (linear saturation)**.** *Define constants* $(L, M) \in \mathcal{R}^+$ *such that* $0 < L \leq M$*. Now, define a function* $\sigma : \mathbb{R} \to \mathbb{R}$*.* σ *is said to be a* linear saturation *if it is continuous, nondecreasing and satisfies*

a. $s\sigma(s) > 0 \qquad \forall s \neq 0$

b. $\sigma(s) = s \qquad$ *when* $|s| \leq L$

c. $|\sigma(s)| \leq M \qquad \forall s \in \mathbb{R}$

Definition 4 (conventional saturation)**.** $\sigma : \mathbb{R} \to \mathbb{R}$ *is said to be a* conventional saturation *if it has a limit* $M \in R+$ *such that*

a. $s\sigma(s) > 0 \qquad \forall s \neq 0$

b. $\sigma(s) = s \qquad when\ |s| \leq M$

c. $|\sigma(s)| = M \qquad when\ |s| > M$

Remark 8. σ *is said to be* saturated *when its argument is not in its linear region. For* linear saturation *this occurs when* $|s| > L$*. For* conventional saturation *this occurs when* $|s| > M$*.*

Remark 9. conventional saturation *is a special case of* linear saturation *with* $L = M$ *and a constant saturation value* M*.*

Definition 5 (vector valued saturaion)**.** *A function* $\sigma : \mathcal{R}^m \to \mathcal{R}^m$ *is an* $\mathcal{R}^m$*-valued saturation function if*

$$\sigma : (x_1, \ldots, x_m) \to (\sigma_1(x_1), \ldots, \sigma_m(x_m)),$$

and, for all $i = 1, \ldots, m$*,* $\sigma_i(\cdot)$ *is a saturation function.*

Lemma 1. *Consider a chain of* n*-integrators, given by (103), which may be represented as* $\dot{x} = A_x x + B_x u$*, with* $x \in \mathbb{R}^n$*,* $u \in \mathbb{R}$ *and*

$$A_x = \begin{bmatrix} 0 & 1 & 0 & \cdots & 0 \\ \vdots & & & & \vdots \\ 0 & \cdots & \cdots & \cdots & 1 \\ 0 & \cdots & \cdots & \cdots & 0 \end{bmatrix}, \quad B_x = \begin{bmatrix} 0 \\ \vdots \\ \vdots \\ 1 \end{bmatrix}, \tag{104}$$

then there exists a linear transformation $y = T_{yx} x$ *which transforms (103) into* $\dot{y} =$

$A_y y + B_y u$ *where,*

$$A_y = \begin{bmatrix} 0 & a_n & \cdots & \cdots & a_n \\ 0 & 0 & a_{n-1} & \cdots & a_{n-1} \\ \vdots & \ddots & \ddots & \ddots & \vdots \\ 0 & \cdots & \cdots & \cdots & a_2 \\ 0 & \cdots & \cdots & \cdots & 0 \end{bmatrix}, \quad B_y = \begin{bmatrix} a_n \\ a_{n-1} \\ \vdots \\ \vdots \\ a_1 \end{bmatrix}, \tag{105}$$

and the elements $a_i \in \mathbb{R} \setminus 0$ *with* $i = 1 \dots n$.

Proof. Given a set of coefficients

$$A = \{a_1, a_2, \cdots, a_n\}, \tag{106}$$

let $A_l \subseteq A$ represent a subset containing the first l elements of A. Define a function $F_k^m(A_l)$ which acts over the set A_l. F_k^m is used to generate the product of combinations of elements taken m at a time from A_l. The number of such combinations is given by the binomial coefficient $\binom{l}{m}$. Hence, $F_k^m(A_l)$ may be treated as a *generating function* that outputs the k^{th} combination of the product of m elements taken from the set A_l without repetition and disregarding order. Note that $F_k^0 = 1$.

In order to generate the transformation T_{yx}, define the function $C(l, m)$, with $l \in [0, \cdots, n]$, $m \in [0, \cdots, l]$ and $m \leq l$, over the set of coefficients A given by (106).

$$C(l, m) = \sum_{k=1}^{\bar{C}_m^l} F_k^m(A_l) \tag{107}$$

$$C(l, 0) = 1, \tag{108}$$

where $\bar{C}_m^l$ is the binomial coefficient $\binom{l}{m}$. The new coordinate system is characterized by

$$y_{n-i} = a_{i+1} \sum_{j=0}^{i} C(i, j) x_{n-j}, \qquad i \in [0, \cdots, n-1], \tag{109}$$

and the transformation T_{yx} is explicitly given by

$$\begin{aligned} T_{yx_{(n-i)(n-j)}} &= a_{i+1}C(i,j) \qquad & i \geq j \\ T_{yx_{(n-i)(n-j)}} &= 0 & i < j, \end{aligned} \tag{110}$$

for $i, j \in [0, \cdots, n-1]$. Additionally, T_{yx} is an upper diagonal matrix with non-zero diagonal entries. Hence, $T_{xy} = T_{yx}^{-1}$ exists. Finally, observing that

$$\begin{aligned} \dot{y} &= T_{yx}A_xT_{yx}^{-1}y + T_{yx}B_xu \\ &= A_yy + B_yu, \end{aligned}$$

it is enough to verify that $A_yT_{yx} = T_{yx}A_x$ and that $T_{yx}B_x = B_y$. This may be carried out using Equations 104, 105 and 110. □

Theorem 6. *For the system given by (103). Given any set of positive constants* $\{(L_i, M_i)\}$, *where* $L_i \leq M_i$ *for* $i = 1, \cdots, n$ *and* $M_i < \frac{1}{2}L_{i+1}$ *for* $i = 1, \cdots, n-1$, *and for any set of functions* $\{\sigma_i\}$ *that are* linear saturations *for* $\{(L_i, M_i)\}$, *there exists a linear coordinate transformation* $y = T_{yx}x$ *such that the bounded control*

$$u = -\sigma_n(y_n + \sigma_{n-1}(y_{n-1} + \cdots + \sigma_1(y_1))), \tag{111}$$

results in a globally asymptotically stable system.

Proof. In short, use the transformation given by Lemma 1 in the proof of Theorem 2.1 in [73]. It is however restated here for completeness.

Use the coordinate transformation $y = T_{yx}x$ given by Lemma 1 and choose the set of coefficients $a_i > 0$. Substituting the nested saturation law given by Eqn (111)

into Eqn (103) and expanding yields the closed loop system

$$\begin{aligned}
\dot{y}_1 &= a_n \quad [y_2 + \cdots + y_n \; -\sigma_n(y_n + \sigma_{n-1}(\cdots \sigma_1(y_1)))] \\
\dot{y}_2 &= a_{n-1}[y_3 + \cdots + y_n \; -\sigma_n(y_n + \sigma_{n-1}(\cdots \sigma_1(y_1)))] \\
&\vdots \\
\dot{y}_{n-1} &= a_2 \quad [\qquad\quad y_n \; -\sigma_n(y_n + \sigma_{n-1}(\cdots \sigma_1(y_1)))] \\
\dot{y}_n &= \qquad\qquad\quad -a_1\sigma_n(y_n + \sigma_{n-1}(\cdots \sigma_1(y_1))).
\end{aligned} \tag{112}$$

The trajectory of y_n is examined first. Choosing a Lyapunov function $V_n = y_n^2$, with $y_n \in \mathcal{R}^1$. Its derivative $\dot{V}_n$ may be written as

$$\dot{V}_n = -2a_1 y_n \left[\sigma_n(y_n + \sigma_{n-1}(y_{n-1} + \cdots + \sigma_1(y_1)))\right].$$

Noting that $a_i > 0$. Definition 3, conditions (a), (b), imply that y_n and $\sigma_n(\cdot)$ are the same sign only if $y_n + \sigma_{n-1}(\cdot)$ is the same sign as y_n. Condition (c) of Definition 3 applied to σ_{n-1} and having chosen $M_{n-1} < \frac{1}{2}L_n$, it can be seen that $\dot{V}_n < 0$ for all $y_n \notin Q_n = \{y_n : |y_n| \leq \frac{1}{2}L_n\}$. If starting outside Q_n, the trajectory of y_n eventually enters Q_n in *finite time*. Since the RHS of Eqn (112) is globally Lipschitz, the derivatives are bounded resulting in the remaining states $y_1 \cdots y_{n-1}$ remaining bounded for any given *finite time*.

Once y_n has entered Q_n, condition (b) of Definition 3 implies σ_n operates in its linear region because the argument to σ_n is bounded as

$$|y_n + \sigma_{n-1}(\cdot)| \leq \frac{1}{2}L_n + M_{n-1} \leq L_n.$$

The equation for the evolution of y_{n-1} is now given by

$$\begin{aligned}
\dot{y}_{n-1} &= \cancelto{0}{a_2 y_n - a_2 y_n} - a_2\sigma_{n-1}(y_{n-1} + \cdots + \sigma_1(y_1)) \\
&= -a_2\sigma_{n-1}(y_{n-1} + \cdots + \sigma_1(y_1)),
\end{aligned}$$

which is similar to the expression for $\dot{y}_n$. Using similar arguments as that used for the evolution of y_n, it can be shown that y_{n-1} enters a set Q_{n-1} in finite time and

remains in Q_{n-1} thereafter with all remaining states being bounded. Continuing in the same fashion, it can be shown that every state y_i for $i \in [1, \cdots, n]$, enters a set $Q_i = \{y_i : |y_i| \leq \frac{1}{2}L_i\}$ in finite time and all saturation functions σ_i are operating in their linear regions. Hence after a certain finite amount of time the governing equations, Eqn (112), becomes

$$\begin{aligned}
\dot{y}_1 &= -a_n y_1 \\
\dot{y}_2 &= -a_{n-1}(y_1 + y_2) \\
&\vdots \\
\dot{y}_n &= -a_1(y_1 + y_2 + \cdots + y_n),
\end{aligned}$$

which is exponentially stable. □

Corollary 2 (Pole location)**.** *If the saturators used are* conventional saturation*, and none of the σ_i are saturated, the poles of the linearized closed loop system reside at $\{-a_1, -a_2, \cdots, -a_n\}$. During periods when the outermost saturated element is the k^{th} saturator, σ_k, the poles of the resulting closed loop linear system reside at $\{-a_1, -a_2, \cdots, -a_{n-k}, 0_1, 0_2, \cdots, 0_k\}$.*

Proof. Using the nested saturation law, the closed-loop n-integrator system may be expressed as

$$\dot{x}_n + \sigma_n(y_n + \sigma_{n-1}(y_{n-1} + \cdots + \sigma_1(y_1))) = 0.$$

When the k^{th} saturator is saturated, and $\sigma_{k+1} \cdots \sigma_n$ are not saturated, the closed loop system is given by

$$\dot{x}_n + y_n + y_{n-1} + \cdots y_{k+1} \pm M_k = 0.$$

This represents a forced linear system where the forcing function is the constant M_k. Examining the homogeneous part

$$0 = \dot{x}_n + y_n + y_{n-1} + \cdots + y_{k+1}.$$

Using Eqn (109) to expand y_i

$$\begin{aligned} 0 = \dot{x}_n &+ a_1 \sum_{j=0}^{0} C(0,j) x_{n-j} \\ &+ a_2 \sum_{j=0}^{1} C(1,j) x_{n-j} + \cdots \\ &+ a_{n-k} \sum_{j=0}^{n-(k+1)} C\left(n-(k+1), j\right) x_{n-j}. \end{aligned}$$

Noting that $x = x_1, \dot{x} = x_2, \cdots, x^{(n-1)} = x_n, x^{(n)} = \dot{x}_n$, and substituting $p = n - k$ for clarity the characteristic equation may be written as

$$\begin{aligned} \Upsilon(\lambda) = \lambda^n & \\ &+ a_1 C(0,0) \lambda^{n-1} \\ &+ a_2 C(1,0) \lambda^{n-1} + a_2 C(1,1) \lambda^{n-2} \\ &\vdots \\ &+ a_p C(p-1,0) \lambda^{n-1} + \cdots + a_p C(p-1,p-1) \lambda^k. \end{aligned}$$

Factoring out λ^k

$$\begin{aligned} \Upsilon(\lambda) = \lambda^k [\lambda^p & \\ &+ a_1 C(0,0) \lambda^{p-1} \\ &+ a_2 C(1,0) \lambda^{p-1} + a_2 C(1,1) \lambda^{p-2} \\ &+ a_p C(p-1,0) \lambda^{p-1} + \cdots + a_p C(p-1,p-1)], \end{aligned}$$

and may be written in its final form as

$$\Upsilon(\lambda) = \lambda^k (\lambda + a_1)(\lambda + a_2) .... (\lambda + a_p),$$

which has k zeros and $p = n - k$ non-zero stable poles at known locations. □

Corollary 3. *During periods when σ_k is the outermost saturated element in the control law of Theorem 6 and the coordinate transformation used is given by Lemma 1,*

then, in steady-state, the magnitude of the k^{th} derivative, $\dot{x}_k$, is given by

$$|\dot{x}_k| = \left| \frac{M_k}{a_{n-k} C(n-(k+1), n-(k+1))} \right|, \tag{113}$$

for $k \in [1, \cdots, n-1]$, and

$$|\dot{x}_k| = |M_k|, \tag{114}$$

for $k = n$.

Proof. If σ_k is saturated, the closed loop system may be written as

$$\dot{x}_n + y_n + y_{n-1} + \cdots y_{k+1} \pm M_k = 0.$$

Using Eqn (109)

$$\begin{aligned} 0 = \dot{x}_n &+ a_1 \sum_{j=0}^{0} C(0,j) x_{n-j} \\ &+ a_2 \sum_{j=0}^{1} C(1,j) x_{n-j} + \cdots \\ &+ a_{n-k} \sum_{j=0}^{n-(k+1)} C\left(n-(k+1), j\right) x_{n-j} \pm M_k. \end{aligned} \tag{115}$$

When the outermost saturated element is σ_k, the dynamics eventually reach a *saturated-equilibrium* region where higher-order derivatives reach zero. So, $x^{(n)} \cdots x^{(k+1)}$, i.e., $\dot{x}_n, x_n \cdots x_{k+2}$ go to zero. The only term left from Eqn (115) is

$$a_{n-k} C(n-(k+1), n-(k+1)) x_{k+1} \pm M_k = 0. \tag{116}$$

Noting that $\dot{x}_k = x_{k+1}$, rearranging Eqn (116) and taking the absolute value of both sides results in Eqn (113). Finally, when $k = n$, the outermost saturator σ_n is saturated and Eqn (115) reduces to

$$\dot{x}_n \pm M_n = 0. \tag{117}$$

Rearranging Eqn (117) and taking magnitudes of both sides results in Eqn (114) □

Corollary 4 (Restricted Tracking)**.** *Consider a nonlinear system with magnitude saturation at the input u given by*

$$\dot{x}_1 = x_2, \cdots, \dot{x}_n = \sigma_{n+1}(u), \tag{118}$$

and a compatible reference signal given by

$$\left[x_d(t), \quad \dot{x}_d(t), \quad \cdots \quad x_d^{(n)}(t) \right]. \tag{119}$$

If $|x_d^{(n)}(t)| \leq L_{n+1} - \epsilon$ for all $t \geq t_0$ and for some $\epsilon > 0$ and given linear saturation *functions σ_i with parameters (L_i, M_i) satisfying,*

$$\begin{aligned} L_i &\leq M_i && i = 1, \cdots, n+1 \\ M_i &< \frac{1}{2} L_{i+1} && i = 1, \cdots, n-1 \\ M_n &\leq \epsilon, \end{aligned}$$

then, the feedback

$$u = x_d^{(n)} - \sigma_n(y_n + \sigma_{n-1}(y_{n-1} + \cdots + \sigma_1(y_1))),$$

with $y = T_{yx} e$ given by Lemma 1, where, $e_i = x_i - x_d^{(i-1)}$ for $i = 1 \cdots n$, results in a globally asymptotically stable system. Additionally if conventional saturation *elements are used, the error dynamics are governed by Corollary 2 and quasi-steady rates governed by Corollary 3.*

Proof. The dynamics of Eqn (118) may be expressed in terms of the error e

$$\dot{e}_1 = e_2, \cdots, \dot{e}_n = -x_d^{(n)} + \sigma_{n+1}(u).$$

With the given control law, if the magnitude of the n^{th} derivative of the command x_d is always such that $|x_d^{(n)}(t)| \leq L_{n+1} - \epsilon$ for all $t \geq t_0$ and $M_n \leq \epsilon$, then the magnitude of the argument of σ_{n+1} is

$$|x_d^{(n)} - \sigma_n(\cdot)| \leq L_{n+1},$$

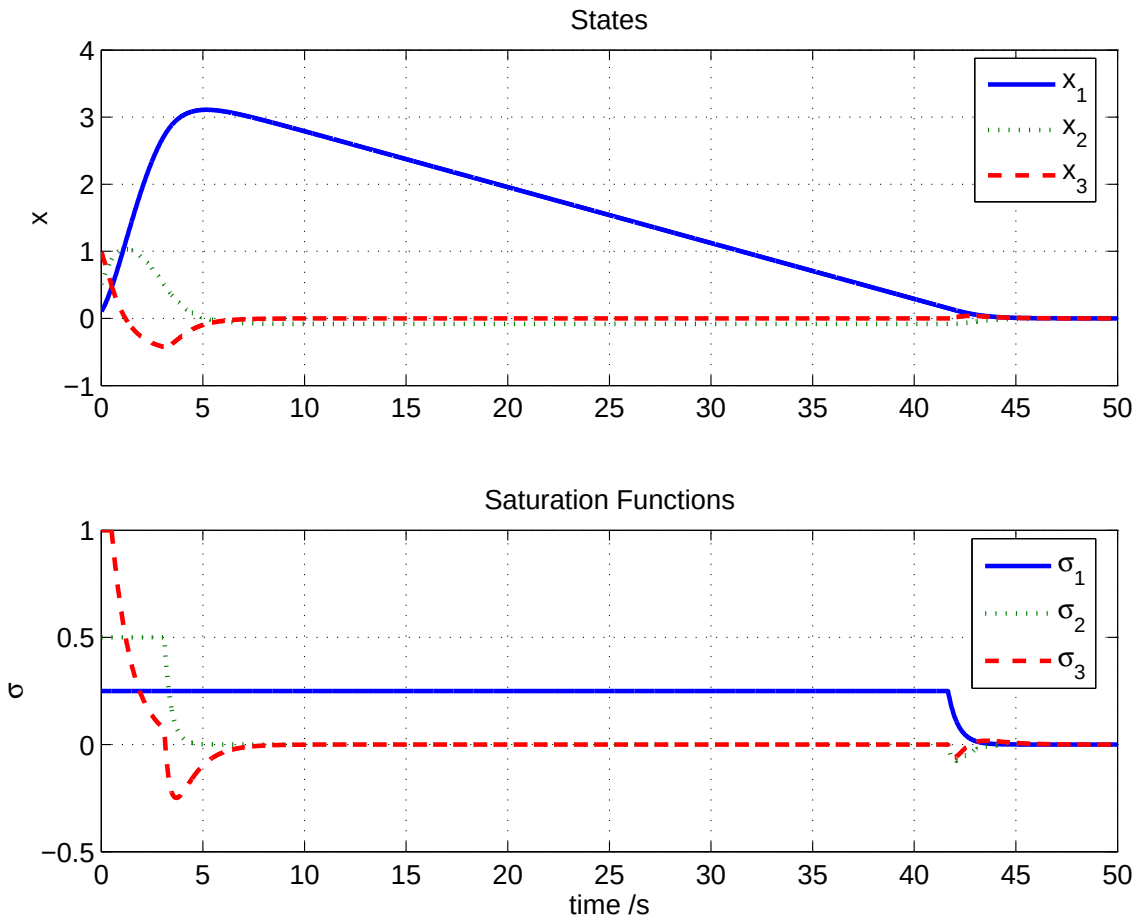

Figure 28: Initial condition response of a 3^{rd} order system

and σ_{n+1} is always in its linear region, resulting in the closed loop error dynamics becoming

$$\dot{e}_1 = e_2, \cdots, \dot{e}_n = -\sigma_n(y_n + \sigma_{n-1}(y_{n-1} + \cdots + \sigma_1(y_1))). \tag{120}$$

The conditions of this corollary and form of Eqn (120) satisfy the requirements of Theorem 6. This implies that the dynamics of e are asymptotically stable and hence x tracks x_d asymptotically. The form of Eqn (120) also allows Corollary 2 and Corollary 3 to be applied directly. □

B.3 Examples

B.3.1 Global Stabilization

Consider the problem of stabilizing the 3^{rd} order system

$$\dot{x}_1 = x_2, \dot{x}_2 = x_3, \dot{x}_3 = u,$$

using bounded control $u \in [-1, 1]$ (conventional saturation) with poles at $\{-1, -3, -2\}$. Then, $\{a_1, a_2, a_3\} = \{1, 3, 2\}$. The transformation required to achieve these poles may be expressed as

$$\begin{bmatrix} y_1 \\ y_2 \\ y_3 \end{bmatrix} = \begin{bmatrix} a_3(a_1 a_2) & a_3(a_1 + a_2) & a_3 \\ & a_2(a_1) & a_2 \\ & & a_1 \end{bmatrix} \begin{bmatrix} x_1 \\ x_2 \\ x_3 \end{bmatrix}.$$

Using the nested saturation law given by Theorem 6 and choosing the saturation element parameters as follows

$$\begin{aligned} M_3 &= 1, & L_3 &= M_3 \\ M_2 &= \frac{1}{2}L_3 - \bar{\epsilon}, & L_2 &= M_2 \\ M_1 &= \frac{1}{2}L_2 - \bar{\epsilon}, & L_1 &= M_1, \end{aligned}$$

where $\bar{\epsilon}$ is a small positive number, that is used to satisfy the inequality $M_i < \frac{1}{2}L_{i+1}$. Additionally the saturation element parameters are chosen $L_i = M_i$ (conventional saturation). Then, the closed loop system is given by

$$\dot{x}_3 + \sigma_3(y_3 + \sigma_2(y_2 + \sigma_1(y_1))) = 0.$$

An initial condition response with $x_0 = [0.1, 0.5, 1.0]$ is shown in Fig. 28. The figure also shows the outputs of the saturation elements.

- 0 - 0.5s, σ_3 is saturated
- 0.5 - 3.1s, σ_2 is saturated

- 3.1 - 41.6s, σ_1 is saturated
- 41.6 - 50s, control law is unsaturated

The only region where the system practically reaches a *saturated-equilibrium* is when σ_1 is saturated, between 10 and 41 seconds. The equilibrium value for $\dot{x}_1$ is given by Corollary 3

$$|\dot{x}_1| = |x_2| = \left|\frac{M_1}{a_2 a_1}\right| = 0.0833$$

and matches the slope of x_1 in Fig. 28.

B.3.2 Restricted Tracking

Consider a chain of 4 integrators where, $\sigma_5(u)$ represents a magnitude saturated actuator.

$$\dot{x}_1 = x_2, \dot{x}_2 = x_3, \dot{x}_3 = x_4, \dot{x}_4 = \sigma_5(u),$$

where σ_5 is a conventional saturation function with parameters (L_5, M_5). A compatible command may be represented as $[x_d, \dot{x}_d, \ddot{x}_d, \dddot{x}_d, \ddddot{x}_d]$. Defining the error as, $e = x - x_d$, the error derivatives may be written as

$$\dot{e} = x_2 - \dot{x}_d$$

$$\ddot{e} = x_3 - \ddot{x}_d$$

$$\dddot{e} = x_4 - \dddot{x}_d$$

$$\ddddot{e} = \sigma_5(u) - \ddddot{x}_d,$$

The control is given by Corollary 4,

$$u = \ddddot{x}_d - \sigma_4(y_4 + \sigma_3(y_3 + \sigma_2(y_2 + \sigma_1(y_1)))),$$

with $|\ddddot{x}_d| \leq L_5 - \epsilon$ and $M_4 \leq \epsilon$, for some $\epsilon > 0$, the saturation function parameters (L_i, M_i) chosen to satisfy the conditions given by Corollary 4 and y_i given by Lemma 1.

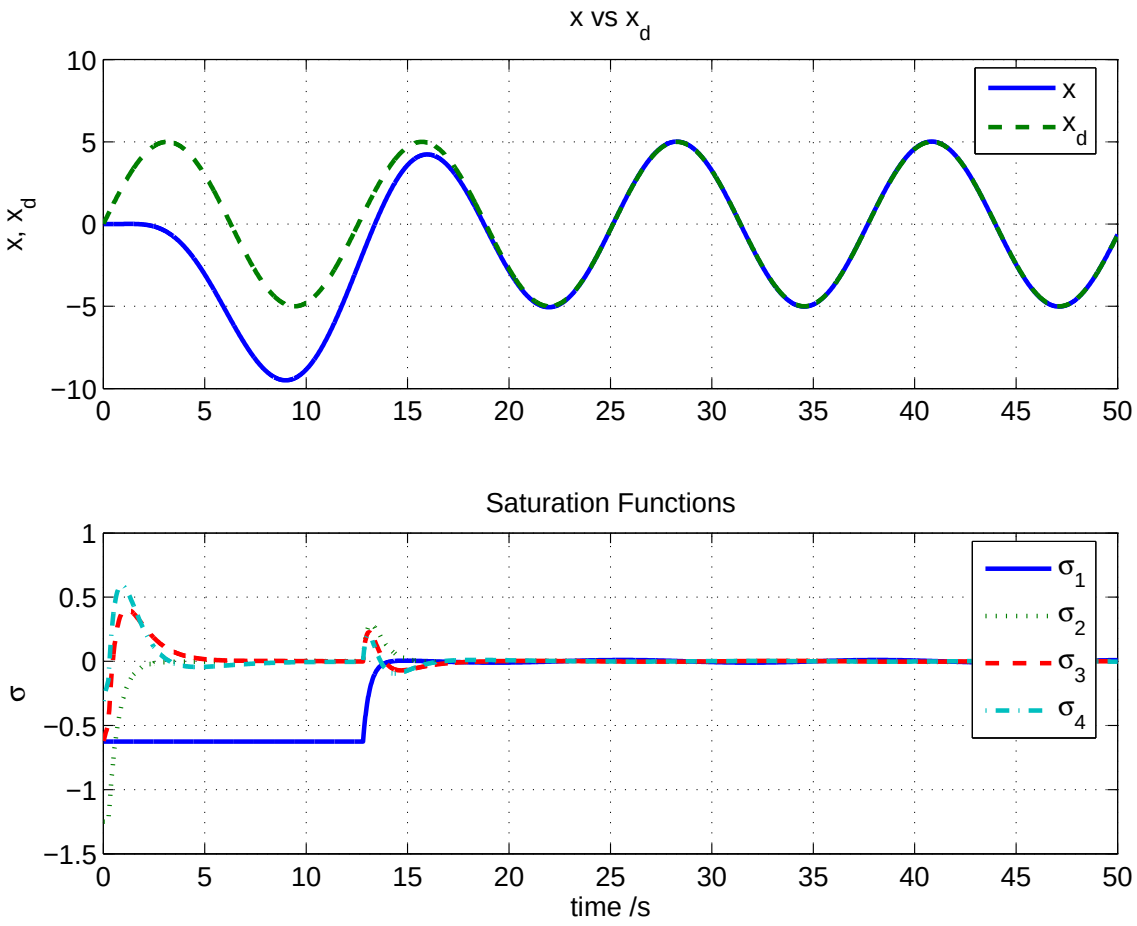

Figure 29: Response to a sinusoidal command for a 4^{th} order system

The coordinate transformation used is $y = T_{yx}e$ where T_{yx} is given by

$$\begin{bmatrix} a_1a_2a_3a_4 & (a_1a_3 + a_2a_3 + a_1a_2)a_4 & (a_1 + a_2 + a_3)a_4 & a_4 \\ 0 & a_1a_2a_3 & (a_1 + a_2)a_3 & a_3 \\ 0 & 0 & a_1a_2 & a_2 \\ 0 & 0 & 0 & a_1 \end{bmatrix}.$$

Here, the poles were taken to be at

$$\{-a_1, -a_2, -a_3, -a_4\} = \{-0.5, -1, -2, -3\}.$$

The saturation function parameters were chosen as

$$\begin{aligned} L_5 &= 10 & M_5 &= L_5 - \bar{\epsilon} \\ \epsilon &= \frac{1}{2}L_5 \\ L_4 &= \epsilon & M_4 &= \epsilon - \bar{\epsilon} \\ L_3 &= \frac{1}{2}L_4 & M_3 &= L_3 - \bar{\epsilon} \\ L_2 &= \frac{1}{2}L_3 & M_2 &= L_2 - \bar{\epsilon} \\ L_1 &= \frac{1}{2}L_2 & M_1 &= L_1 - \bar{\epsilon}, \end{aligned}$$

where $\bar{\epsilon}$ is a small positive number chosen to satisfy $M_i < L_i$. If Corollary 3 is evaluated for various saturation elements being saturated.

$$\begin{aligned} |\dot{e}_4| &= |M_4| \quad when, \sigma_4 \text{ is saturated} \\ |\dot{e}_3| &= \left|\frac{M_3}{a_1}\right| \quad when, \sigma_3 \text{ is saturated} \\ |\dot{e}_2| &= \left|\frac{M_2}{a_1a_2}\right| \quad when, \sigma_2 \text{ is saturated} \\ |\dot{e}_1| &= \left|\frac{M_1}{a_1a_2a_3}\right| \quad when, \sigma_1 \text{ is saturated.} \end{aligned} \tag{121}$$

The response of this system to a sinusoidal command compatible with $x_d = 5\sin(0.5t)$ and zero initial conditions is illustrated in Fig. 29.

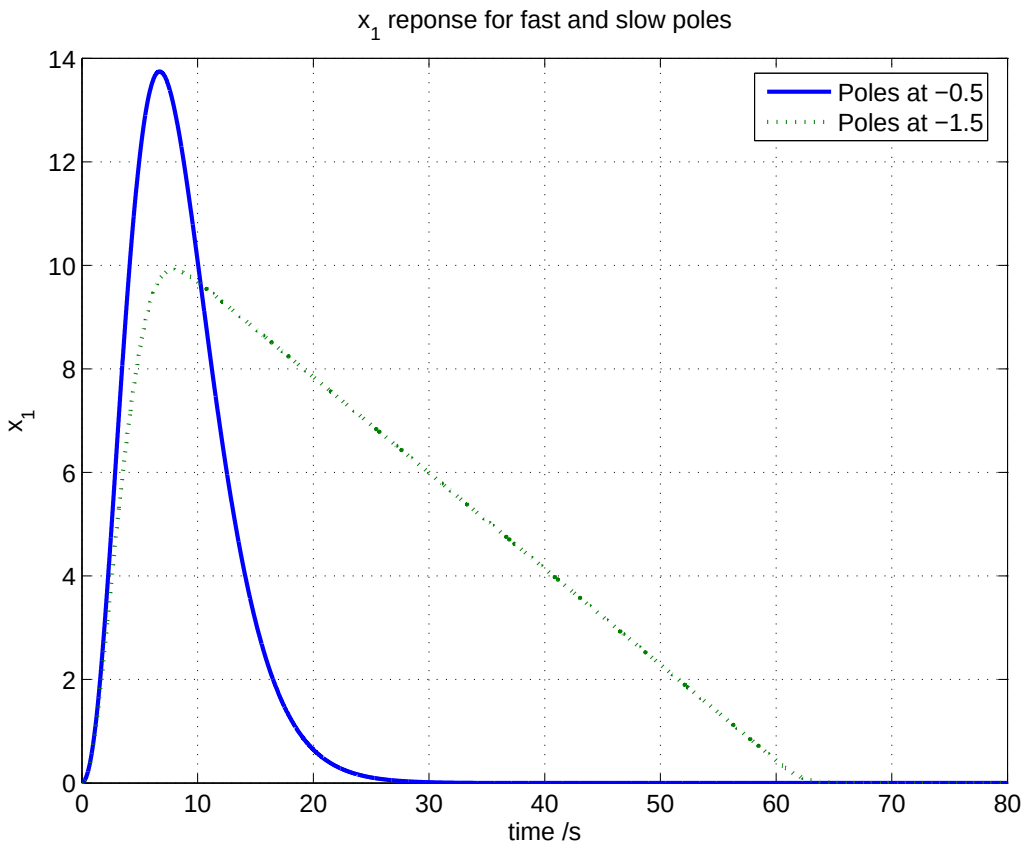

Figure 30: Comparison of the initial condition response, for a 4^{th} order system. The solid curve settles faster and has all poles at -0.5 whilst the dashed-curve settles slower and has poles at -1.5.

From Eqn (121) notice that as the bandwidth i.e., a_i is increased, the error rates in *saturated-equilibrium* decrease. Hence for higher bandwidth, the overall settling time can be higher, which is perhaps counter-intuitive. This aspect is further illustrated in Fig. 30 where it is observed that the control law with faster poles (all at -1.5) takes longer to be regulated back to 0 than the system with slower poles (all at -0.5). The initial condition used was $x_0 = [0, 0.1, 1, 2]^T$ with zero command.

REFERENCES

[1] Abraham, R., Marsden, J. E., and Ratiu, T., "Manifolds, Tensors, Analysis, and Applications". Springer Verlag, Berlin, 1988.

[2] Aeronautical Design Standard, *Handling Qualities Requirements for Military Rotorcraft, ADS-33E*. Redstone Arsenal, Alabama: United States Army Aviation and Missile Command, March 2000.

[3] Bateman, A. and Lin, Z., "An analysis and design method for linear systems under nested saturation," *Systems & Control Letters*, vol. 48, pp. 41–52, 2003.

[4] Bemporad, A., Casavola, A., and Mosca, E., "Nonlinear control of constrained linear systems via predictive reference management," *IEEE Transactions on Automatic Control*, vol. 42, pp. 340–349, March 1997.

[5] Bernstein, D. S. and Michel, A. N., "A chronological bibliography on saturating actuators," *International Journal of Robust and Nonlinear Control*, vol. 5, pp. 375–380, 1995.

[6] Brinker, J. and Wise, K., "Flight testing of a reconfigurable flight control law on the x-36 tailless fighter aircraft," *AIAA Journal of Guidance, Control, and Dynamics*, vol. 24, no. 5, pp. 903–909, 2001.

[7] Calise, A. J., Hovakimyan, N., and Idan, M., "Adaptive output feedback control of nonlinear systems using neural networks," *Automatica*, vol. 37, pp. 1201–1211, aug 2001. Special Issue on Neural Networks for Feedback Control.

[8] Calise, A. J., Lee, S., and Sharma, M., "Development of a reconfigurable flight control law for tailless aircraft," *AIAA Journal of Guidance, Control, and Dynamics*, vol. 24, no. 5, pp. 896–902, 2001.

[9] Calise, A. J., Sharma, M., and Lee, S., "Adaptive autopilot design for guided munitions," *AIAA Journal of Guidance, Control, and Dynamics*, vol. 23, no. 5, 2000.

[10] Frazzoli, E., Dahleh, M. A., and Feron, E., "Real-time motion planning for agile autonomous vehicles," *AIAA Journal of Guidance, Control, and Dynamics*, vol. 25, no. 1, pp. 116–129, 2002.

[11] Gavrilets, V., Mettler, B., and Feron, E., "Nonlinear model for a small-sized acrobatic helicopter," in *AIAA Guidance, Navigation and Control Conference*, no. 2001-4333, (Montréal, Quebec, Canada), Aug. 2001.

[12] Gavrilets, V., Mettler, B., and Feron, E., "Control logic for automated aerobatic flight of miniature helicopter," in *AIAA Guidance, Navigation and Control Conference*, no. AIAA-2002-4834, (Monterey, CA), August 2002.

[13] Haddad, W. M., *Control-System Synthesis: The Fixed-Structure Approach*. Unpublished, 1995. AE6351 Robust Control Course Notes.

[14] Haddad, W. M. and Chellaboina, V., *Nonlinear Dynamical Systems and Control: A Dissipative Systems Approach*. Pre-Print, 2002.

[15] Hanus, R., Kinnaert, M., and Henrotte, J. L., "Conditioning technique, a general anti-windup and bumpless transfer methods," *Automatica*, vol. 23, no. 6, pp. 729–739, 1987.

[16] H.Khalil, *Nonlinear Systems*. Macmillan Publishing Company, New York, 1992.

[17] Hornik, K., Stinchcombe, M., and White, H., "Multilayer feedforward networks are universal approximators," *Neural Networks*, vol. 2, no. 5, pp. 359–366, 1989.

[18] Hovakimyan, N. and Calise, A. J., "Adaptive output feedback control of uncertain multi-input multi-output systems using single hidden layer neural networks," *International Journal of Control*, 2002. submitted.

[19] Hovakimyan, N., Kim, N., Calise, A., Prasad, J., and Corban, J. E., "Adaptive output feedback for high-bandwidth control of an unmanned helicopter," in *AIAA Guidance, Navigation and Control Conference*, 2001.

[20] Hu, T. and Lin, Z., *Control Systems with Actuator Saturation : Analysis and Design*. Birkhaüser, 2001.

[21] Hu, T. and Lin, Z., "Composite quadratic lyapunov functions for constrained linear systems," *IEEE Transactions on Automatic Control*, vol. 48, pp. 440–450, March 2003.

[22] Hu, T., Lin, Z., and Chen, B. M., "An analysis and design method for linear systems subject to actuator saturation and disturbance," *Automatica*, vol. 38, pp. 351–359, 2002.

[23] Isidori, A., "Nonlinear Control Systems I". Springer Verlag, Berlin, 1994.

[24] Isidori, A., "Nonlinear Control Systems II". Springer Verlag, Berlin, 1999.

[25] Jadbabaie, A. and Hauser, J., "On the stability of receding horizon control with a general terminal cost," *IEEE Transactions on Automatic Control*, vol. 50, pp. 674–678, May 2005.

[26] Jadbabaie, A., Yu, J., and Hauser, J., "Unconstrained receding horizon control of nonlinear systems," *IEEE Transactions on Automatic Control*, vol. 46, pp. 776–783, May 2001.

[27] Johnson, E. N., *Limited Authority Adaptive Flight Control*. PhD thesis, Georgia Institute of Technology, School of Aerospace Engineering, Atlanta, GA 30332, Dec 2000.

[28] Johnson, E. N. and Calise, A. J., "Limited authority adaptive flight control for reusable launch vehicles," *AIAA Journal of Guidance, Control, and Dynamics*, vol. 26, pp. 906–913, Nov-Dec 2003.

[29] Johnson, E. N., Calise, A. J., and Corban, J. E., "Reusable launch vehicle adaptive guidance and control using neural networks," in *AIAA Guidance, Navigation and Control Conference*, no. 4381, 2001.

[30] Johnson, E. N. and Kannan, S. K., "Adaptive flight control for an autonomous unmanned helicopter," in *AIAA Guidance, Navigation and Control Conference*, no. AIAA-2002-4439, (Monterey, CA), August 2002.

[31] Johnson, E. N. and Schrage, D. P., "System integration and operation of a research unmanned aerial vehicle," *AIAA Journal of Aerospace Computing, Information and Communication*, vol. 1, pp. 5–18, Jan 2004.

[32] Kannan, S. K. and Johnson, E. N., "Adaptive trajectory based flight control for autonomous helicopters," in *AIAA Digital Avionics Conference*, no. 358, (Irvine, CA), October 2002.

[33] Karason, S. P. and Annaswamy, A. M., "Adaptive control in the presence of input constraints," *IEEE Transactions on Automatic Control*, vol. 39, no. 11, pp. 2325–2330, 1994.

[34] Kim, B. S. and Calise, A. J., "Nonlinear flight control using neural networks," *AIAA Journal of Guidance, Control, and Dynamics*, vol. 20, no. 1, pp. 26–33, 1997.

[35] Kim, N., Calise, A. J., Hovakimyan, N., Prasad, J., and Corban, J. E., "Adaptive output feedback for high-bandwidth flight control," *AIAA Journal of Guidance, Control, and Dynamics*, vol. 25, no. 6, pp. 993–1002, 2002.

[36] Kothare, M. V., Campo, P. J., Morari, M., and Nett, C. N., "A unified framework for the study of anti-windup designs," *Automatica*, vol. 30, no. 12, pp. 1869–1883, 1994.

[37] La Civita, M., Messner, W. C., and Kanade, T., "Modeling of small-scale helicopters with integrated first-principles and system-identification techniques," in *Proceedings of the 58th Forum of the American Helicopter Society*, vol. 2, (Montreal, Canada), pp. 2505–2516, June 2002.

[38] La Civita, M., Papageorgiou, G., Messner, W. C., and Kanade, T., "Design and flight testing of a gain-scheduled $\mathcal{H}_\infty$ loop shaping controller for wide-envelope flight of a robotic helicopter," in *Proceedings of the 2003 American Control Conference*, (Denver, CO), pp. 4195–4200, June 2003.

[39] La Civita, M., Papageorgiou, G., Messner, W. C., and Kanade, T., "Design and flight testing of a high bandwidth $\mathcal{H}_\infty$ loop shaping controller for a robotic helicopter," in *AIAA Guidance, Navigation and Control Conference*, no. AIAA-2002-4846, (Monterey, CA), August 2002.

[40] Lauvdal, T., *Stabilization of Linear Systems with Input Magnitude and Rate Saturations*. PhD thesis, Norwegian University of Science and Technology, Department of Engineering Cybernetics, Trondheim, Norway, 1998.

[41] Lavretsky, E. and Hovakimyan, N., "Positive μ-modification for stable adaptation in a class of nonlinear systems with actuator constraints," in *Proceedings of the 2004 American Control Conference*, (Boston, MA), 2004.

[42] Leitner, J., Calise, A. J., and Prasad, J. V. R., "Analysis of adaptive neural networks for helicopter flight controls," *AIAA Journal of Guidance, Control, and Dynamics*, vol. 20, pp. 972–979, Sep-Oct 1997.

[43] Lewis, F. L., "Nonlinear network structures for feedback control (survey paper)," *Asian Journal of Control*, vol. 1, no. 4, pp. 205–228, 1999.

[44] Lin, Y. and Sontag, E. D., "Universal formula for stabilization with bounded controls," *Systems & Control Letters*, vol. 16, pp. 393–397, 1991.

[45] Mazenc, F. and Praly, L., "Adding integrations, saturated controls and stabilization for feedforward systems," *IEEE Transactions on Automatic Control*, vol. 41, nov 1996.

[46] Menon, P., Chatterji, G., and Cheng, V., "Two-time-scale autopilot for high performance aircraft," in *AIAA Guidance, Navigation and Control Conference*, 1991.

[47] Mettler, B., *Identification Modeling and Characteristics of Miniature Rotorcraft*. Kluwer Academic Publishers, 2002.

[48] Munzinger, C., "Development of a real-time flight simulator for an experimental model helicopter," Master's thesis, Georgia Institute of Technology, School of Aerospace Engineering, Atlanta, GA 30332, Jul 1997.

[49] Murray, P. M. R. M. and Praly, L., "Nonlinear rescaling of control laws with application to stabilization in the presence of magnitude saturation," in *Nonlinear Control Systems Design Symposium*, (Enschede, Netherlands), July 1998.

[50] Narendra, K. S. and Annaswamy, A. M., "A new adaptive law for robust adaptation without persistent excitation," *IEEE Transactions on Automatic Control*, vol. 32, pp. 134–145, Februrary 1987.

[51] OSD, "Unmanned aircraft systems roadmap 2005-2030," tech. rep., Office of the Secretary of Defense, 2005.

[52] Pappas, G. J., "Avoiding saturation by trajectory reparameterization," in *IEEE Conference on Decision and Control*, (Kobe), 1996.

[53] Peng, Y., Vrancic, D., and Hanus, R., "Anti-windup, bumpless, and conditioned transfer techniques for pid controllers," *IEEE Controls Systems Magazine*, vol. 16, pp. 48–57, August 1996.

[54] Pittet, C., Tarbouriech, S., and Burgat, C., "Stability regions for linear systems with saturation controls via circle and popov cirteria," in 36^{th} *IEEE Conference on Decision and Control*, vol. 5, December 1997.

[55] Prasad, J. V. R. and Lipp, A. M., "Synthesis of a helicopter nonlinear flight controller using approximate model inversion," in *Mathematical and Computer Modelling*, vol. 18, pp. 89–100, August 1993.

[56] Rawlings, J. B. and Muske, K. R., "The stability of constrained receding horizon control," *IEEE Transactions on Automatic Control*, vol. 38, no. 10, pp. 1512 – 1516, 1993.

[57] Rysdyk, R. T. and Calise, A. J., "Nonlinear adaptive flight control using neural networks," *IEEE Controls Systems Magazine*, vol. 18, pp. 14–25, Dec 1998.

[58] Rysdyk, R. T. and Calise, A. J., "Adaptive model inversion flight control for tiltrotor aircraft," *AIAA Journal of Guidance, Control, and Dynamics*, vol. 22, no. 3, pp. 402–407, 1999.

[59] Saberi, A., Lin, Z., and Teel, A. R., "Control of linear systems with saturating actuators," *IEEE Transactions on Automatic Control*, vol. 41, pp. 368–378, March 1996.

[60] Sanders, C. P., DeBitetto, P. D., Feron, E., Vuong, H. F., and Levenson, N., "Hierarchical control of small autonomous helicopters," in 37^{th} *IEEE Conference on Decision and Control*, vol. 4, (Tampa, Florida), December 1998.

[61] Selmic, R. R. and Lewis, F. L., "Deadzone compensation in motion control systems using neural networks," *IEEE Transactions on Automatic Control*, vol. 45, pp. 602–613, April 2000.

[62] Selmic, R. R. and Lewis, F. L., "Neural-network approximation of piecewise continuous functions: application to friction compensation," *IEEE Transactions on Neural Networks*, vol. 13, pp. 745–751, May 2002.

[63] Sontag, E. D., "An algebraic approach to bounded controllability of linear systems," *International Journal of Control*, vol. 39, pp. 181–188, 1984.

[64] Sontag, E. D., "Controllability is harder to decide than accessibility," *SIAM Journal of Control and Optimization*, vol. 26, pp. 1106–1118, 1988.

[65] Sontag, E. D., "Some complexity questions regarding controllability," in 27^{th} *IEEE Conference on Decision and Control*, vol. 2, (Austin, Texas), December 1988.

[66] Sontag, E. D., *Mathematical Control Theory : Deterministic Finite Dimensional Systems*. Springer, 2^{nd} ed., 1998.

[67] Spooner, J. T., Maggiore, M., Ordóñez, R., and Passino, K. M., *Stable Adaptive Control and Estimation for Nonlinear Systems, Neural and Fuzzy Approximator Techniques*. Wiley, 2002.

[68] Stevens, B. L. and Lewis, F. L., *Aircraft Control and Simulaion*. John Wiley & Sons, New York, 2003.

[69] Sussman, H. J. and Kokotovic, P. V., "The peaking phenomenon and the global stabilization of nonlinear systems," *IEEE Transactions on Automatic Control*, vol. 36, pp. 424–440, April 1991.

[70] Sussmann, H. J., Sontag, E. D., and Yang, Y., "A general result on the stabilization of linear systems using bounded controls," *IEEE Transactions on Automatic Control*, vol. 39, dec 1994.

[71] Sussmann, H. J. and Yang, Y., "On the stabilizability of multiple integrators by means of bounded feedback controls," in *Proceedings of the 30th IEEE Conference on Decision and Control*, (Brighton, UK), 1991.

[72] Teel, A. R., "Feedback stabilization : Nonlinear solutions to inherently nonlinear problems," Tech. Rep. UCB/ERL M92/65, Electronics Research Laboratory, University of California, Berkeley, CA 94720, June 1992.

[73] Teel, A. R., "Global stabilization and restricted tracking for multiple integrators with bounded controls," *Systems & Control Letters*, vol. 18, pp. 165–171, 1992.

[74] Teel, A. R., "A nonlinear small gain theorem for the analysis of control systems with saturation," *IEEE Transactions on Automatic Control*, vol. 41, no. 9, pp. 1256–1270, 1996.

[75] Teel, A. R., "Semi-global stabilization of linear systems with position and rate-limited actuators," *Systems & Control Letters*, vol. 30, pp. 1–11, 1997.

[76] Zaccarian, L. and Teel, A. R., "A common framework for anti-windup, bumpless transfer and reliable designs," *Automatica*, vol. 38, no. 10, pp. 1735–1744, 2002.

VITA

Suresh Kumar Kannan was born on August 8, 1974, in Dharmapuri, Tamil Nadu, India. In 1992 he entered the University of Manchester, UK, obtaining an MEng in Aerospace Engineering in 1996. During 1995 and 1996 he worked as a visiting researcher at Rolls-Royce Civil Aero Engines Limited in Derby, UK. In Fall 1996, he entered the School of Aerospace Engineering at Georgia Institute of Technology for graduate studies. He was awarded a Master of Science in Aerospace Engineering in 2002. His interests include nonlinear systems, adaptive control and unmanned systems.